VŠB – Technical University of Ostrava
Faculty of Mechanical Engineering
Department of Power Engineering

Diploma Thesis

Numerický výpočet posledního stupně a difuzoru v experimentální parní turbíně T10MW

Numerical calculation of the last stage and diffuser in the experimental steam turbine T10MW

Student: Bc. Breno Chaves e Silva
Diploma thesis supervisor: Ing. Zdeněk Šmída
Diploma thesis consultant: doc. Ing. Michal Hoznedl, PhD.

VŠB - Technical University of Ostrava
Faculty of Mechanical Engineering
Department of Energy Engineering

Diploma Thesis Assignment

Student: **Breno Chaves e Silva, BSc**

Study Programme: N2301 Mechanical Engineering

Study Branch: 2302T006 Energy Engineering

Title: Numerical Calculation of the Last Stage and Diffuser of the Experimental Steam Turbine T10MW
Numerický výpočet posledního stupně a difuzoru experimentální parní turbíny T10MW

The thesis language: English

Description:

3D CFD calculation of the 3rd (last) stage and diffuser in T10MW experimental turbine (configuration Boiler Feed Pump Turbine) will be done. The diploma thesis should include the following points:

1. 3D model of steam in last stage and diffuser will be done on the base of provided geometry.
2. 3D mesh of geometry.
3. Setting of CFD solver, calculation for at least two operational regimes with boundary conditions set on the base of experimental measurement.
4. Data postprocessing, comparison between measured and calculated data, determination of stage flow parameters, losses and outlet flow fields.

In the case of persisting problems with the divergence of CFD calculation, in other words in case of the impossibility to calculate the given geometry, for example from the reason of the limited computing capacity of your pc. Simplify geometry or analyze partial calculated data with emphasis on the detailed justification for this step.

References:

MORAN, J. and Michael, SHAPIRO N., Howard. Fundamentals of Engineering Thermodynamics – 5th Edition. New York: John Wiley & Sons, 2006, 831 p., ISBN 978-0-07-150821-6.
BLOCH, P., Heinz and Murai P. SINGH. Steam Turbines – Design, Applications and Re-Rating – 2nd Edition. New York: McGraw-Hill Companies, Inc., 2009, 414 p. ISBN: 978-0-471-72793-4
LEYZEROVICH, S. Alexander. Steam Turbines for Modern Fossil-Fuel Power Plants. Lilburn: Fairmont Press, 2008, 350 p. ISBN: 0-88173-549-3.
SCHOBEIRI, M. T. Turbomachinery Flow Physics and Dynamic Performance. Berlin, Heidelberg: Springer, 2005, 522 p. ISBN: 3-540-22368-1.
ftp.energia.bme.hu. ANSYS FLUENT Tutorial Guide. [online]. © 2012, [cit. 2018-03-11]. Available from: < ftp://ftp.energia.bme.hu/pub/Tuzelestechnika/MSc/flu_tg.pdf >

Extent and terms of a thesis are specified in directions for its elaboration that are opened to the public on the web sites of the faculty.

Supervisor: **Ing. Zdeněk Šmída**

Date of issue: 21.12.2018
Date of submission: 20.05.2019

doc. Ing. Stanislav Honus, Ph.D.
Head of Department

prof. Ing. Ivo Hlavatý, Ph.D.
Dean

Student's affidavit

I declare that I have prepared the whole diploma thesis including appendices independently under the leadership of the diploma thesis supervisor, and I stated all the documents and literature used.

In the thesis, I used internal information about the technical parameters of the steam turbine obtained from the company Doosan Škoda Power, the company agrees to their disclosure

„Jsem si vědom/-a toho, že se při odborných konzultacích zajišťovaných ze strany Doosan Škoda Power (dále jen „DSPW") mohu seznámit s informacemi, které představují obchodní tajemství nebo jsou informacemi důvěrné povahy. Výslovně se zavazuji, že nebudu s utajovanými informacemi nakládat v rozporu s instrukcemi či zájmy DSPW, zejména utajované informace nesdělím žádné třetí osobě ani dalším zaměstnancům DSPW, ani neumožním sdělení utajovaných informací takovým osobám. Současně uděluji DSPW licenci k veškerému užití Závěrečné práce a jejího obsahu, tj. DSPW má zejména právo obchodně využívat vše obsažené v Závěrečné práci. Prohlašuji, že DSPW náleží veškerá práva k jakýmkoliv výsledkům technické tvůrčí činnosti (vynálezy a užitné vzory), předmětům průmyslového výtvarnictví (průmyslové vzory), jakož i označením (ochranné známky a označení původu) a také konstrukčním schématům polovodičových výrobků (tzv. topografie polovodičových výrobků) (dále jen „Průmyslová práva"), přímo či nepřímo obsažených v Závěrečné práci, tj. DSPW má zejména právo obchodně využívat dle svého uvážení Průmyslová práva, dále Průmyslová práva upravovat, neomezeně s nimi nakládat a poskytovat dalším osobám, atd.

Text práce a publikace související s prací předložím DSPW ke kontrole, jestli neobsahují důvěrné informace DSPW, nejpozději 14 dní před odevzdáním ve škole nebo jiným zveřejněním. Prohlašuji, že dokončenou i nedokončenou práci odevzdám DSPW v elektronické podobě nejpozději do 31.7. roku, kdy plánuji odevzdat závěrečnou práci ve škole."

In Ostrava on May 20, 2019.

.....

Student's signature

I declare that:

- I am aware that Act No. 121/2000 Coll., Act on copyright, rights related to copyright and amending some laws (the Copyright Act), in particular Section 35 (Use of a work in the civil or religious ceremonies or in official events organized by public authorities, in the context of university performance and use of university work) and Section 60 (university work) shall apply to my final diploma thesis
- I understand that VŠB – Technical University of Ostrava (hereinafter referred to as "VŠB-TUO") has the right to use this final diploma thesis non-commercially for its internal use (Section 35 Subsection 3 of the Copyright Act)
- if requested, a copy of this diploma thesis will be deposited with the thesis supervisor,
- if VŠB-TUO is interested, I will make a licensing agreement with it permitting to use the thesis within the scope of Section 12 Subsection 4 of the Copyright Act,
- I can only use my thesis, or grant a license to use it with the consent of VŠB-TUO, which is authorized in such a case to demand an appropriate contribution to the costs that were incurred by VŠB-TUO to create the thesis (up to the actual amount),
- I understand that - according to Act No. 111/1998 Coll., on higher education institutions and on changes and amendments to other acts (Higher Education Act), as amended - that this diploma thesis will be available for public before the defence at the thesis supervisor's workplace, and electronically stored and published after the defence at the Central Library of VŠB-TUO, regardless of the outcome of its defence.

In Ostrava on May 20, 2019.

.....

Signature of the author

Name and surname of the thesis author: Bc. Breno Chaves e Silva

Permanent address of the thesis author: Rua Alvaro Menezes, 386, S. A. Do Monte, Brasil

ANNOTATION OF DIPLOMA THESIS

CHAVES E SILVA, BRENO. *3D Numerical calculation of the last stage and diffuser in the experimental steam turbine T10MW*: Diploma Thesis. Ostrava: VŠB – Technical University of Ostrava, Faculty of Mechanical Engineering, Department of Power Engineering, 2019, 102 p. Supervisors: doc. Ing. Michal Hoznedl, PhD., Ing. Zdeněk Šmída.

This master thesis deals with the modeling of the complete flow of steam turbine stage. The introduction presents a summary of information about the company Doosan Škoda Power. Next chapters are devoted to the distribution of steam turbines and their working process. Last chapter of theory deals with the theory of flow. The practical part is focused on the design geometry inverse model steam round blades in Autodesk Inventor, design of mesh in ANSYS Meshing and 3D numerical calculation of the turbine stage in ANSYS Fluent 19.1. It also has setting of CFD solver, calculation for at least two operational regimes with boundary conditions set on the base of experimental measurement. Data postprocessing, comparison between measured and calculated data, determination of stage flow parameters, losses and outlet flow fields.

KEYWORDS

Steam turbine, ANSYS, Fluent, Numerical calculation, Turbine stage, Friction loss

ANOTACE DIPLOMOVÉ PRÁCE

CHAVES E SILVA, BRENO. *Numerický výpočet posledního stupně a difuzoru v experimentální parní turbíně T10MW:* Diplomová práce. Ostrava: VŠB – Technická univerzita Ostrava, Fakulta strojní, Katedra energetiky, 2019, 102 s. Vedoucí práce: doc. Ing. Michal Hoznedl, PhD., Ing. Zdeněk Šmída.

Diplomová práce se zabývá problematikou modelování proudění páry kompletním turbínovým stupněm. V úvodu je prezentován souhrn informací o společnosti Doosan Škoda Power. Další kapitoly se věnují rozdělení parních turbín a jejich pracovnímu procesu. Poslední kapitola teoretické části se zabývá teorií proudění. Praktická část se věnuje návrhu geometrie inverzního modelu páry v Autodesk Inventoru, tvorbě výpočetní sítě v ANSYS Meshing a 3D numerickému výpočtu turbínového stupně v ANSYS Fluent 19.1. V diplomové práci jsou také uvedeny nastavení CFD řešiče a výpočet pro nejméně dva provozní režimy s okrajovými podmínkami stanovenými na základě experimentálního měření. Následné zpracování dat, porovnání naměřených a vypočtených dat, stanovení fázových průtokových parametrů, ztrát a výstupních tokových polí.

KLÍČOVÁ SLOVA

Parní turbína, ANSYS, Fluent, numerický výpočet, turbínový stupeň, třecí ztráty

Content

Content

PICTURE LIST

PICTURE LIST

TABLE LIST

List of symbols, quantities and abbreviations

Nomenclature

Quantity	Name	Unit
A	Work	J
CLF	Courant number	-
D	Diameter	m
D_b	Diameter of the overbanding edges OL	m
$D_{p,OL}$	Beam diameter OL	m
$D_{p,RL}$	RL average diameter	m
F	Strong	N
G_{RL}	Mass flow in the distributor blade	$kg \cdot s^{-1}$
M	Moment of force	$N \cdot m$
M_{H2O}	Molar mass of water	$kg \cdot kmol^{-1}$
M_k	Torque induced by compressive force	$N \cdot m$
N_{NL}	Blade performance	W
N_v	Ventilation performance	W
P	Performance	W
R	Universal molar gas constant	$J \cdot kmol^{-1} \cdot K^{-1}$
Re	Reynolds number	-
Re_{krit}	Critical Reynolds Number	-
S_{1R}	Channel cross section at the rotor inlet	m^2
S_{2R}	Channel cross-section of the rotor exit	m^2
T	Temperature	K
T_a	Admission temperature	K
$T_{e,ize}$	Isoentropic emission temperature	K
T_v	Time scale of molecular diffusion	s
T_t	Time scale	s
T_{1R}	Inlet temperature to the rotor	K
$T_{2R,ize}$	Isoentropic temperature at the rotor outlet	K

List of symbols, quantities and abbreviations

Quantity	Name	Unit
Z_t	Loss power	W
a	Specific work for one kilogram of working substance	$J \cdot kg^{-1}$
$a_{c,ize}$	Iso-entropic measurements	$J \cdot kg^{-1}$
a_t	Specific technical work	$J \cdot kg^{-1}$
$a_{t,ize}$	Iso-entropic technical work	$J \cdot kg^{-1}$
a_{zvuk}	The speed of sound	$m \cdot s^{-1}$
c_{RL}	RL on the middle	m
c_1	Absolute speed at rotor inlet	$m \cdot s^{-1}$
c_2	Absolute speed at rotor exit	$m \cdot s^{-1}$
c_{2S}	Absolute velocity at stator output	$m \cdot s^{-1}$
c_{2x}	Axial absolute speed at rotor exit	$m \cdot s^{-1}$
c_{0x}	Axial absolute speed at stage inlet	$m \cdot s^{-1}$
c_{1u}	Perimeter component of the absolute velocity at the input of the rotor	$m \cdot s^{-1}$
c_{2u}	Peripheral component of the absolute velocity at the rotor outlet	$m \cdot s^{-1}$
c'	Absolute velocity at stator input	$m \cdot s^{-1}$
d	Internal pipe diameter	m
$d_{H,0}$	Hydraulic diameter indicating the dimension of the largest possible vortex at the inlet to the channel	m
$d_{H,2}$	Hydraulic diameter denoting the dimension of the largest possible swirl at the outlet of the channel	m
h	Entalpie	$J \cdot kg^{-1}$
h_a	Admission enthalpy	$J \cdot kg^{-1}$
h_e	Emission enthalpy	$J \cdot kg^{-1}$
$h_{e,ize}$	IsoEntropic emission enthalpy	$J \cdot kg^{-1}$
h_0	Enthalpy of steam entering the inter-channel channel	$J \cdot kg^{-1}$
i_T	Turbulence intensity	$\%$
k	Specified constant	-

List of symbols, quantities and abbreviations

Quantity	Name	Unit
k_τ	Friction coefficient	-
k_{tur}	Turbulent kinetic energy	$m^2 \cdot s^{-2}$
l_v	The length of the valve part OL	m
l	Length dimension (geometric scale)	m
l_{OL}	Length OL	m
l_{RL}	Length RL	m
m	Weight	kg
$\dot{m}_{pary}$	Actual steam flow in the inter-channel channel	$kg \cdot s^{-1}$
$\overline{\dot{m}_{pary}}$	The average value of the actual steam flow in the inter-path channel	$kg \cdot s^{-1}$
$\dot{m}_0$	Mass flow of steam at the inlet to the inter-channel channel	$kg \cdot s^{-1}$
$\dot{m}_{0,skut}$	Actual measured steam flow	$kg \cdot s^{-1}$
$\dot{m}_{0,1/50}$	1/50 of the mass flow of steam at the inlet to the inter-channel channel	$kg \cdot s^{-1}$
$\dot{m}_2$	Steam mass flow at the exit from the mezilop. channel	$kg \cdot s^{-1}$
$\dot{m}_{2,1/58}$	1/58 mass flow of steam at the inlet. channel	$kg \cdot s^{-1}$
n	Rotor speed	s^{-1}
p	Pressure	Pa
p_{hyb}	Momentum	$kg \cdot m \cdot s^{-1}$
p_0	Static pressure at the stage input	Pa
$p_{0,supersonic}$	Initial pressure at the inlet to the stage	Pa
p_{1R}	Rotor inlet pressure	Pa
p_2	Static pressure at the output of the stage	Pa
$p_{2R,ize}$	Iso-entropic pressure at the rotor outlet	Pa
r	Degree of reaction	-
r_{H2O}	Specific gas constant for water	$J \cdot kg^{-1} \cdot K^{-1}$
r_{OP}	Apparent reaction	%
$r_{OŠ}$	Top reaction	%

List of symbols, quantities and abbreviations

Quantity	Name	Unit
r_2	Beam radius OL	m
r_2	Beam radius OL	m
s	Average width of gap between OK and stator	m
s_b	Void in the overbanding gland	m
u	Peripheral speed	$m \cdot s^{-1}$
t_0	Static inlet temperature	K
t_2	Static output temperature from step	K
t_{RL}	RL pitch on center	m
v	Specific volume	$m^3 \cdot kg^{-1}$
v_m	Specific volume of steam at the end stage	$m^3 \cdot kg^{-1}$
w	Relative speed	$m \cdot s^{-1}$
$w_{k,s}$	Average pipeline speed	$m \cdot s^{-1}$
w_k	Flow rate of fluid (speed scale)	$m \cdot s^{-1}$
w_1	Relative speed at the rotor inlet.	$m \cdot s^{-1}$
w_2	Relative output speed from the rotor	$m \cdot s^{-1}$
w_∞	Speed of free flow	$m \cdot s^{-1}$
x_k	Distance from the leading edge	m
z_{OL}	Number of blades OK	-
z_{RL}	Number of RK blades	-
Δc_u	Difference of peripheral components of absolute speeds	$m \cdot s^{-1}$
Δh	Real enthalpy gradient	$J \cdot kg^{-1}$
Δh_{ize}	Iso entropic enthalpy gradient	$J \cdot kg^{-1}$
Δh_R	Enthalpy gradient in the rotor	$J \cdot kg^{-1}$
Δh_{RC}	Total enthalpy gradient in the rotor	$J \cdot kg^{-1}$
$\Delta h_{R,ize}$	Iso entropic rotor enthalpy	$J \cdot kg^{-1}$
Δh_S	Enthalpy gradient in the stator	$J \cdot kg^{-1}$
Δh_{SC}	The total enthalpy gradient in the stator	$J \cdot kg^{-1}$
$\Delta h_{S,ize}$	The isotropic enthalpy gradient of the stator	$J \cdot kg^{-1}$

Quantity	**Name**	**Unit**
$\Delta h_{ST,ize}$	Iso entropic enthalpy gradient	$J \cdot kg^{-1}$
$\Delta h_{ST,C,ize,\max}$	Total maximum enthalpy gradient in degree	$J \cdot kg^{-1}$
ΔM_k	Torque loss	$N \cdot m$
ΔP_τ	Friction performance	W
ε	(Speed) of dissipation	$m^2 \cdot s^{-3}$
η	Kolmogorov's length scale	m
$\eta_{dyn,visk}$	Dynamic viscosity	$kg \cdot m^{-1} \cdot s^{-1}$
η_{TV}	Efficiency from temperatures	-
η_{TD}	Thermodynamic efficiency	-
κ	Poisson constant	-
ν	Kinematic viscosity	$m^2 \cdot s^{-1}$
ρ	Density	$kg \cdot m^{-3}$
ρ_0	Density of steam at the interstellar channel inlet	$kg \cdot m^{-3}$
ρ_2	Density of steam at the outlet of the stage	$kg \cdot m^{-3}$
τ	Time	s
ω	The angular velocity	$rad \cdot s^{-1}$
$\zeta' \cdot \psi'$	Correlation moment	-

Abbreviations

Abbreviation	Importance
CFD	(Computational fluid dynamics) Calculation of fluid dynamics
CLF	Courant - Fridrichs Levi) Courant Number
DNS	(Direct Numerical Simulation) Direct numerical simulation method
EES	(Engineering Equation Solver) Software for technical calculations
LES	(Lagre Eddy Simulation) The method of large vortices
MFR	Moving Frame Rotation Rotates geometry
NT	Low-pressure turbine
OL	Circulation blade
RANS	(Reynolds Averaged Navier Stokes equations) Time-averaging method
RL	Distribution blade
RNG	(Re-Normalization Group)
SST	(Shear stress transport) Reynolds shear stress
ST	Medium pressure turbine
T1MW	Designation of an experimental turbine
VK	Input Confusor
VT	High pressure pipe
VVER	Water - water power reactor
VystK	Output channel
2D	Two-dimensional
3D	Three-dimensional

0. Introduction

This diploma thesis will deal with turbine steam flow, which is a very complex scientific discipline, which is not even fully understood at present. Previously, these tasks were computed by very complicated computational methods, which were often not solvable at all. These calculations could be replaced by practical experiments, but they were much more demanding, both economically and temporally. Progress in this area has been brought about by the development of computing technology, with which new possibilities for numerical simulation of current fields have been opened. This has created a new science discipline called CFD. However, it should be added that numerical computations can not replace real experiments on real machines, either in terms of the necessary structural simplifications on geometries, the imperfections of the computational network or the mathematical errors occurring in the calculation. However, they provide a very good idea of how a flowing medium is behaving or an easy comparison of different kinds of simulations.

The work will be developed in collaboration with Doosan Škoda Power's research and development department and its goal is to explain to the reader the process of 3D numerical calculation of the steam turbine stage from the creation of the basic geometry of the inverse model to the analysis of the results. It verifies the measurement results of the experimental triple-stage Boiler Feed Pump Turbines (BFPTs) T10MW. The work will be based on practical experiments that have already been carried out in the Doosan Škoda Power laboratory in Pilsen. It will endeavor to verify these experiments and justify any differences in the results.

The first chapter of the theoretical part will deal with the history and present of Doosan Škoda Power and its development department, for which the thesis is being processed.

The second chapter will deal with the theory of steam turbines in terms of equipment description, distribution, history, but especially with regard to their working process, with an emphasis on the transformation of energy in the individual types of turbine blade shifting.

The last chapter of the theoretical part of the thesis will provide information on turbulent flow theory. It will try to define and infer some basic equations of this non-stationary and complicated process. In addition, individual turbulence models used for numerical flow calculations will be described, eg in ANSYS Fluent.

The practical part of the diploma thesis will have two basic sections. The first part will deal with the 3D model of steam in last stage and diffuser will be done on the base of provided geometry and the 3D mesh of geometry of the experimental steam turbine T10MW.

The second part will describe the setting of CFD solver, calculation for at least two operational regimes with boundary conditions set on the base of experimental measurement.

Data postprocessing, comparison between measured and calculated data, determination of stage flow parameters, losses and outlet flow fields. Both chapters will consist of the geometry, computer network, boundary conditions, numerical calculation, and result analysis.

From both calculations, torque generated by the compressive force will be obtained. The difference in torques is the so-called loss moment, which is used to calculate the loss or friction power. There are a number of computational relationships for determining loss, friction, or ventilation performance. Some of these formulas are 20 to 30 years old, so it is the effort of this work to update these relationships and to make corrections of constants that may no longer be current due to the development of the construction of steam turbine blades.

The last chapter will include a plot showing the comparison of some important calculated parameters with the experimental data obtained by the measurements, as well as the assessment of any differences and a plot of General characteristic of low pressure turbine under variable flow showing the ventilation phenomena region.

How all these steps have been taken and, in particular, what the outcome will be assessed in the conclusion, see Chapter 5.

1. Doosan Škoda Power company

1.1 History

The diploma thesis is written in cooperation with Doosan Škoda Power, so it is necessary to write a few sentences about the history of this company.

Figure 1-1: Emil Škoda [2]

The beginning of the Škoda Company dates back to 1859, when Count Valdstejn founded a branch of its foundries and machinery in Plzen. In 1866 he joined the Emil Škoda factory as chief engineer and three years later he bought it in 1869. The first turbine was manufactured in Škoda's factories in 1904. It was equal to the 550 kW steam shaft steam turbine. Custom design of the Škoda turbine was achieved in 1911. The development and production of new machines helped to develop energy and industry in the period of the First Republic. The quality of production is demonstrated, for example, by two three-way condensing steam turbines with a unit capacity of 23 MW with steam heating installed in the Třebovice power plant. These machines were in operation until 1960.

During the Second World War, Škoda's factories were used for military purposes by the Third Reich, and in the raid in April 1945, over 70% of the factory was destroyed.

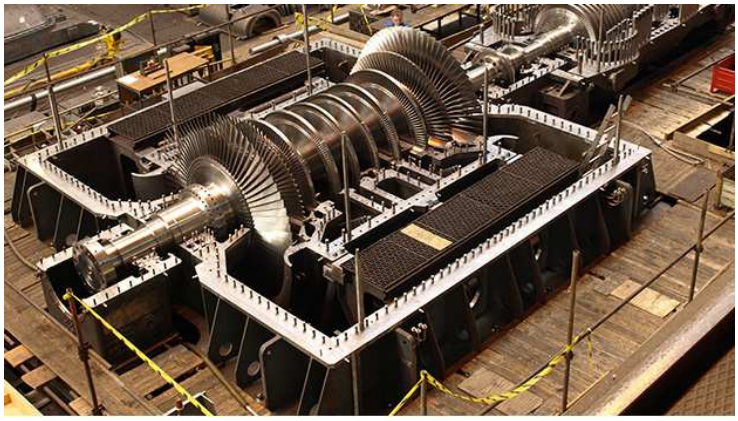

Figure 1-2: Steam Turbines for Nuclear Power Plants from Doosan Skoda [3]

During communism, the enterprise was nationalized, but production and development of new turbines did not cease. In 1969 a new turbine hall of impressive proportions was built, which allowed production to be concentrated together with research into one location. A great

success was a series of twenty-eight steam turbines of 220 MW. These machines were used to produce electricity in nuclear power plants with VVER type pressure reactors and the first was built in 1975. Another important milestone was a four-valve condensing steam turbine of 500 MW produced in 1976.

In 1991, a 1000 MW steam turbine was built on the output steam for nuclear power plants. This year's product range was also enriched by industrial high-speed turbines. However, with the onset of democracy, the period of privatization of the Škoda syndicate began.

Several subsidiaries were set up in 1993 and one of them was Škoda Turbíny. However, the subsequent merger of the subsidiaries in 1998 led to the renaming of Energo Škoda. However, this name lasted until 2004, when the name of the company changed to Škoda Power. For the next two years, ie in 2006, the transformation of Škoda Power s.r.o. to a joint stock company. However, the development did not continue on the technological side. In 2007, a steam turbine for the supercritical block at Ledvice Power Plant was built at 660 MW. In 2007 Doosan Škoda Power retrofitted high pressure components in two 1000 MW turbines at the Temelin nuclear power plant, Czech Republic, supporting safe, reliable and economical operation until at least 2042. Another important step was made in 2009, when Škoda Power became a subsidiary of Doosan Heavy Industries and Construction. In 2011, buildings and facilities were reconstructed in experimental laboratories. In 2012, the last important step has been to renaming the company to Doosan Škoda Power. [4], [5]

Figure 1-3: Logo development Doosan Škoda Power [4]

Nowadays Doosan Škoda Power develops high-temperature steam turbines for coal-fired power plants that meet strict emissions targets by operating at increasingly high temperatures (currently around 600–620 °C) using ultra-supercritical steam technology. Its nuclear power plant-optimised turbines handle enormous steam flow parameters and ensure resilience to water drop erosion at high temperatures. Turbines operate up to 1250 MW, ensuring that the pressure and expansion of individual components are maintained within normal parameters. [6]

1.2 Research and Development

Doosan Škoda Power has its own R & D department, which focuses primarily on improving the efficiency of energy conversion, an important step towards saving fuel and protecting the environment. In addition to developing its own steam turbine design, Doosan is dedicated to research into cogeneration units, refrigeration equipment and heat cycles using municipal waste and biomass as fuel. [4]

2. Theory of Boiler Feed Pump Turbines (BFPT) and steam turbines

2.1 Boiler Feed Pump Turbines (BFPTs)

The design of a boiler feed pump turbine features some unique characteristics that presents certain challenges in terms of efficiency management, varying operating ranges, and many other features. In order better understand the accepted designs of Boiler Feed Pump Turbines (BFPTs), it is important to know how the operation of steam turbines used to drive boiler feed pumps can fundamentally improve fossil and nuclear plants. Much like the design of mechanical drive turbines, feed pump turbines also feature the same thermodynamic objectives as the main turbine and all of the engineering difficulties with optimal blade design, rotor and bearing harmonic conditions, ideal flow path definitions, and so on. However, some distinctions can make a BFPT design particularly distinct from a regular mechanical drive turbine. Figures (2 - 1) shows a basic heat balance diagram for a plant using a boiler feed pump turbine arrangement.

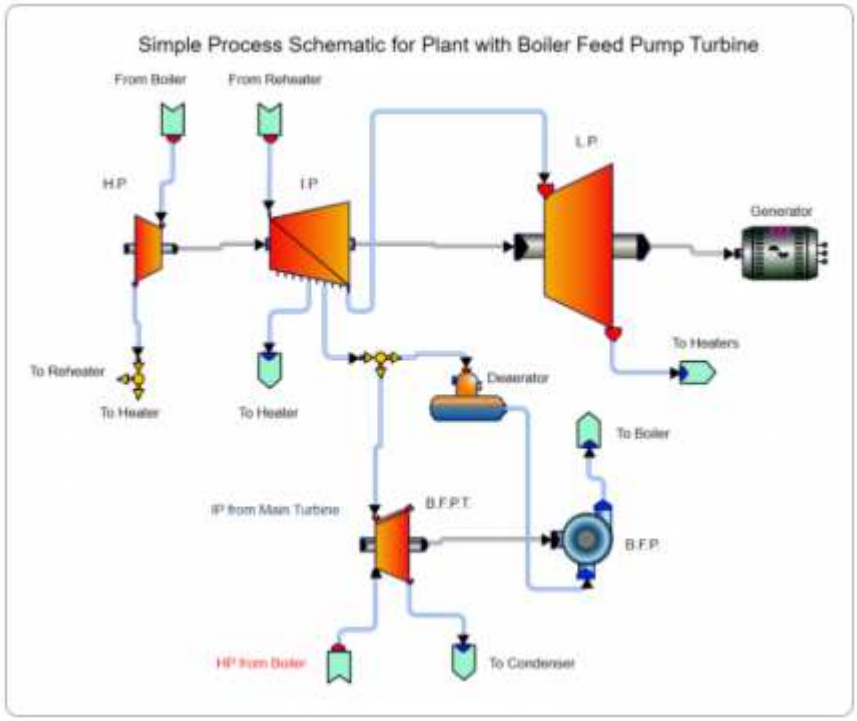

Figure 2-1: Simple Process Diagram for Plant with Boiler Feed Pump Turbine [1]

Inherent in its name, the BFPT must be fully compatible with the boiler feed pump. In other words, the necessary power and speed of the BFPT are determined by the requirements of the pump. In a fully integrated and dynamic system such as this, a large portion of the design requires developing a proper heat balance that will optimize the plant performance. In

general, the boiler feed pump turbine uses both steam from the boiler and the main turbine to drive the mechanical shaft connected to the boiler feed pump. This arrangement has proven highly successful in efficiently applying the steam's thermal energy throughout the plant. In certain arrangements, the BFPT can instead accept steam from cold reheat lines, main unit crossover piping lines, and different extractions from the main turbine. Regardless of the source, one distinction specifically unique to the BFPT is that it must accept steam from two separate sources.

In reference to schematic in Figure (2 – 1), the BFPT accepts steam at different pressures from both the boiler and the main turbine. The low-pressure steam extracted from the main turbine, generally between the high-pressure (HP) turbine and intermediate pressure (IP) turbine sections, will range from 75 psig to 250 psig. On the other hand, high-pressure steam directed from the boiler can reach pressures as high as 2400 psig, even 3500 psig in supercritical plants. The ability to utilize two vastly separate steam sources is made possible with the use of two separate inlet designs for the BFPT. The inlet designs for both the high pressure and the lower pressure sections of the BFPT consist of a series of valves driven by an actuator. The percentage in which each of these valve sections are open controls the different operating conditions of the plant. Three main operating points are considered for the feed pump turbine based on solely the lower pressure steam conditions coming from the main turbine. The conditions with these valves wide open (VWO), 40% of the main unit load (MUL), and the run out point (65% of MUL) all define the operating ranges of this section of the turbine. The range associated with each of these points allow the engineer to size the correct areas of the LP nozzles.

High-pressure steam from the boiler can be used to start the BFPT without using an auxiliary steam source. These start up requirements determine the nozzle sizing for the HP steam inlet section. As seen above, in order to achieve an optimal and efficient design for a BFPT, a number of different intermediate design points must be considered due to the expansive operating range that this particular turbine experiences. The analysis of different off-design curves becomes crucial in the design of boiler feed pump turbines and is a must for any engineers looking to improve their axial turbine design for boiler feed pump turbines.

2.2 Energy machines

Energy machines are devices that transform or modify energy or their wearers. It divides: [7]

- **Primary machines** (combustion engines, wind turbines) convert primary energy sources into a more noble form of energy.

- **Secondary machines** (steam turbines, compressors, pumps) convert the transformed form of energy into a different kind of energy.
- **Tertiary machines** (inverters, transformers, heat exchangers) modify parameters of the same kind of energy.

2.3 Steam turbines

Steam turbines are secondary energy machines in which the steam enthalpy is changed to the kinetic steam energy, and by partial braking on the rotor blades the mechanical energy of the turbine rotor is obtained.

Unlike steam engines that have large dimensions, they work at low speed and low efficiency; steam turbines are incomparably more efficient and more dynamic devices with high efficiency and great performance. [8]

2.4 History of steam turbines

The first device that may be classified as a reaction steam turbine was little more than a toy, the classic Aeolipile, described in the 1st century by Hero of Alexandria in Roman Egypt. In 1551, Taqi al-Din in Ottoman Egypt described a steam turbine with the practical application of rotating a spit. Steam turbines were also described by the Italian Giovanni Branca (1629) and John Wilkins in England (1648). The devices described by Taqi al-Din and Wilkins are today known as steam jacks. In 1672 an impulse steam turbine driven car was designed by Ferdinand Verbiest. A more modern version of this car was produced some time in the late 18th century by an unknown German mechanic. In 1775 at Soho James Watt designed a reaction turbine that was put to work there. In 1827 the Frenchmen Real and Pichon patented and constructed a compound impulse turbine. [10]

Figure 2-2: Aeolipile from Heron of Alexandria [9]

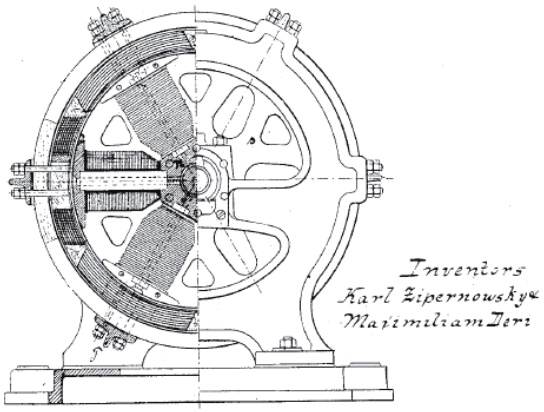

Figure 2-3: Dynamo Electric Machine [11]

The modern steam turbine was invented in 1884 by Sir Charles Parsons, whose first model was connected to a dynamo that

generated 7.5 kilowatts (10.1 hp) of electricity. The invention of Parsons' steam turbine made cheap and plentiful electricity possible and revolutionized marine transport and naval warfare. Parsons' design was a reaction type. His patent was licensed and the turbine scaled-up shortly after by an American, George Westinghouse. The Parsons turbine also turned out to be easy to scale up. Parsons had the satisfaction of seeing his invention adopted for all major world power stations, and the size of generators had increased from his first 7.5 kilowatts (10.1 hp) set up to units of 50,000 kilowatts (67,000 hp) capacity. Within Parson's lifetime, the generating capacity of a unit was scaled up by about 10,000 times, and the total output from turbo-generators constructed by his firm C. A. Parsons and Company and by their licensees, for land purposes alone, had exceeded thirty million horse-power. [10]

A number of other variations of turbines have been developed that work effectively with steam. The de Laval turbine (invented by Gustaf de Laval) accelerated the steam to full speed before running it against a turbine blade. De Laval's impulse turbine is simpler, less expensive and does not need to be pressure-proof. It can operate with any pressure of steam, but is considerably less efficient.[citation needed] Auguste Rateau developed a pressure compounded impulse turbine using the de Laval principle as early as 1896, obtained a US patent in 1903, and applied the turbine to a French torpedo boat in 1904. He taught at the École des mines de Saint-Étienne for a decade until 1897, and later founded a successful company that was incorporated into the Alstom firm after his death. One of the founders of the modern theory of steam and gas turbines was Aurel Stodola, a Slovak physicist and engineer and professor at the Swiss Polytechnical Institute (now ETH) in Zurich. His work Die Dampfturbinen und ihre Aussichten als Wärmekraftmaschinen (English: The Steam Turbine and its prospective use as a Heat Engine) was published in Berlin in 1903. A further book Dampf und Gas-Turbinen (English: Steam and Gas Turbines) was published in 1922.

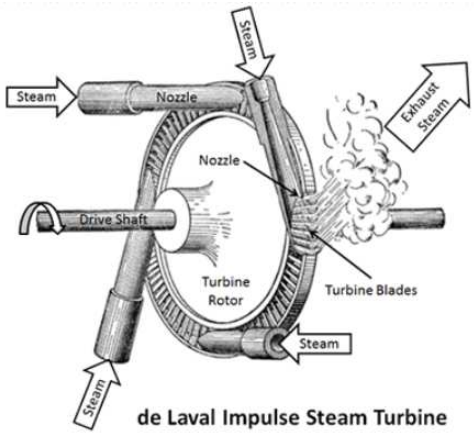

Figure 2-4: Laval Impulse Steam Turbine [11]

The Brown-Curtis turbine, an impulse type, which had been originally developed and patented by the U.S. company International Curtis Marine Turbine Company, was developed in the 1900s in conjunction with John Brown & Company. It was used in John Brown-engined merchant ships and warships, including liners and Royal Navy warships. [10]

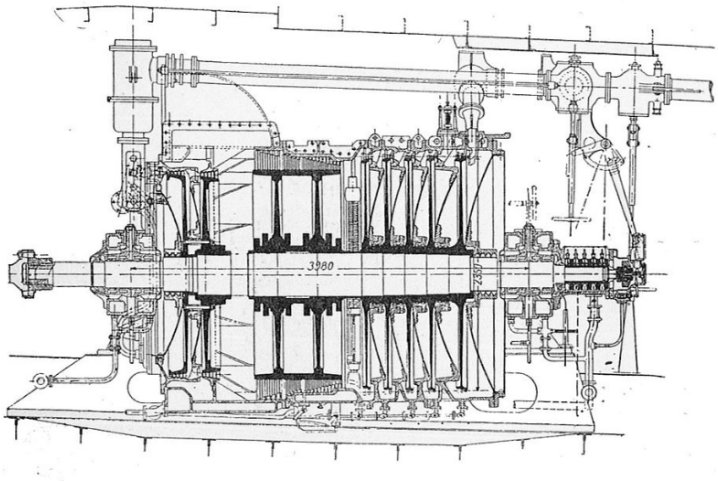

Figure 2-5*: Turbine Diagram of an AEG marine steam turbine 1905 [9]*

2.5 Division of steam turbines

Steam turbines can be divided into many aspects and parameters. The following subchapter will provide a comprehensive summary of how to divide. [8]

2.5.1 According to admission steam pressure

Depending on the admission pressure or inlet vapor, the turbines are divided:

- **Low pressure** - for pressures less than 2.5 MPa.
- **Medium pressure** - for pressures from 2.5 to 6.4 MPa.
- **High pressure** - for pressures greater than 6.4 MPa.

2.5.2 Depending on the type of blades

Division by type of blade is also called a division according to the principle of energy conversion. It is a turbine:

- **Equal-pressure (action)** - Expansion of steam occurs especially in the stator (distribution) part of the stage.
- **Overpressure (reaction)** - steam expansion takes place throughout the stage, both in the stator and the rotor.
- **Curtis wheels** - this is a special type of flat-bladed gear.

2.5.3 According to admission steam parameters

Depending on the admission or inlet vapor parameters, the turbines are divided:

- **With overheated admission steam** - this is a standard implementation of steam turbines eg for heating plants.
- **With saturated admission steam** - this is the implementation of steam turbines for nuclear power plants with pressurized water reactors.

2.5.4 Depending on the use of emission steam

Depending on the use of the emission or output vapor, the turbines are divided:

- **Condensing** - a condenser is placed behind the turbine, where the pressure is very low (about 6 kPa). Usual use eg in heating plants.
- **Backpressure** - turbine pressure is higher than barometric pressure. These turbines are mainly used where there is a great need for process steam.
- **The sampling** - backpressure and condensing turbines have nowadays implemented steam extraction for various purposes eg for regenerative water supply heaters, degasifiers or power pump drives.

2.5.5 Depending on the number of degrees

The basic construction element of the turbine is the stage (stator + rotor). Depending on the number of stages, steam turbines are distributed:

- **Single-stage** - All steam expansion takes place on one stage.
- **Multi Stage** - Expansion of steam takes place on several stages of the turbine.

2.5.6 According to the predominant direction of steam flow

Depending on the direction the steam flows through the device, the turbines are divided:

- **Axial** - steam flows parallel to the axis of rotation of the machine. This is 95% of today's steam turbines.
- **Radial** - steam flows perpendicular to the axis of rotation of the machine. These turbines are hardly seen today. They were manufactured at the 1st Brno machine shop.
- **Radial axial (centripetal)** - steam enters the turbine perpendicular to the axis of rotation and then extends parallel to the axis of rotation. Several of these turbines were produced by Škoda Turbíny.

2.5.7 Depending on the type of steam sampling

Depending on the type of steam sampling for different purposes, the turbines are divided:

- **With an unregulated take-off** - as the name says, the vapor pressure is not regulated for these steam take-offs. The sampling takes place at one or more locations of the turbine and these take-offs are used, for example, for regenerative water supply heaters.
- **With a controlled take-off** - the number of these withdrawals is limited because the steam goes out of the heat cycle system, such as heat for the consumer.

2.5.8 Depending on the number of turbine bodies

Depending on the number of bodies, turbines can be divided:

- **One - body** - these are primarily smaller types of turbines.
- **Multiple bodies** - Expansion takes place in several turbine bodies eg VT - ST - NT. Individual intercoolers or moisture separators can be placed between the units.

2.5.9 According to the turbine mobility

Based on mobility, we divide the turbines:

- **Mobile** - This type of turbine is mainly used on ships such as the Russian mobile nuclear power station with steam steam turbine.
- **Stationary** - fixed turbines eg in heating plants or plants.

2.6 The principle of work of steam turbines

The principle of steam turbine activity is the transformation of water vapor enthalpy into the mechanical energy of the rotor shaft of the turbine.

If the overpressure blade is used, the steam expansion in both the stator and the rotor takes place, that is, the entire stage. If the equipotential blade is used, expansion occurs only in the stator part of the turbine stage.

Expansion is a process in which pressure and temperature drop and, together with a specific volume, the flow rate of the flow medium increases. Thus, the enthalpy of the steam decreases with the pressure component and the kinetic energy of steam increases. In contact with circular blades, the kinetic energy is passed to the rotor and changes to mechanical energy, respectively turbine work.

Steam turbines are considered to be high-speed machines, so the water vapor molecule will run them very quickly and will not be able to pass on the heat of the turbine body. That is

why we consider the ideal working process of steam turbine expansion as an *isotropic process*.

Applying the previous knowledge of the change of heat to the formula $dq = 0\left[J \cdot kg^{-1}\right]$ of the second formulation of the first thermodynamic law (2.1), the equation of the technical work of the ideal isotropic process (2.3) will be obtained by mathematical modifications (2.2). What is the mechanical job of the turbine:

$$dq = dh - da_t = c_p \cdot dT - v \cdot dp \tag{2.1}$$

$$\begin{aligned} dq &= dh - da_t = c_p \cdot dT - v \cdot dp \\ dq &= 0 \\ da_t &= dh \\ da_t &= c_p \cdot dT \\ a_{t,ize} &= c_p \cdot (T_a - T_{e,ize}) \\ \underline{\underline{a_{t,ize}}} &= h_a - h_{e,ize}\left[J \cdot kg^{-1}\right] \end{aligned} \tag{2.2}$$

$$a_{t,ize} = \Delta h_{ize} = h_a - h_{e,ize}\left[J \cdot kg^{-1}\right] \tag{2.3}$$

Equation (3.3) is also called an isotropic enthalpy gradient $\Delta h_{ize}\left[J \cdot kg^{-1}\right]$.

However, as seen in Figure (2 – 6), in fact, the turbine is unable to process the ideal enthalpy gradient as losses occur. The actual enthalpy gradient is therefore $\Delta h\left[J \cdot kg^{-1}\right]$. Thanks to this knowledge it is possible to determine the internal thermodynamic efficiency of the turbine from equation (2.4).

$$\eta_{td} = \frac{a_t}{a_{t,ize}} = \frac{\Delta h}{\Delta h_{ize}} \frac{h_a - h_e}{h_a - h_{e,ize}}\left[-\right] \tag{2.4}$$

As can be seen from the foregoing knowledge, the larger the enthalpy gradient, the greater the work done by the turbine. However, it must be borne in mind that each stage of the turbine, ie the stator + rotor, is able to transform only a certain maximum enthalpy gradient. Therefore, because of the increase in efficiency, the turbines are built on several stages. [8]

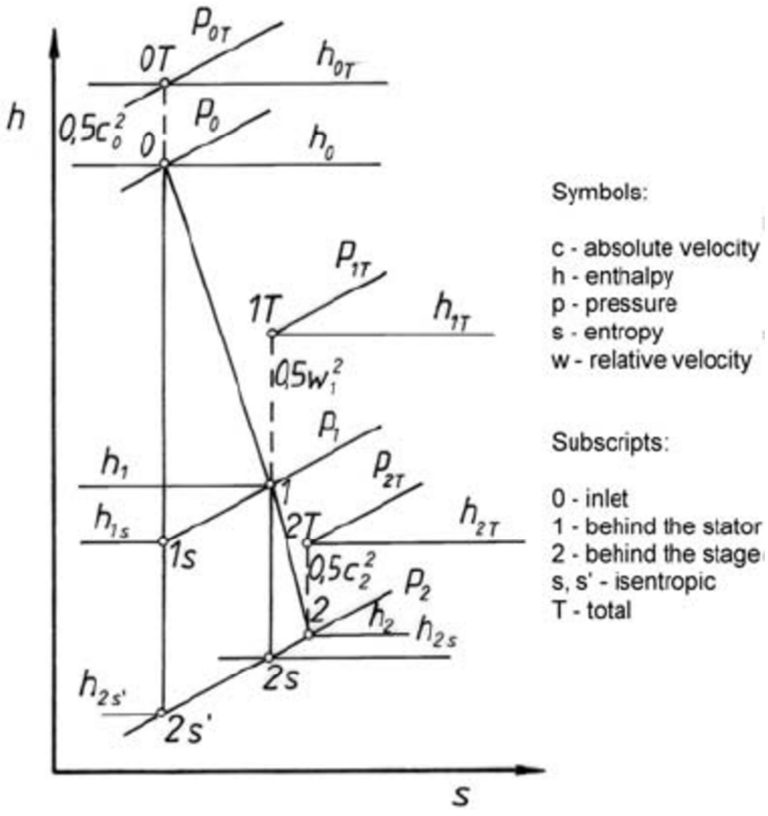

Figure 2-6: Enthalpy-entropy diagram for a turbine stage [13]

2.7 Energy transformation analysis of axial steam turbine

2.7.1 Pressure in axial stage

Axial steam turbines are nowadays more than 95% used in power and industry. Therefore, energy transformation analysis will be performed on the stage of the axial turbine.

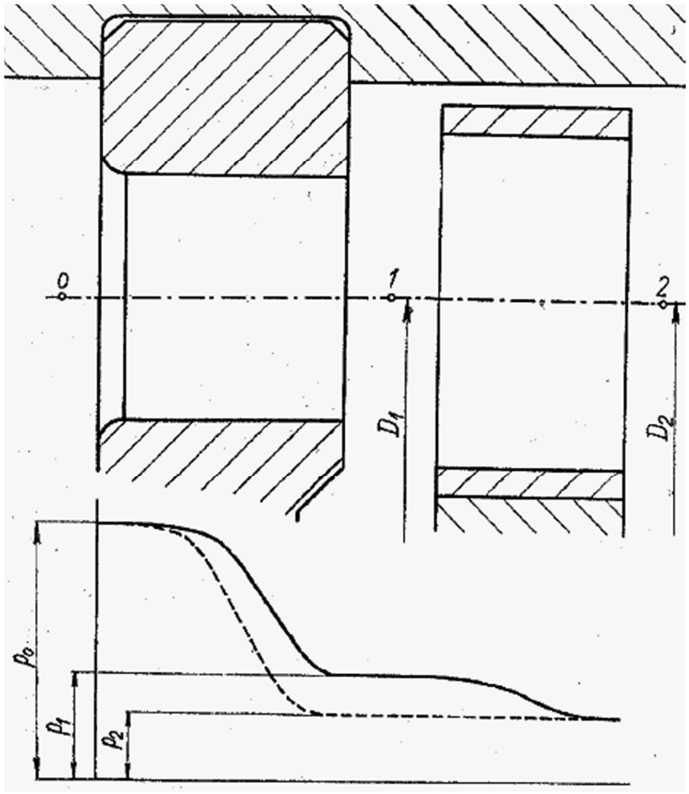

Figure 2-7: Degree of axial steam turbine, course of pressures [4]

In the figure above, you can see the distribution and circular blades in the cut. The graphical representation of the pressure pattern shows the expansion in the stage, and since the expansion takes place in both the stator and the rotor part, it is a pressure stage. [4]

2.7.2 Speed course in axial scale

The figure (2 - 8) is the same step but with the input and output speeds plotted. Since this is a plane vane grid, the circumferential velocity is the same for both the rotor and the stator and has a value u.

The steam enters the stator at absolute speed c'. *The shape of the stator blade copies the direction of the absolute velocity vector* c. Due to the expansion of the steam in the stator part the pressure drops and the absolute speed increases to the absolute velocity at the output of the stator c_{2S}, this speed is equal to the absolute speed at the input of the rotor c_1. In the rotor, however, the steam is in a relative environment, so there is a relative velocity w. From

knowledge of speed c_1 and u, you can draw a triangle and get a relative speed at the rotor inlet w_1.

The shape of the rotor blade copies the direction of the relative velocity vector w. There are two cases now.

If there is an equal degree, the expansion in the rotor is no longer running and the relative velocities are equal $w_1 = w_2$ or is the overpressure stage and then the relative speed at the inlet to the rotor is greater than the relative velocity at the outlet of the rotor $w_1 > w_2$. In any case, steam escapes from the rotor at relative speeds at the outlet of the rotor w_2 and by connecting to the peripheral speed u and the triangle representation gives the absolute speed at the rotor exit c_2, which is also the input speed to the next stage. [8]

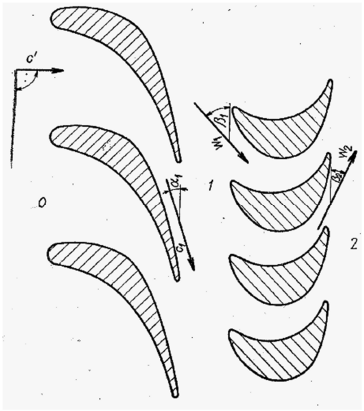

Figure 2-8: A flat bladed grid of the equal-stage stage of an axial steam turbine [4]

2.7.3 Speed triangles in axial scale

Figures (2 - 9) show the speed triangles of the above step. Absolute velocity at stator input c' has a value of approximately $20 \div 30 \left[m \cdot s^{-1}\right]$. Conversely, the absolute velocity at the output of the stator c_{2S} is very high. At pressurized levels, it is lower than the speed of sound, and in the case of equal degrees its value may exceed the speed of sound.

As previously mentioned, the circumferential velocities have a constant value in the plane blade grid $u = u_S = u_R$. Too high circumferential velocity could cause tearing of the blade hinges due to large centrifugal forces.

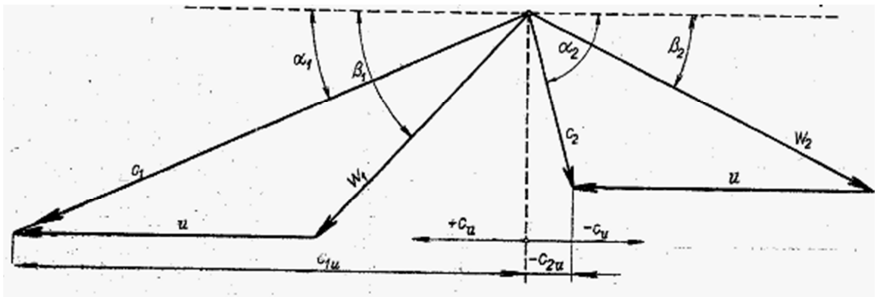

Figure 2-9: Speed triangles of equal-grade axial steam turbine [4]

More detailed descriptions of the above figures will be made in subchapters 2.7.3 and 2.7.4, which deal with the overpressure and equal blade of the turbine stages. [8]

2.7.4 Optimization of speeds and angles

It is also an attempt to optimize some angles to achieve better steam turbine parameters. E.g. angle α_1 is an effort to bring value as close as possible 0°. However, this is not realistic and in reality its size is around $\alpha_1 = 12° \div 16°$.

Also the absolute speed at the rotor outlet c_2 should be as small as possible. This speed is related to the angle $\alpha_2^{'} = 180° - \alpha_2 - \beta_2$, which connects vectors to velocity c_2 and u. This angle should be as close as possible to the value 90°. In practice, however, its value $\alpha_2^{'} = 180° - (80° \div 88°)$.

2.7.5 Euler's equation

The energy transformation in turbines is described by Euler's equation. To understand the function of Euler's equation correctly, you need to answer two basic questions.

2.7.5.1 What is the transformation of energy?

The answer is given by the equation of the second Newtonian law (2.5), the Law of Force, which reads:

"If a body acts on a force, then the body moves with an acceleration that is directly proportional to the applied force and inversely proportional to the weight of the body." [15]

More often this law is expressed as power F is equal to the momentum change of momentum p_{hyb}. This can be expressed by equation (2.5). Momentum p_{hyb} can be broken down as the product of the mass and the difference of the peripheral components of the absolute velocities Δc_u.

$$F = \frac{dp_{hyb}}{d\tau} = \frac{d(m \cdot \Delta c_u)}{d\tau} \left[N\right] \tag{2.5}$$

Adjusting the equation to the shape:

$$F \cdot \tau = m \cdot \Delta c_u \tag{2.6}$$

Several mathematical adjustments will now be made (2.7) to clarify the quantities of turbine energy transformations.

First, the equation is multiplied by the radius r. This will gain momentum M. The next step is to multiply the equation by the angular velocity ω. On the left side of the equation, then power is obtained P and the peripheral speed on the right side u. Will multiply performance further P time τ, work will be gained A. Then carry out the weight equation m, the labor value per kilogram of the working substance will be assigned a.

$$
\begin{aligned}
&F \cdot \tau = m \cdot \Delta c_u \quad /\cdot r \\
&F \cdot r \cdot \tau = m \cdot r \cdot (c_{1u} - c_{2u}) \\
&M \cdot \tau = m \cdot r \cdot (c_{1u} - c_{2u}) \quad /\cdot \omega \\
&M \cdot \omega \cdot \tau = m \cdot r \cdot \omega \cdot (c_{1u} - c_{2u}) \\
&P \cdot \tau = m \cdot u \cdot (c_{1u} - c_{2u}) \\
&A = m \cdot u \cdot (c_{1u} - c_{2u}) \quad /: m \\
&\underline{\underline{a = u \cdot (c_{1u} - c_{2u}) \left[J \cdot kg^{-1} \right]}}
\end{aligned}
$$

$$a = u \cdot (c_{1u} - c_{2u}) \left[J \cdot kg^{-1} \right] \tag{2.8}$$

The equation of the specific work is also called First expression of Euler's equation (2.8). What does this writing say about energy transformation? If the peripheral velocity is obtained, the equation (2.9) will be obtained.

$$u = \pi \cdot D \cdot n \left[m \cdot s^{-1} \right] \tag{2.9}$$

The steam turbine is an effort to get mechanical energy, work. Therefore, all the transformational processes lead to this work. Based on equations (2.8) and (2.9), it can be stated that the amount of work that can be discharged from the turbine depends on the rotor speed n, the dimensions of the blades represented here by the diameter D and the curvature of the current in the planar blade grid, represented here by the peripheral components of the absolute velocities c_{1u} a c_{2u}.

As mentioned in subchapter 2.6.4, it is an attempt to optimize some angles to certain ideal values. If an angle is then set $\alpha_2' = 90°$, the mathematical modification (2.10) of the equation of the *second expression of Euler equation* (2.11), which applies to axial machines, is obtained.

$$
\begin{aligned}
&c_{2u} = c_2 \cdot \cos \alpha_2' \\
&c_{2u} = c_2 \cdot \cos 90° \\
&\underline{\underline{c_{2u} = 0 \left[m \cdot s^{-1} \right]}}
\end{aligned}
\tag{2.10}
$$

$$a = u \cdot c_{1u} \left[J \cdot kg^{-1} \right] \tag{2.11}$$

2.7.5.2 In what parts and how does the energy transform?

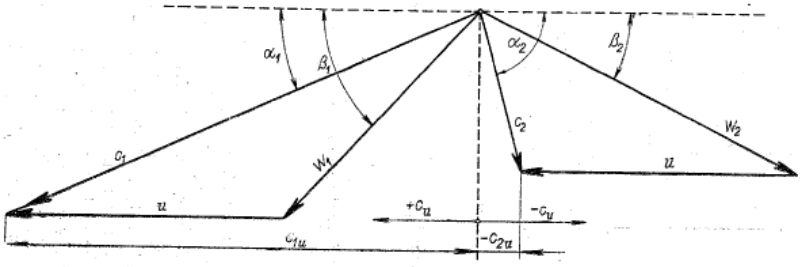

Figure 2-10: Speed triangles of equal-grade axial steam turbine [4]

Once again there is a picture of the speed triangles. Individual members in the velocity triangle can be mathematically replaced, for example, with the Kosin sentence (2.12), which allows you to calculate the angle in a triangle based on the knowledge of all three of its sides, or to calculate the triangle side based on the knowledge of the two sides and the angle between them. [19]

$$\begin{aligned} w_1^2 &= c_1^2 + u^2 - 2 \cdot c_1 \cdot u \cdot \cos\alpha_1 \\ \underline{w_2^2 &= c_2^2 + u^2 - 2 \cdot c_2 \cdot u \cdot \cos\alpha_2} \end{aligned}, \tag{2.12}$$

It is also possible to replace the other members of the right sides of the equations with the following modifications:

$$\begin{aligned} c_{1u} &= c_1 \cdot \cos\alpha_1 \\ c_{2u} &= c_2 \cdot \cos\alpha_2 \end{aligned}, \tag{2.13}$$

By setting the equation of the specific work (2.11) the equation of the maximum specificity of the steam turbine (3.14) can be obtained.

$$w_1^2 = c_1^2 + u^2 - 2 \cdot c_{1u} \cdot u$$

$$\underline{w_2^2 = c_2^2 + u^2 - 2 \cdot c_{2u} \cdot u}$$

$$c_{1u} = \frac{c_1^2 + u^2 - w_1^2}{2 \cdot u}$$

$$\underline{c_{2u} = \frac{c_2^2 + u^2 - w_2^2}{2 \cdot u}}$$

$$a = u \cdot (c_{1u} - c_{2u}) = u \cdot \left(\frac{c_1^2 + u^2 - w_1^2}{2 \cdot u} - \frac{c_2^2 + u^2 - w_2^2}{2 \cdot u} \right) = u \cdot \left(\frac{c_1^2 - c_2^2}{2 \cdot u} + \frac{w_2^2 - w_1^2}{2 \cdot u} + \frac{-u^2 + u^2}{2 \cdot u} \right) =$$

$$\underline{\underline{a = \frac{c_1^2 - c_2^2}{2} + \frac{w_2^2 - w_1^2}{2} \left[J \cdot kg^{-1} \right]}}$$

$$a = \frac{c_1^2 - c_2^2}{2} + \frac{w_2^2 - w_1^2}{2} \left[J \cdot kg^{-1} \right] \tag{2.14}$$

2.7.5.2.1 Stator energy transformation

From the formula of the second formulation of the first thermodynamic law (2.1) the equation of the total energy of the working medium is determined. There is no heat exchange with the surroundings $dq = 0$, stator stands, does not work so he is $da_t = 0$.

Thus, the enthalpy change occurs in the total energy equation (2.15) Δh_S, and since steam enters the stator at a certain velocity and also flows out at some other velocity, the equation also includes an increase in the kinetic energy in the stator $\frac{1}{2}\Delta c_S^2$. [4], [16]

$$dq = dh - da_t \quad \Rightarrow \quad dq = 0 \quad \Rightarrow \quad da_t = 0$$

$$\Delta h_{SC} = \Delta h_S + \frac{1}{2}\Delta c_S^2 \tag{2.15}$$

$$\begin{aligned} &\left(h_{1S} - h_{2S}\right) + \frac{1}{2}\left(c_{1S}^2 - c_{2S}^2\right) = 0 \\ &\underline{h_{1S} - h_{2S} = \frac{1}{2}\left(c_{2S}^2 - c_{1S}^2\right)} \end{aligned} \tag{2.16}$$

When the enthalpy drops, the absolute velocity of the stator output must increase c_{2S}^2. Therefore, it is a confirmation that the stator is expanding (2.16).

2.7.5.2.2 Energy transformation in the rotor

Here also, the equation of the second formula of the first thermodynamic law (2.1) determines the equation of the total energy of the working medium. There is no heat exchange with the surroundings $dq = 0$, but the rotor does work, so it's already here da_t.

Thus, in the equation of total energy (2.17) there is an enthalpy change Δh_R, and since steam enters the rotor at a certain speed and also exits with some other velocity, the equation also includes an increase in the kinetic energy in the rotor $\frac{1}{2}\Delta c^2$. [4], [16]

$$dq = dh - da_t \quad \Rightarrow \quad dq = 0$$

$$\Delta h_{RC} = \Delta h_R + \frac{1}{2}\Delta c^2 \tag{2.17}$$

$$\begin{aligned} &\Delta h_{RC} = \Delta a_t \\ &\Delta h_R + \frac{1}{2}\Delta c_R^2 = \Delta a_t \\ &\left(h_{1R} - h_{2R}\right) + \frac{c_1^2 - c_2^2}{2} = \frac{c_1^2 - c_2^2}{2} + \frac{w_2^2 - w_1^2}{2} \\ &\underline{h_{1R} - h_{2R} = \frac{w_2^2 - w_1^2}{2}} \end{aligned} \tag{2.18}$$

The Equation of Maximum Energy (2.14) is added to the equation of total energy (2.17). Mathematical modifications (2.18) show that all work is done from the turbine rotor.

2.8 Types of turbine blades

As mentioned in subchapter (3.4.2), there are two basic types of turbine blades and one special type designed for input stages to stabilize the steam flow.

The following subchapter deals with the description and mutual differences of these three types of blades. However, it is first necessary to define the concept of the *degree of reaction.*

2.8.1 Degree of reaction

It is a type of paddle type. It can be defined as the ratio of the entropic entropy of the rotor $\Delta h_{R,ize}$ to the iso-level gradient. $\Delta h_{ST,ize}$.

$$r = \frac{\Delta h_{R,ize}}{\Delta h_{S,ize} + \Delta h_{R,ize}} = \frac{\Delta h_{R,ize}}{\Delta h_{ST,ize}} [-] \qquad (2.19)$$

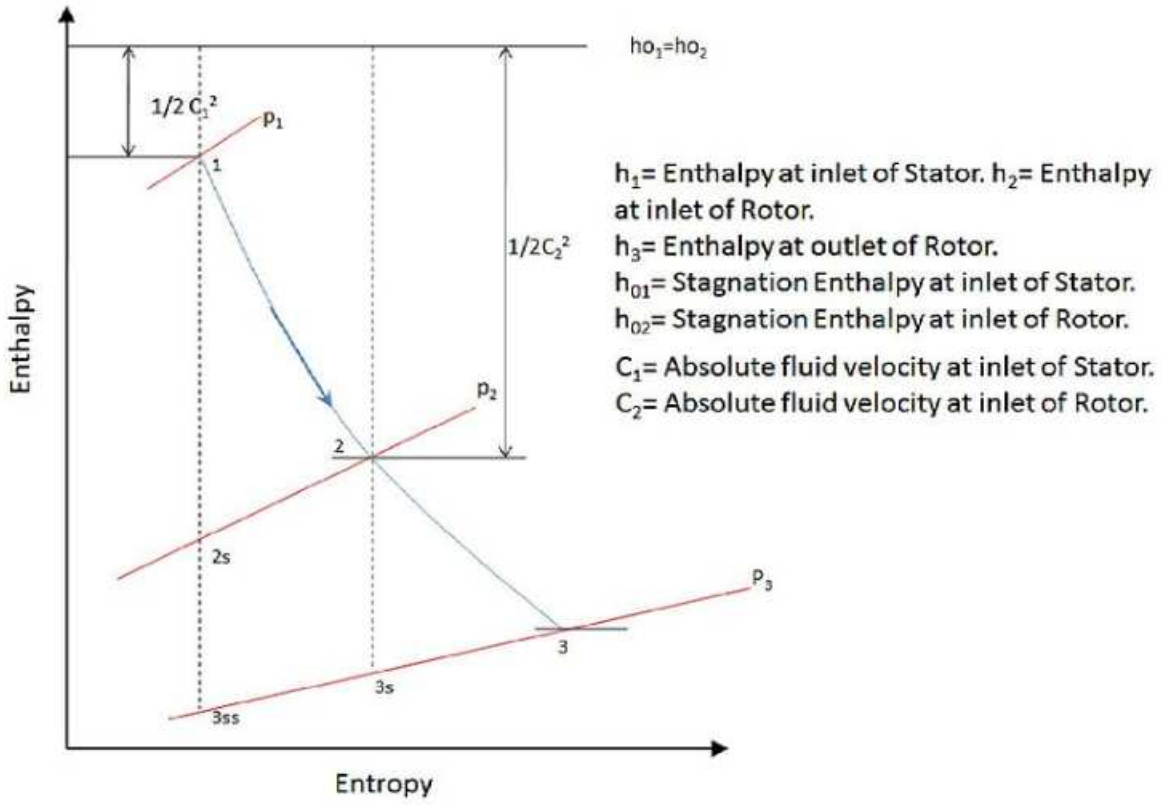

Figure 2-11: Enthalpy vs. Entropy diagram for stage flow in turbine [16]

In the reaction step $r = 0{,}5[-]$ it is an overpressure blade. In these stages the pressure in front of the circulating blades is greater than the pressure behind them. Number 0.5 indicates that about half the enthalpy gradient is processed in the stator part and half in the rotor part.

In the reaction step $r = 0[-]$ it is a flat-bladed blade because the pressure before and behind the run-up blades is the same and all the enthalpy gradient is processed in the distribution blades.

Nowadays, however, the turbines do not follow precisely these constants. There are turbines with a reaction rate of 0 to over 0.5. Even flat-bottomed turbines work with a little reaction, usually around 2 to 3% on the blade of the blades.

However, in order to simplify concepts in theory, we will continue to work with constants $r = 0[-]$ for equal blade and 0.5 for overpressure blade. [8]

2.8.2 Overpressure (reaction) stage

The overpressure reaction stage is characterized by long and slender blades. The shape of the blades is the same in the stator and rotor parts, which is advantageous in the design and manufacture of the blades.

The degree of reaction in any actual blade is always greater than 0. As has been said, ideally the reaction rate is equal to 0.5. This indicates the processing of the half of the enthalpy gradient on the stator and half of the enthalpy gradient on the rotor. The following inequalities of important variables (2.20), such as enthalpy, temperature, pressures and velocities, represent the expansion of steam in the rotor part.

$$\begin{aligned} &\Delta h_{R,ize} > 0 \\ &h_{1R} - h_{2R,ize} > 0 \\ &h_{1R} > h_{2R} \\ &c_p \cdot T_{1R} > c_p \cdot T_{2R,ize} \\ &T_{1R} > T_{2R,ize} \\ &p_{1R} > p_{2R,ize} \\ &w_2 > w_1 \end{aligned} \qquad (2.20)$$

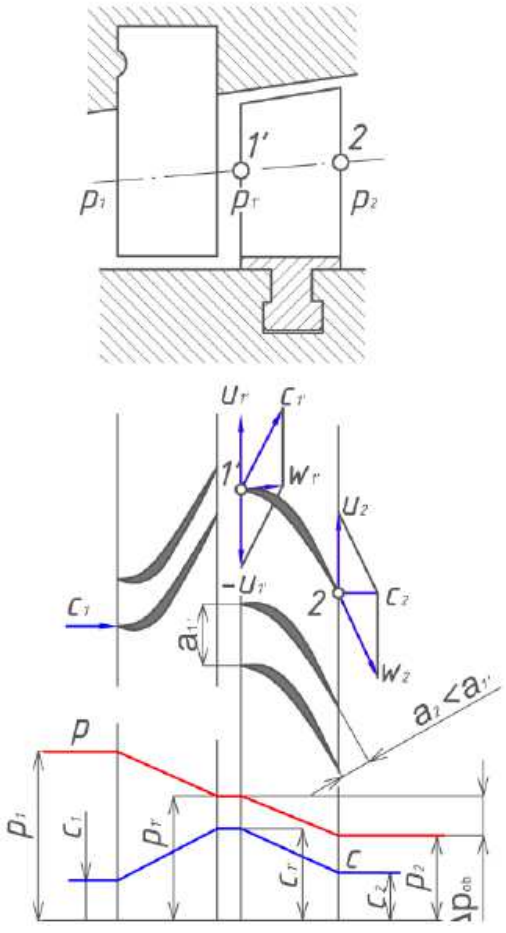

Figure 2-12: Cylindrical section of the overpressure and the course of pressures and speeds [17]

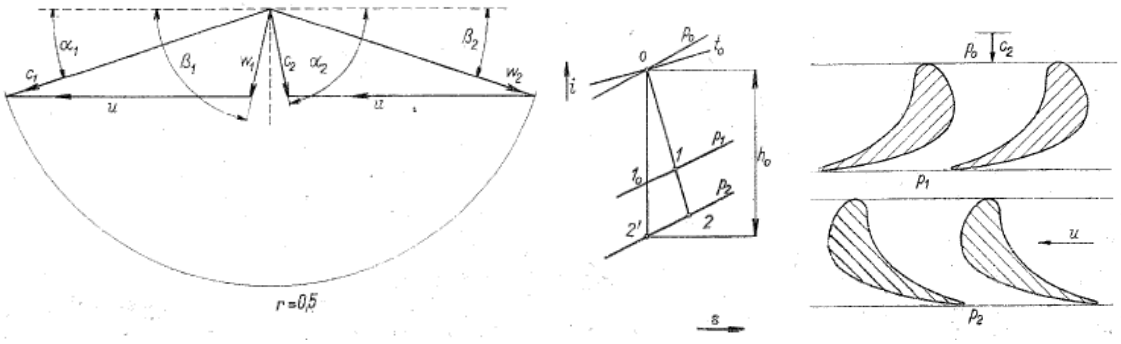

Figure 2-13: Speed triangles, h - with a diagram and cut with overpressure blades [4]

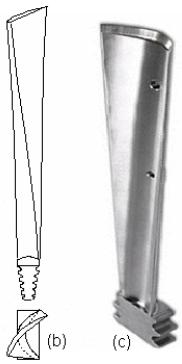

Figure 2-14: Overpressure blades [18]

The interplanar channel has, in both the stator and the rotor, the shape of a tapering nozzle. This shape ensures gradual expansion across the entire stage. It is also important to minimize the clearance between the distributor and circular blades to reduce the loss of steam from the ducts of the circulating blades.

This method of blowing the turbine is most often used in the last stages, because it processes well the small enthalpy gradients. However, due to the erosion of wet steam, these blades are made from the most expensive materials and therefore their price is very high. [8]

The following diagram shows how expansion works in the turbine overpressure.

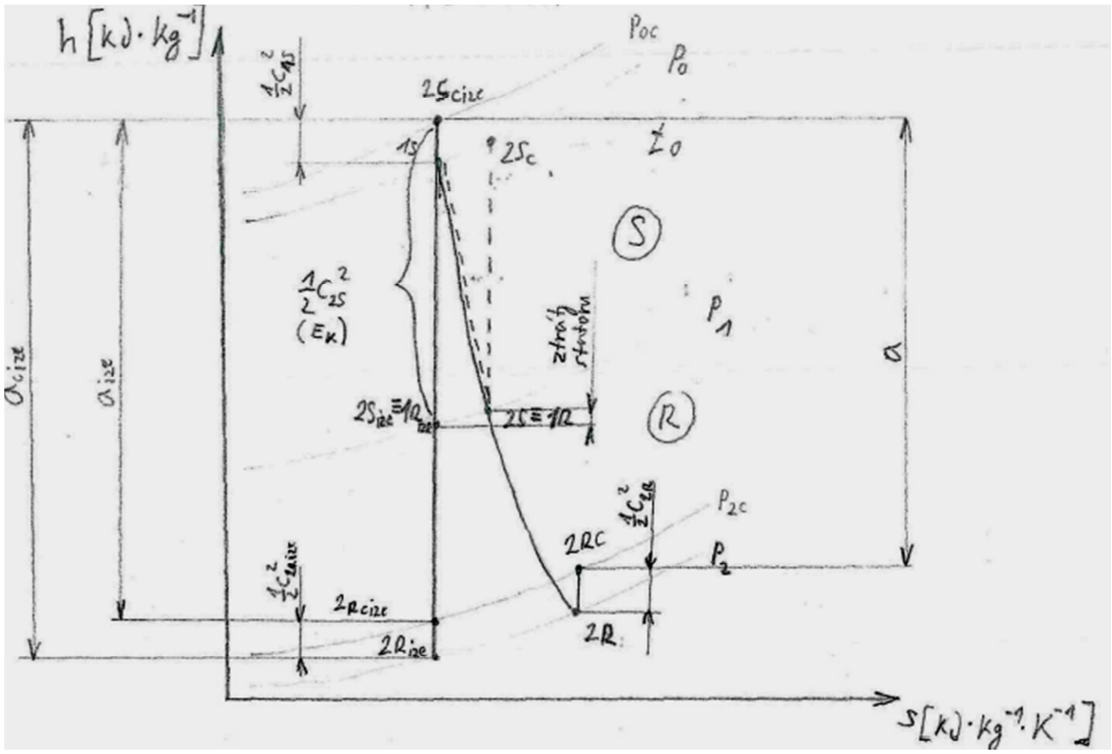

Figure 2-15: h - s steam expansion diagram in overpressure [4]

Mathematical adjustments (2.21) represent the calculation of the isotropic measurement work $a_{c,ize}$, which is equal to the total maximum enthalpy gradient in the degree $\Delta h_{ST,C,ize,\max}$. Which is equal to the total maximum This work can also be calculated as the product of the peripheral velocity and the absolute velocity at the input of the rotor c_1.

$$\begin{aligned} &\Delta h_{ST,C,ize,\max} = a_{c,ize} = u \cdot c_{1u} \\ &\alpha_1 = 0 \quad \Rightarrow \quad \cos\alpha_1 = 1 \quad \Rightarrow \quad c_{1u} = c_1 \\ &\underline{\underline{\Delta h_{ST,C,ize,\max} = a_{c,ize} = u \cdot c_1}} \left[J \cdot kg^{-1}\right] \end{aligned} \tag{2.21}$$

To compare the enthalpy gradient of each blade species, the peripheral speed will now be selected $u \doteq 280 \left[m \cdot s^{-1}\right]$.

The absolute speed at the rotor input has the magnitude of the approaching sound velocity $c_1 \leq a_{zvuk} \doteq 300 \left[m \cdot s^{-1}\right]$. Normally, however, its size varies from 260 to 280 $\left[m \cdot s^{-1}\right]$. Thus, it can be argued that the circumferential velocity is approximately the same as the absolute velocity at the rotor inlet $u \doteq c_1$. *The result of equation (2.22) is that the overpressure turbine stage is able to process the enthalpy gradient approximately equal to the quadratic angular velocity* u.

$$\begin{aligned} &u \doteq c_1 \doteq \sqrt{\Delta h_{ST,C,ize,\max}} \\ &\underline{\underline{\Delta h_{ST,C,ize,\max} \doteq u^2}} \end{aligned} \tag{2.22}$$

E.g. when both the circumferential and absolute velocity values of 280 $\left[m \cdot s^{-1}\right]$ are selected, an enthalpy gradient is obtained which is capable of processing one degree of overpressure turbine.

$$\begin{aligned} &\Delta h_{ST,C,ize,\max} = a_{c,ize} = u \cdot c_1 = u^2 = 280^2 = 78400 \\ &\underline{\underline{\Delta h_{ST,C,ize,\max} = 78400 \left[J \cdot kg^{-1}\right]}} \end{aligned} \tag{2.23}$$

The selected overpressure stage is capable of handling gradient $78400 \left[J \cdot kg^{-1}\right]$at maximum.

2.8.3 Equal (action) stage

Equal-action, action stage is characterized by short, massive blades wrapped around the circumference to protect against vibration and vibration.

The degree of action of the blade is ideally equal to 0. This indicates that the entire enthalpy gradient is processed on the distribution blades. The equations below (2.23) of important variables such as enthalpy, temperature, pressure and velocity confirm that there is no expansion in therotor.

$$\begin{aligned} \Delta h_R &= 0 \\ h_{1R} &= h_{2R} \\ T_{1R} &= T_{2R} \\ S_{1R} &= S_{2R} \\ p_{1R} &= p_{2R} \\ w_2 &= w_1 \end{aligned} \qquad \textbf{(2.23)}$$

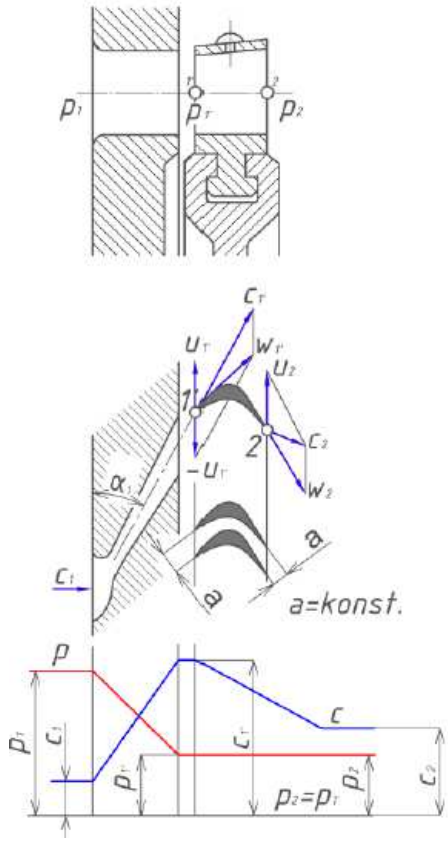

Figure 2-16: Cylindrical cross-section cylindrical section and the course of pressures and velocities [19]

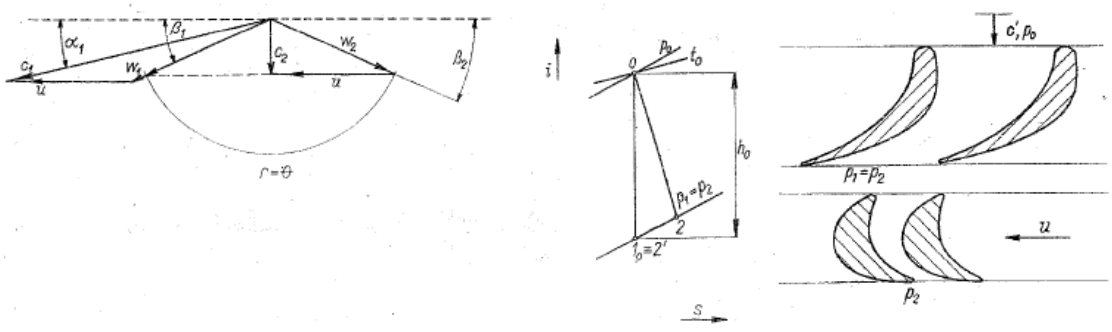

Figure 2-17: Speed triangles, h - s diagram, and cut with equal blades [4]

The interplanar channel of the distributor blades may be in the form of a convergent divergent nozzle or Laval nozzles. This also means that the absolute velocity at the output of the stator can be substantially greater than the speed of the sound $c_{2S} = c_1 > a_{zvuk} \approx 600\left[m \cdot s^{-1}\right]$ and in this case the so-called supercritical flow is achieved.

There is no expansion in the rotor and the pressure before and after the rotor is constant. This indicates that there is no loss of steam before and behind the impeller. For this reason, it is possible to maintain a relatively large clearance between the stator and the rotor.

The intersection cross section of the intersection channel in the rotor part is also constant throughout the blade length. There is no current curve or force effect. However, when the steam passes through the impeller, the absolute velocity decreases and thus a part of the kinetic energy is passed to the impeller. This method of paddling is used at the input stages because it is well tolerated by higher pressure loads and greater enthalpy gradients. [8]

The following diagram shows how the expansion in the equal-stage turbine stage looks.

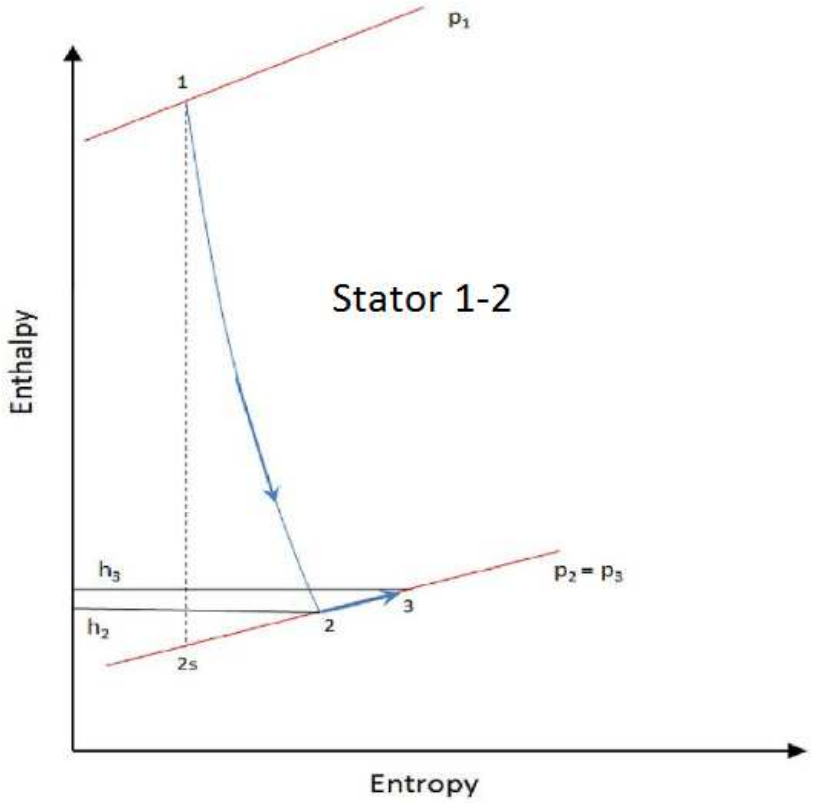

Figure 2-18: Steam expansion diagram in Equal Level [16]

From the velocity triangles of Figure (2 - 17), it follows that the peripheral component of the absolute velocity at the rotor inlet c_{1u} is approximately 2 times greater than the peripheral speed u. *The result of equation (2.24) is that the equipotential turbine stage is able to process the enthalpy drop approximately equal to twice the quadrant of the angular velocity* u.

$$c_1 \doteq 2 \cdot u \doteq \sqrt{2 \cdot \Delta h_{ST,C,ize,\max}}$$
$$\underline{\underline{\Delta h_{ST,C,ize,\max} \doteq 2 \cdot u^2}} \qquad (2.24)$$

E.g. if both the peripheral and absolute velocity values are selected 280 $\left[m \cdot s^{-1}\right]$ an enthalpy gradient is obtained that is capable of processing one stage of a flat-bladed turbine.

$$\Delta h_{ST,C,ize,\max} = a_{c,ize} = u \cdot c_1 = 2 \cdot u^2 = 2 \cdot 280^2 = 156800$$
$$\Delta h_{ST,C,ize,\max} = \underline{\underline{156800\left[J \cdot kg^{-1}\right]}} \tag{2.25}$$

The equal-degree selected in this way is able to maximally handle the gradient $156\,800\left[J \cdot kg^{-1}\right]$.

2.8.4 Curtis wheel

C - Wheel is a special type of flat-blade that is used to handle a large enthalpy gradient. It is installed in the inlet section of the steam turbines and is called the control stage because it serves to regulate and stabilize the steam flow before entering the next stages. The disadvantage of this blade is less efficient than the conventional flat or overpressure stage.

It consists of a stator part I and a rotor which has two (or three) wings of the impeller blades. In one stage, there are two rows of impellers II and IV on the rotor, and between them there are so called reversible blades III located in the stator housing, see Figure (2 - 19).

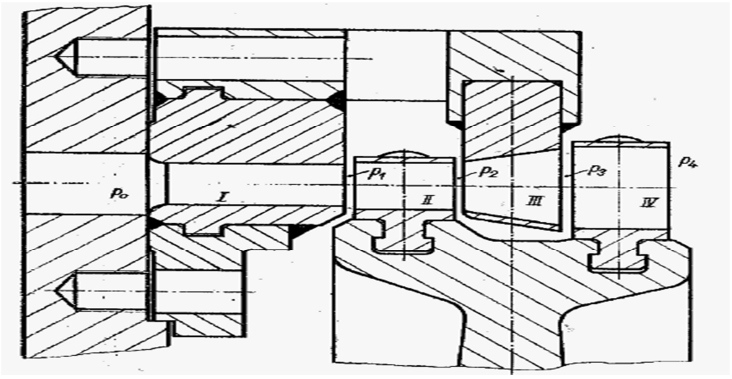

Figure 2-19: Cylindrical section Curtis [4]

Steam has a great absolute speed at the rotor exit after passing through the first ring of the orbital blades c_2, therefore it is brought into return blades in which only the absolute velocity vector is rotated and it goes into the next wreath. Curtis's level is usually a free space in which the current is settled and compared, and then the equal degrees are followed. [8]

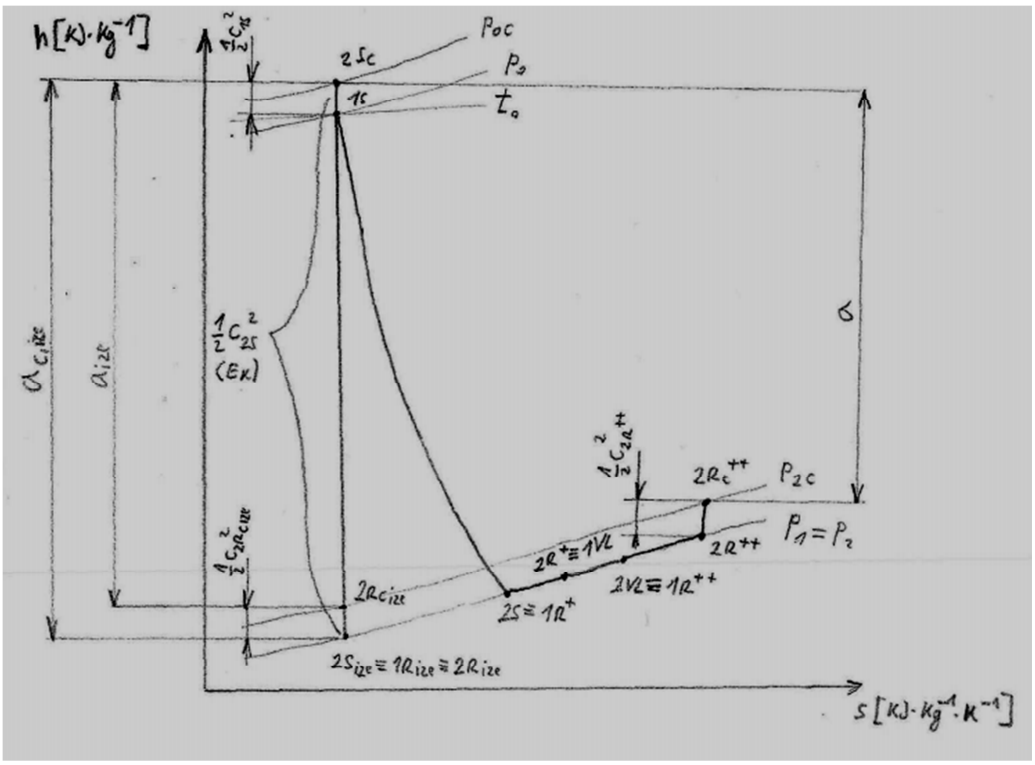

Figure 2-20: h - s steam expansion diagram C - round [4]

Assuming the angle $\alpha_1 \doteq 0°$ (near zero) and the absolute speed at the outlet of the second ring of the rotor blades c_4 it extends approximately parallel to the axis of rotation, i.e. $\alpha_4 \doteq 90°$. It can then be stated that the peripheral component of the absolute velocity at the inlet to the rotor is equal to the absolute velocity at the inlet to the rotor $c_{1u} = c_1$. Z it follows, as in previous cases, that the maximum enthalpy gradient and the specific work of the degree are equal to the product (2.26).

$$\Delta h_{ST,C,ize,\max} = \underline{\underline{a_{c,ize} = u \cdot c_1 \left[J \cdot kg^{-1}\right]}} \tag{2.26}$$

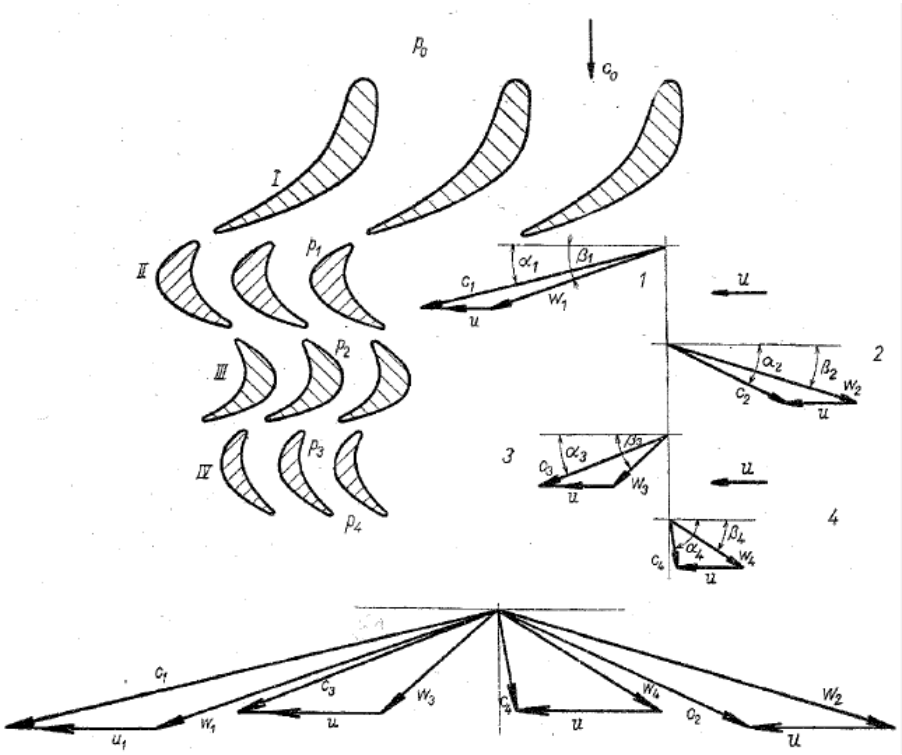

Figure 2-21: Plane paddle lattice and velocity triangles of Curtis degree [4]

From the velocity triangles in Figure (2 - 21) it follows that the peripheral component of the absolute velocity at the inlet to the rotor c_{1u} is approximately 4 times greater than circumferential speed u. *The result of Equation (2.27) is that the Curtis turbine stage is capable of processing an enthalpy gradient approximately equal to four times the square of the angular velocity* u.

$$c_1 \doteq 4 \cdot u \doteq \sqrt{4 \cdot \Delta h_{ST,C,ize,\max}}$$
$$\underline{\underline{\Delta h_{ST,C,ize,\max} \doteq 4 \cdot u^2}} \qquad (2.27)$$

E.g. if both circumferential and absolute velocity values are selected 280 $\left[m \cdot s^{-1}\right]$ it receives an enthalpy gradient that can handle one Curtis degree.

$$\Delta h_{ST,C,ize,\max} = a_{c,ize} = u \cdot c_1 = 4 \cdot u^2 = 4 \cdot 280^2 = 313600$$
$$\Delta h_{ST,C,ize,\max} = \underline{\underline{313600\left[J \cdot kg^{-1}\right]}} \qquad (2.28)$$

The Curtis degree chosen in this way is able to process the gradient at maximum $313600\left[J \cdot kg^{-1}\right]$.

2.8.5 Conclusion and comparison of blading

At the end of the above-mentioned subchapters, it can be stated that the turbine turbomachining can handle about two times the enthalpy gradient than the overpressure blading. This makes it possible to use a smaller number of stages and thereby reduce the cost

and size of the turbine, respectively, the rotor shaft. However, the overpressure blading is not so heavily stressed, it allows smoother pressure changes and also achieves greater efficiency. Equal-pressure padding has greater frictional losses, swirling and current tearing, so its efficiency is lower. Although Curtis's grade can handle a quadruple enthalpy gradient over the pressure stage, it has the lowest efficiency.

All three methods of blading have their advantages and disadvantages, so turbines most often consist of a combination of these steps. The Curtis stage is installed at the inlet and the equal-pressure paddle is installed, and overpressure bladed stages are performed on the outlet side.

Note: In the practical part of the thesis is used a special method of blading, which is neither equal pressure nor overpressure, but it is called blading with increased reaction.

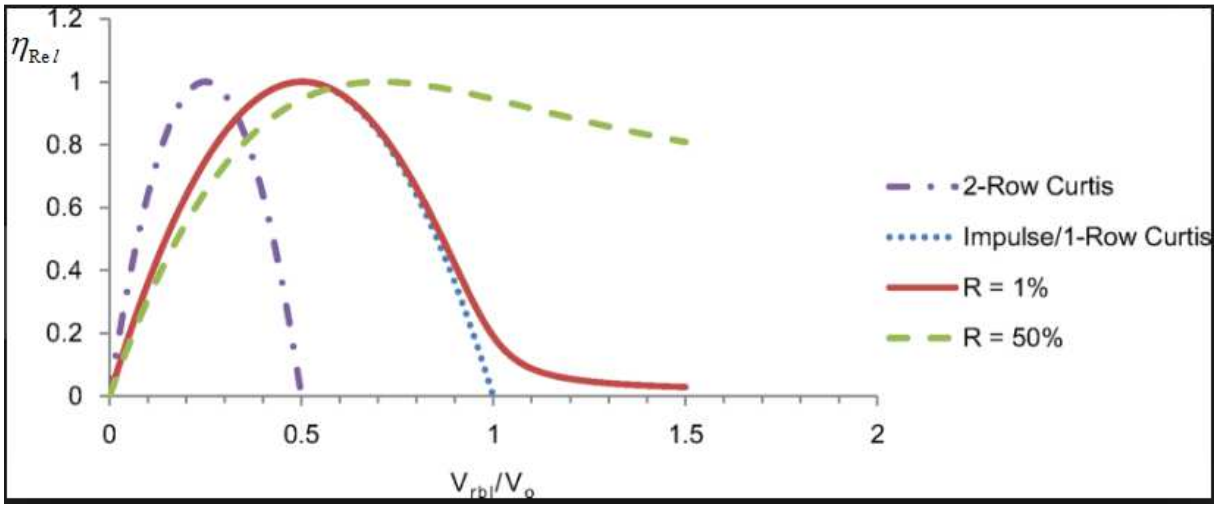

Figure 2-22: Dependence of relative stage efficiency with different type of blading to the ratio of circumferential speed to input absolute speed to the rotor [20]

3. The theory of turbulent flow

3.1 Introduction to Flow

There are two types of flow of real fluids, laminar or turbulent flow. The nature of the movement of the fluid particles determines the kind of matter.

If the velocity profile of the flow field is delimited by the mean velocity value, it is a laminar flow in which there is minimal mass and energy transfer between the fluid layers. Thus, laminar flow can be calculated by direct numerical simulation without the need to model equations.

In the next chapter, however, the turbulent flow will be mentioned, which can be defined as the non-stationary non-periodic movement of the fluid particles produced at higher flow rates. There is no more direct simulation here, since the increase in speed starts to increase the influence of inertia forces, which cause random streamlines, which then change their direction and size. Thus, turbulent flow is characterized by a complicated internal structure.

The so-called boundary layer is formed, which forms a laminar sublayer with a minimum thickness. As the name implies, there is a laminar flow. Behind the laminar sublayer lies a transition sublayer where current disturbances are already present and behind it there is a fully developed turbulent flow.

An example is shown in Figure (3 - 1). A thin plate that is flowed by a stream of fluid in which the pressure is constant throughout. As can be seen on the left side of the figure, the fluid velocity increases up to the free-flow rate. The zero speed of the plate is due to the viscosity. The boundary layer thickness is zero at the leading edge and its maximum size at the trailing edge. In the boundary layer, the streamlines do not have the shape of parallel lines but diverging curves. [8], [22]

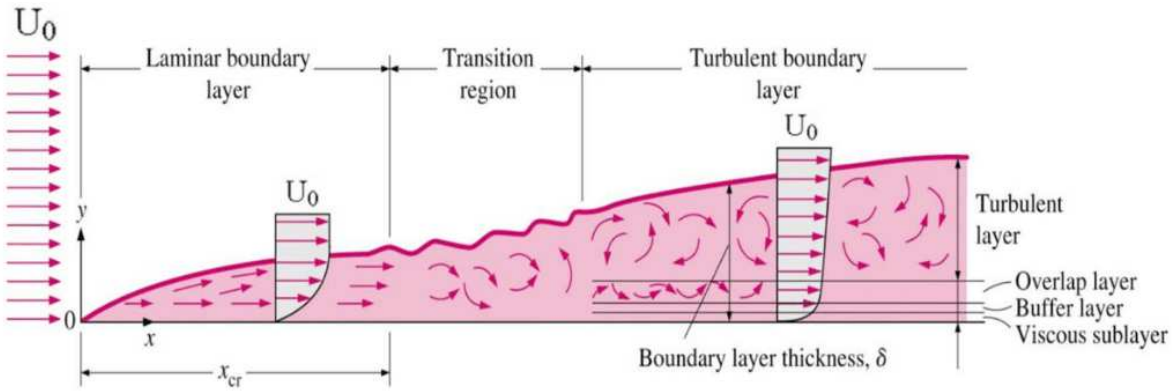

Figure 3-1: The boundary layer and sublayers [21]

3.2 Reynolds number

It is a dimensionless calculation criterion that determines the boundary between laminar and turbulent flow.

If one-dimensional flow in the pipeline is considered, the Reynolds number is calculated from the mean velocity in the pipeline $w_{k,s}\ [m \cdot s^{-1}]$, the inner diameter of the pipe $d\ [m]$ and kinematic viscosity $\nu\ [m^2 \cdot s^{-1}]$.

$$\mathrm{Re} = \frac{w_{k,s} \cdot d}{\nu}\ [-] \tag{3.1}$$

In this case, the critical value is $\mathrm{Re}_{krit} = 2230\ [-]$. It follows that it is $\mathrm{Re} \leq \mathrm{Re}_{krit}$ it is a laminar flow and if it is $\mathrm{Re} \geq \mathrm{Re}_{krit}$ it is a turbulent flow.

In the previous example of a slab flowed by parallel current, the Reynolds number is calculated from the free current velocity $w_{\infty}\ [m \cdot s^{-1}]$, distance from the leading edge $x_k\ [m]$ and kinematic viscosity $\nu\ [m^2 \cdot s^{-1}]$.

$$\mathrm{Re} = \frac{w_{\infty} \cdot x_k}{\nu}\ [-] \tag{3.2}$$

In this case the Reynolds number is critical $\mathrm{Re}_{krit} = 5 \cdot 10^5\ [-]$. [8]

Blade profiles have a characteristic dimension for calculating the Reynolds number of the blade.

3.3 Turbulent flow properties

3.3.1 Random movement

Turbulent flow is characterized by random movement of fluid particles. By fluid particle is meant a volume that contains a large number of fluid molecules. The random motion itself is composed of an ordered central motion and random fluctuations (Brownian motion).

Fluid molecules impinge on other molecules as they move, slowing down this impact and transferring some of their momentum to other molecules, which then accelerate. Thus, momentum is shared between layers of fluid at different speeds, and this is manifested by increasing resistance to the main flow direction. This is called *internal fluid friction*. [22]

3.3.2 Tangent Voltage

Tangential stress is due to fluid friction, velocity gradient, and fluid momentum change due to their penetration between adjacent layers. This unsteady movement is called *additional turbulent tension*. [22]

3.3.3 Turbulent viscosity

The kinematic viscosity of turbulent flow is no longer a constant, as was the case with the viscosity of laminar flow. It is now referred to as a function that depends on the state of the flowing fluid and the position of the point to which it is related. It therefore depends on the momentum sharing due to random fluctuations and the remoteness of the point from the wall. These assumptions depend on the velocity profile of the turbulent flow, whose shape is no longer parabolic, as in laminar flow, but it is flatter in nature. [22]

3.3.4 Diffuse nature of turbulence

Due to velocity gradients in fluctuations, viscous stresses and dissipations, or irreversible changes of one form of energy to another, arise. Due to the decrease in the kinetic energy of the turbulence, the internal energy of the fluid increases, therefore it is necessary to continuously supply energy to the system, if not, turbulence ceases and the speed and return to laminar flow is reduced. [22]

3.4 Turbulent flow

The general definition says that flow can be called turbulent, if its variables show chaotic and random fluctuations, both in space and in time.

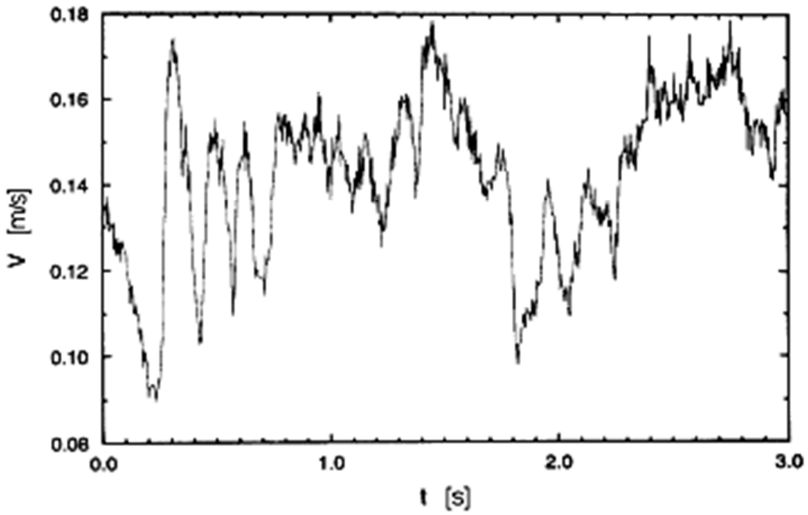

Figure 3-2: Speed-time dependence of fully developed turbulent flow [22]

The father of the first work on the theory of turbulent flow is Osborne Reynolds, who published it in 1883. He introduced the first equations that try to physically describe this flow. However, even today, this task is not completely resolved. Although chaos and nonlinear dynamic systems have made considerable progress, there is still no way to fully understand the nature of turbulence.

Turbulence occurs in many technical fields and their basic elements are turbulent beliefs.

3.4.1 Classification of turbulent flow based on time scales

Osborne Reynolds introduced the concept of Reynolds number, which has already been defined in subchapter 3.2. However, it is now appropriate to elaborate on this concept.

As already described in the chapter above, the Reynolds number is a dimensionless criterion dependent on the characteristic length dimension (scale) $l\,[m]$ and velocity of flowing fluid (velocity scale) $w_k\,[m\cdot s^{-1}]$. These terms will hereinafter be referred to as macroscale. Furthermore, the Reynolds number is inversely proportional to the dependent kinematic viscosity $\nu\,[m^2\cdot s^{-1}]$, which expresses the molecular properties of the flowing fluid.

$$\mathrm{Re}=\frac{w_k\cdot l}{\nu}\cdot\frac{l}{l}=\frac{w_k\cdot l^2}{\nu\cdot l}=\frac{l^2\cdot\frac{1}{\nu}}{l\cdot\frac{1}{w_k}}=\frac{\frac{l^2}{\nu}}{\frac{l}{w_k}}=\frac{T_\nu}{T_t}[-] \tag{3.3}$$

Mathematical modifications (3.3) represent the expression of Reynolds number as a ratio of the time scale of molecular diffusion $T_\nu\,[s]$ to time scale $T_t\,[s]$ indicating the transmission of turbulent vortices of the macroscale $l\,[m]$. Then it pays: [24]

- $T_\nu < T_t\ tj.\ \mathrm{Re}<1$ **Laminar flow.** Molecular diffusion marches predominate and turbulent vortices disintegrate.
- $T_\nu \approx T_t\ tj.\ \mathrm{Re}\approx 1$ **Transition state.** The laminar flow changes to turbulent beyond the critical Reynolds number. This flow is initially periodic, but the further increase in Reynolds number increases instability, decreases periodicity, and flows become turbulent.
- $T_\nu > T_t\ tj.\ \mathrm{Re}>1$ **Turbulent flow.** Turbulent beliefs persist. However, most of the flow meets the parameters of turbulent flow, although low parameters.
- $T_\nu >> T_t\ tj.\ \mathrm{Re}>>1$ **Fully developed turbulent flow.** It indicates that the effect of molecular diffusion is negligible due to the swirl dynamics. It can be stated that turbulent vortices are in this case almost non-viscous.

3.4.2 Dissipation rate

As mentioned in subchapter 3.3.4, dissipation is the irreversible change of one form of energy to another. These changes are important because turbulent vortexes lose their kinetic energy and change them to increase the enthalpy of the flowing medium. Thus, dissipation is the rate ratio $w_k \left[m \cdot s^{-1}\right]$ and macroscale $l\left[m\right]$. [22]

$$\varepsilon = \frac{w_k^{\ 3}}{l}\left[m^2 \cdot s^{-3}\right] \tag{3.4}$$

3.4.3 Kolmogorov scale

This is a micro-scale for better description of dissipation areas. It is determined by the relation of kinematic viscosity $\nu \left[m^2 \cdot s^{-1}\right]$ and dissipation $\varepsilon \left[m^2 \cdot s^{-3}\right]$.

$$\eta = \left(\frac{\nu^3}{\varepsilon}\right)^{\frac{1}{4}}\left[m\right] \tag{3.5}$$

Or it can also be determined from the length macroscale $l\left[m\right]$ and Reynolds numbers $\mathrm{Re}\left[-\right]$ from a relationship.

$$\frac{\eta}{l} = \mathrm{Re}^{-\frac{3}{4}} \Rightarrow \eta = \mathrm{Re}^{-\frac{3}{4}} \cdot l\left[m\right] \tag{3.6}$$

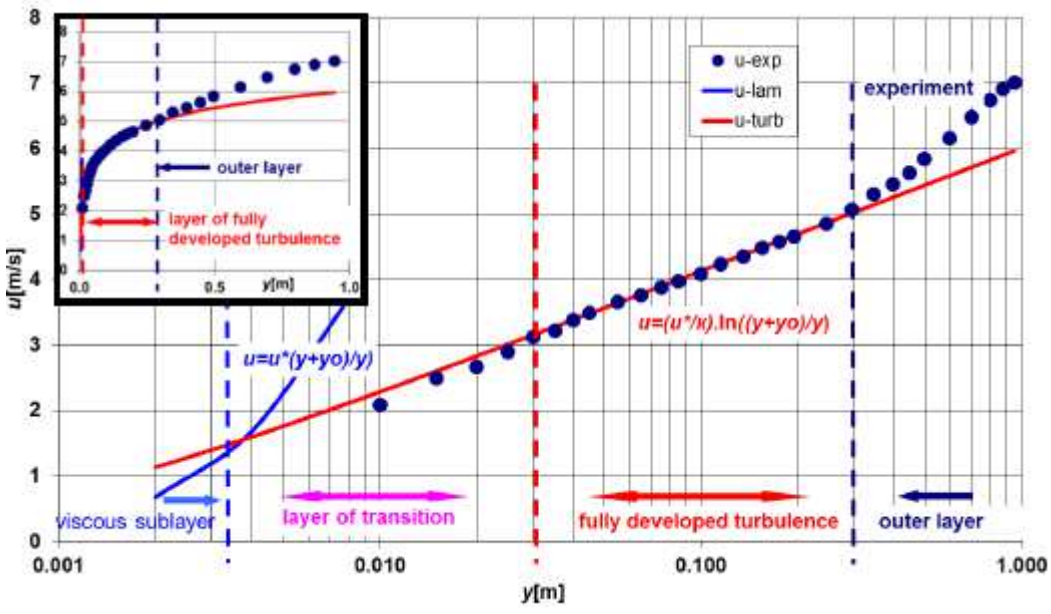

Figure 3-3: Distribution of layer near the wall - in linear and logarithmic coordinates [22]

In the above figure (3 - 3) you can see the difference in clarity of using decadic and logarithmic coordinates. [24]

3.4.4 Turbulent vortex splitting

The turbulent flow swirls have dimensions lying in the region of the microscale $\eta\,[m]$ up to the macro scale $l\,[m]$. Depending on the location, the beliefs are divided: [22]

- By the Wall:
  - Hairy beliefs – hairpin
  - Cracking – bursts
  - Strips – stress

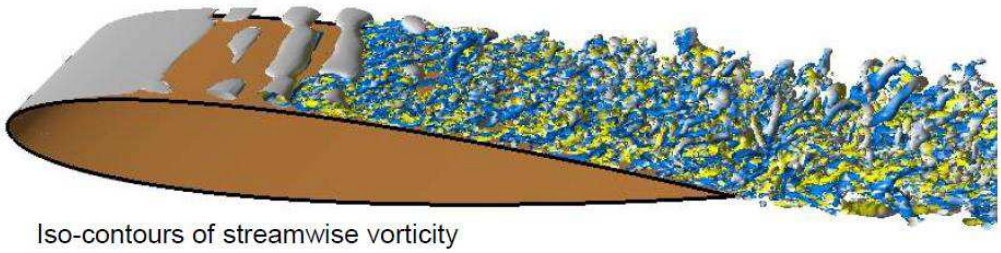

Figure 3-4: Development of turbulent flow on the wing [23]

3.4.5 Techniques of turbulent flow modeling

As mentioned in subchapter 3.4, there is not yet a clear physical model of the nature of turbulent flow. Therefore, three different theoretical approaches based on empirical findings in experiments or on practical applications that have been constructed using basic fluid flow equations are used. [22]

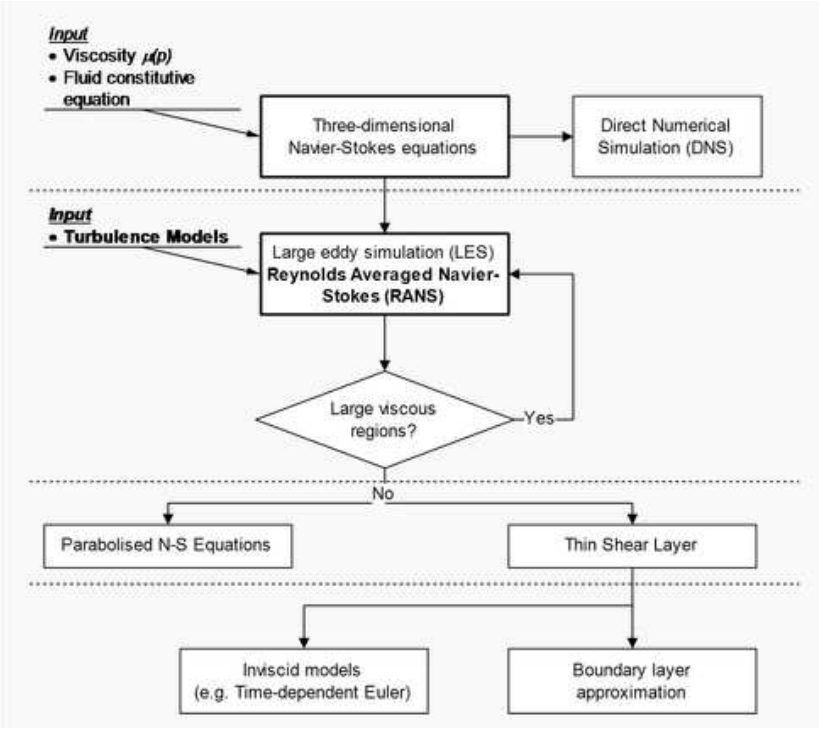

Figure 3-5: Block diagram of individual methods of mathematical modeling of turbulent flow [24]

.

3.4.6 DNS direct numerical simulation method

The advantage of the Direct Numerical Simulation (DNS) method is the ability to directly simulate turbulent flow in a particular task with high accuracy. The disadvantage of high calculation accuracy and very fine computing networks are the high demands on computer technology. The number of nodes for the DNS method can be estimated from the Kolmogorov micro scale, which shows the dimension of the smallest turbulent vortices, see subchapter 3.4.3. This means that the number of nodal points increases exponentially with the increase of Reynolds number. [22]

3.4.7 LES large vortex method

The large vortex method (LES - Lagre Eddy Simulation), based on spatial filtration methods, is based on the modeling of large vortices as spatial and time-dependent features that can be affected in a computing network. Large-scale turbulent beliefs deplete current by kinetic energy. Their influence is highly dependent on their location in the flow field and the time of occurrence. So they are modeled directly in three-dimensional and time-dependent shape. Small scale turbulent vortex structures induced by cascade energy transfer from large vortices are generally isotropic, meaning that they are very little involved in transport phenomena, but through which viscosities cause turbulent kinetic energy to dissipate to heat. Small vortices are parameterized by so-called subgrid models and removed by filtering the turbulent field. The computing complexity depends on the choice of filter bandwidth that corresponds to the network cell size. This implies the narrower band the finer the network and the higher the computing power, but the more accurate the calculation. [8] [22]

3.4.8 RANS Reynolds centering method RANS

Time centering method. RANS - Reynolds Averaged Navier Stokes equations are used to create static models of turbulent flow that are most commonly used in engineering practice. These static models are performed on the basis of time averaging of turbulent flow quantities and on the following time centering procedure of balance equations. [22]

3.4.9 Comparison of mathematical methods of turbulence modeling

In the Figure below (3 - 6) you can see the application of each of the above calculation methods to Figure (3 - 2). The most accurate, but the most complicated computing capacity is the DNS method.

The LES method achieves good quality results, but the computing power is also considerable. In contrast, the RANS method has a somewhat different approach to the problem. These are, at present, the best combination of quality and difficulty in calculation. Therefore, it is also the most widely used in practice. [8] [22]

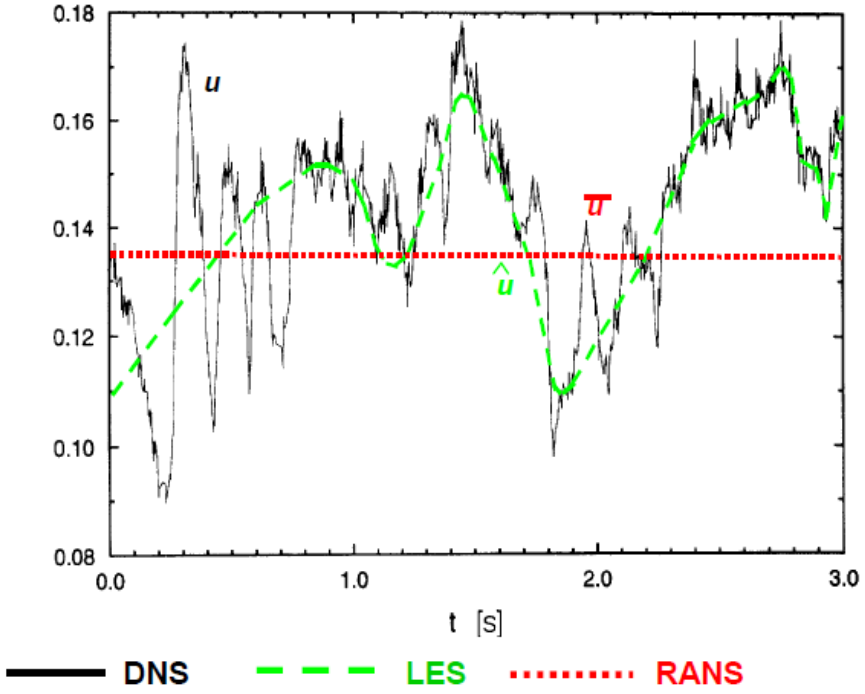

Figure 3-6: Mathematical methods of turbulent flow modeling [22]

3.5 Equations for Turbulent Flow Calculation

In the following subchapters, several equations will be derived that are used in mathematical calculations of turbulent flow. As the issue is quite extensive and complex, which is not the goal of this work, only a summary of the most basic information will be carried out.

In the beginning, it is necessary to determine what laws and equations are actually available for this issue. From the previous subchapters, it is assumed that at least:

- State equation
- Law of Conservation of Mass (Continuity Equation)
- Energy conservation law (energy equation)
- Law of Conservation of Momentum (Navier Stockes Equation, N - S Equation)

In the literature, these equations are often referred to only for laminar flow. However, turbulent flow is used here, so it is necessary to adjust these equations and introduce fluctuations (fluctuations) of the necessary variables.

You need to implement *Reynolds rules*.

3.5.1 Reynolds rules

Time centering is often a technically manageable task. The Reynolds rules, or rules on averaging, are applied to variables that can be broken down into a time-centered and fluctuating $a = \bar{a} + a'$ a $b = \bar{b} + b'$, with:

$$\overline{(a)} = \frac{1}{T}\int_0^T a \cdot d\tau = \overline{(\bar{a} + a')} = \overline{(\bar{a})} + \overline{a'} = \bar{a} + \overline{a'} \Rightarrow \bar{a}' = 0 \tag{3.7}$$

Thus, the following Reynolds rules apply to the quantities so written:

$$\begin{aligned}
&\overline{\bar{a}} = \bar{a} \\
&\overline{\bar{a} \cdot a'} = \overline{(\bar{a} \cdot a')} = \overline{\bar{a} \cdot a'} = 0 \\
&\overline{a + b} = \overline{(\bar{a} + a') + (\bar{b} + b')} = \overline{(\bar{a} + \bar{b}) + (a' + b')} = \overline{(\bar{a} + \bar{b})} + \overline{(a' + b')} = \bar{a} + \bar{b} \\
&\overline{a \cdot b} = \overline{(\bar{a} + a') \cdot (\bar{b} + b')} = \overline{(a \cdot b + a'b + a \cdot b' + a' \cdot b')} = \\
&= \overline{(\bar{a} \cdot \bar{b})} + \overline{(a' \cdot \bar{b})} + \overline{(\bar{a} \cdot b')} + \overline{(a' \cdot b')} = \overline{(\bar{a} \cdot \bar{b})} + \overline{(a' \cdot b')}
\end{aligned} \tag{3.8}$$

Where $\overline{a' \cdot b'}$ is a correlation moment that indicates the relationship between fluctuation components and is generally non-zero like $\overline{a'^2}, \overline{a' \cdot b'^2}, \overline{a'^2 \cdot b'^2}$. This property is typical of turbulence because, in other linear wave theories, non-linear members are often equal to zero. [24]

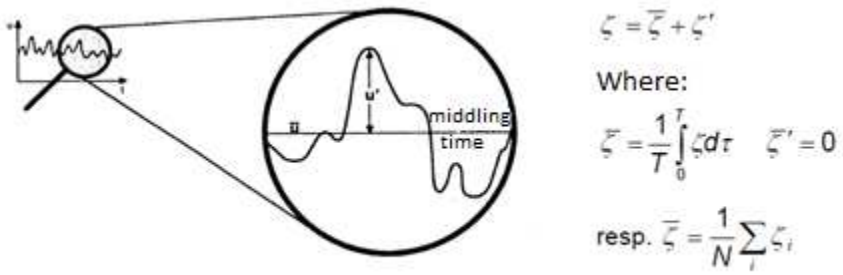

Figure 3-7: Fluctuation (irregular motion) and time centered part [22]

The above rules can be modified as shown in Figure (3 - 7) for further mathematical adjustments as follows:

$$\begin{aligned}
&\overline{\bar{\zeta}} = \bar{\zeta} \\
&\overline{\bar{\zeta} + \zeta'} = \overline{(\bar{\zeta} + \zeta')} = \bar{\zeta} + \overline{\zeta'} = \bar{\zeta} \\
&\overline{\bar{\zeta} \cdot \zeta'} = 0 \\
&\overline{\zeta + \psi} = \bar{\zeta} + \bar{\psi} \\
&\overline{\zeta \cdot \psi} = \bar{\zeta} \cdot \bar{\psi} + \overline{\zeta' \cdot \psi'} \\
&\frac{\overline{\delta\zeta}}{\delta X} = \frac{\delta\bar{\zeta}}{\delta X}
\end{aligned} \tag{3.9}$$

Where $\overline{\zeta' \cdot \psi'}$ is a correlation moment that indicates the relationship between fluctuation components. [24]

3.5.2 Equation of state

Here a state equation for real water vapor will be introduced. However, it should first be noted that the real gas state equation is very complex and therefore simplified and idealized in various ways. The equation (3.10) is based on the classical equation for ideal gas. However, it also contains elements that are a function of temperature a_0, a_1, a_2, a_3. These terms are calculated from empirical formulas that have been determined by experiments, see equation (3.11). For the purpose of this work, only a constant is needed a_0, therefore, the computational equations of the other constants are not given. [23]

$$p \cdot v = R \cdot T \cdot \left[a_0 + a_1 \cdot \left(\frac{p}{10^6} \right) + a_2 \cdot \left(\frac{p}{10^6} \right)^4 + a_3 \cdot \left(\frac{p}{10^6} \right)^{16} \right] \tag{3.10}$$

$$a_0 = \frac{0{,}11534}{\left(\frac{T}{100} \right)^2} + \frac{0{,}04381}{\left(\frac{T-210}{100} \right)^2} - 0{,}000539 \,[-] \tag{3.11}$$

Thus, the state equation for the real fluid is of the form:

$$p \cdot v = R \cdot T \cdot a_0 \tag{3.12}$$

3.5.3 Continuity Equation

Equation (3.13) represents a law of conservation of mass and, at the same time, a continuity equation for laminar flow in a general differential shape for a tube (without cross-section change). It is calculated from the fluid density $\rho \left[kg \cdot m^{-3} \right]$, from derivative $\frac{\delta}{\delta t}$ by time, speed of flowing fluid $w_k \left[m \cdot s^{-1} \right]$ and from turbulent kinetic energy $k_{tur} \left[m^2 \cdot s^{-2} \right]$.

$$\frac{\delta \rho}{\delta t} + \frac{\delta \rho \cdot w_k}{\delta k} = 0 \tag{3.13}$$

Now it is necessary to introduce fluctuations and center the given equation. A continuity equation is then obtained for compressible turbulent flow. [23]

$$\frac{\delta \overline{\rho}}{\delta t} + \frac{\delta \left(\overline{\rho} \cdot \overline{w}_k \right)}{\delta k} + \frac{\delta \overline{\left(\rho' \cdot w_k' \right)}}{\delta k} = 0 \tag{3.14}$$

3.5.4 Energy equation

Equation (3.15) represents the law of conservation of energy and simultaneously the energy equation for laminar flow in general differential form

$$\frac{\delta h}{\delta t}-\frac{1}{\rho}\cdot\frac{\delta p}{\delta t}=\frac{\tau_{kl}}{\rho}\cdot\frac{\delta w_k}{\delta l}-\frac{1}{\rho}\cdot\frac{\delta q_k}{\delta k}+\frac{q_V}{\rho} \tag{3.15}$$

Now it is necessary to introduce fluctuations and center the given equation. Then an energy equation is obtained for compressible turbulent flow. [23]

$$\begin{aligned} &c_p\frac{\delta\left(\overline{\rho}\cdot\overline{T}\right)}{\delta t}+\frac{\delta\left(\overline{\rho}\cdot\overline{w}_k\cdot\overline{T}\right)}{\delta k}-\left(\frac{\delta\overline{p}}{\delta t}+\overline{w}_k\cdot\frac{\delta\overline{p}}{\delta k}\right)=\overline{\tau}_{kl}\cdot\frac{\delta\overline{w}_k}{\delta l}-\frac{\delta\overline{q}_k}{\delta k}+q_V-\\ &-c_p\cdot\frac{\delta\left(\rho'\cdot T'\right)}{\delta t}-c_p\cdot\frac{\delta\left(\overline{j'_k\cdot T'}\right)}{\delta k}+\overline{w'_k\cdot\frac{\delta p'}{\delta k}}+\overline{\tau'_{kl}\cdot\frac{\delta w'_k}{\delta l}} \end{aligned} \tag{3.16}$$

3.5.5 Navier Stockes equation

An N-S equation in differential form with fluctuations introduced is considered:

$$\frac{\delta\left(\overline{u}_i+u'_i\right)}{\delta t}+\frac{\delta\left(\overline{u}_i+u'_i\right)\cdot\left(\overline{u}_j+u'_j\right)}{\delta X_j}=-\frac{1}{\rho}\cdot\frac{\delta\left(\overline{p}+p'\right)}{\delta X_i}+\nu\cdot\frac{\delta^2\left(\overline{u}_i+u'_i\right)}{\delta X_j^{\,2}}+f_i \tag{3.17}$$

It is supposed to be members $f_i=\overline{f}_i,\rho=\overline{\rho}$, it is then possible to write a Reynolds equation of motion, which is very similar to the N-S equation, but has an additional left-hand member.

$$\frac{\delta\overline{u}_i}{\delta t}+\frac{\delta\overline{u}_i\cdot\overline{u}_j}{\delta X_j}+\frac{\delta}{\delta X_j}\cdot\overline{u'_i\cdot u'_j}=-\frac{1}{\rho}\cdot\frac{\delta\overline{p}}{\delta X_i}+\nu\cdot\frac{\delta^2\overline{u}_i}{\delta X_j^{\,2}}+f_i \tag{3.18}$$

Rovnice pro fluktuační složky pak je:

$$\frac{\delta\left(u'_i\right)}{\delta t}+\frac{\delta\overline{u}_i\cdot u'_j}{\delta X_j}+\frac{\delta u'_i\cdot\overline{u}_j}{\delta X_j}+\frac{\delta\left(u'_i\cdot u'_j\right)}{\delta X_j}=-\frac{1}{\rho}\cdot\frac{\delta\left(p'\right)}{\delta X_i}+\nu\cdot\frac{\delta^2\left(u'_i\right)}{\delta X_j^{\,2}}+f_i \tag{3.19}$$

The Reynolds turbulent stresses are shaped $-\rho\overline{u'_i\cdot u'_j}$. Figure (3 - 8) shows the deformation effects of these stresses in turbulent flow. A cube represents a volume of fluid in which fluid of different speeds is mixed by vortex. [24]

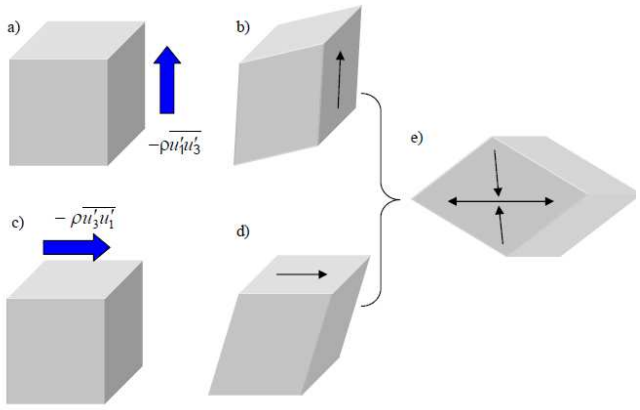

Figure 3-8: Deformation effects of Reynolds turbulent stresses [22]

3.5.6 Reynolds voltage

Starting from Figure (3 - 8), it is important to realize that there are a total of nine components of Reynolds stresses, in which symmetry applies, similarly to viscosity stresses.

$$\begin{bmatrix} \overline{u_1' \cdot u_1'} & \overline{u_1' \cdot u_2'} & \overline{u_1' \cdot u_3'} \\ \overline{u_2' \cdot u_1'} & \overline{u_2' \cdot u_2'} & \overline{u_2' \cdot u_3'} \\ \overline{u_3' \cdot u_1'} & \overline{u_3' \cdot u_2'} & \overline{u_3' \cdot u_3'} \end{bmatrix} = \begin{bmatrix} \overline{u_1' \cdot u_1'} & \overline{u_1' \cdot u_2'} & \overline{u_1' \cdot u_3'} \\ \overline{u_1' \cdot u_2'} & \overline{u_2' \cdot u_2'} & \overline{u_2' \cdot u_3'} \\ \overline{u_1' \cdot u_3'} & \overline{u_2' \cdot u_3'} & \overline{u_3' \cdot u_3'} \end{bmatrix} \tag{3.20}$$

In general, Reynolds stress generates a tensor or a generalized vector of nine members. There are six independent members. There is a problem here because a very complex system of six differential equations arises. Therefore, the effort is to simplify the Reynolds stress in *turbulence models.*

3.5.7 Boussinesqu's turbulent viscosity hypothesis

This hypothesis is the basis of turbulence models and describes the turbulence state by means of turbulent viscosity, which is expressed by the speed scale $u_{rych}\ [m \cdot s^{-1}]$ and length scale $l\ [m]$.

$$\mu_t \approx l \cdot u_{rych} \tag{3.21}$$

The analogy of Figure (3 - 9) between laminar and turbulent flow is assumed to be true. In laminar flow, Newton's equation applies to shear stress and turbulent flows are turbulent stresses and flows proportional to the mean velocity, temperature, and so forth.

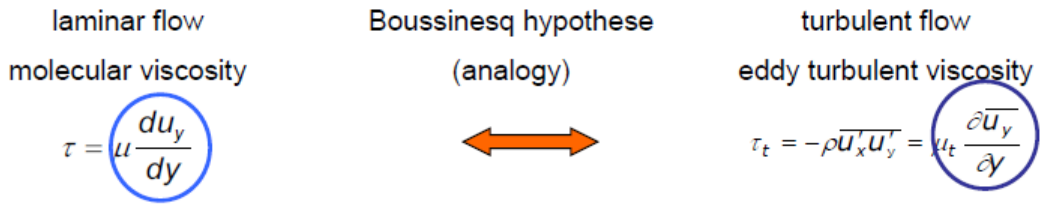

Figure 3-9: Boussinsqu's hypothesis [22]

Thus, turbulent kinetic energy is calculated as:

$$k_{tur} = \frac{1}{2} \cdot \overline{u'_j \cdot u'_j}$$
$$k_{tur} = \frac{1}{2} \cdot \sum_{j=1\ldots3} \overline{u'_j \cdot u'_j} = \frac{1}{2} \cdot \left(\overline{u'^2_1} + \overline{u'^2_2} + \overline{u'^2_3} \right) \tag{3.22}$$

It should be noted that turbulent viscosity is not a physical property of a fluid, but is a flow property. It depends largely on the value of turbulence and can vary considerably at different locations in the flow field.

Thus, if the Reynolds equation of motion (3.18) is adjusted to equation (3.23).

$$\frac{\delta \overline{u}_i}{\delta t} + \frac{\delta \overline{u}_i \cdot \overline{u}_j}{\delta X_j} = -\frac{1}{\rho} \cdot \frac{\delta \overline{p}}{\delta X_i} + \nu \cdot \frac{\delta^2 \overline{u}_i}{\delta X_j^2} + \nu_t \cdot \frac{\delta^2 \overline{u}_i}{\delta X_j^2} \cdot + f_i \tag{3.23}$$

Turbulence models are divided according to the number of complementary differential equations in terms of turbulent viscosity in the jet field:

- Non-algebraic models
- Single-equation models
- Two-equation models

Below is a summary of basic flow solutions with emphasis on turbulent solution methods and models that are used here.

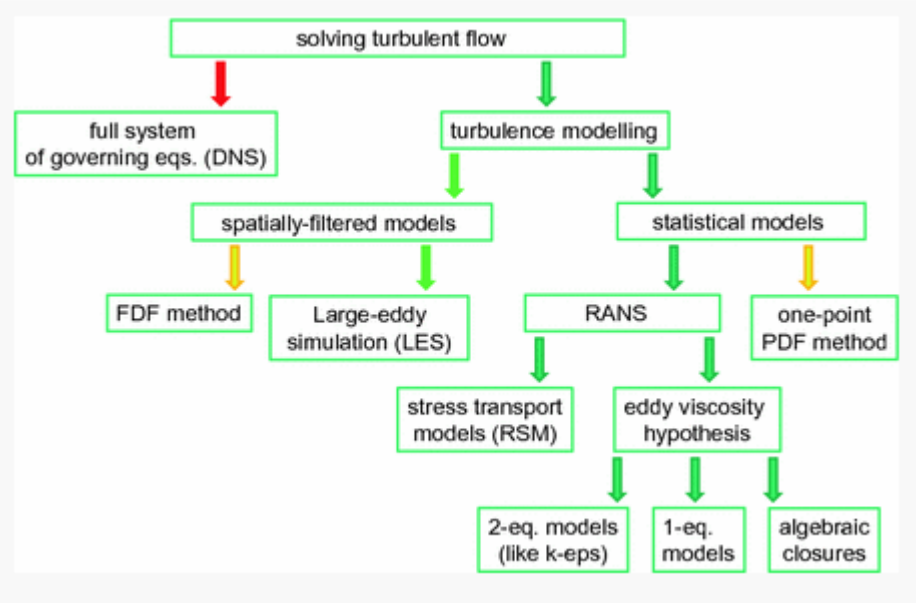

Figure 3-10: Block diagram of mathematical models of turbulence [25]

3.6 The most widely used turbulence models in Doosan Škoda Power

All of these models are used by Ansys FLUENT software, and each one is appropriate in a different situation.

3.6.1 Spalart - Allmaras turbulent model

It is a one-equation model created for aeropro-spatial tasks. The simulation is reliable and more and more popular because it can work on relatively rough computing networks with satisfactory results. Turbulent viscosity is calculated by direct solution of its transport equation. [22]

3.6.2 Turbulent model Standard K – ε

It is the most popular two-equation model and is used as a base model for further simulations. It contains the kinetic energy equation that is formed by subtracting the centered momentum equation from the undiluted equation. The second equation is the dissipation equation, which is based on the physical nature of the model. This model is used only for fully developed turbulent flow. [22]

3.6.3 Turbulent model RNG K – ε

This model is a superstructure of the standard turbulent model K - ε and its advantage is improved analysis of fast voltage currents and turbulence effects. Although this method is about one tenth slower than the Standard model, it is more accurate due to better analysis in the closing areas. [22]

3.6.4 Turbulent model SST, K - ω

This is a very popular two-equation model that will be used in this work. SST formulation solves calculations of tangential shear stresses a k - ω the formulation, in turn, allows the fluid to behave on the inner boundary layer. Therefore, this model is directly applicable to the entire flow range, from the laminar layer to the wall, the transition layer to the fully developed turbulent part of the stream.

3.7 Conclusion of flow theory

The conclusion of this chapter is that the theory of turbulent flow is an evolving scientific discipline and current knowledge of turbulence does not allow to create a clear and coherent model by which turbulence can be calculated. Therefore, several basic models and equations have been introduced that are used in models currently in use. As can be seen, it is an advanced mathematics containing systems of differential equations that are difficult to manipulate. However, these equations are implemented into computational programs such as ANSYS Fluent, and have been presented here for convenience only.

4. 3D numerical calculation of BFPT T10MW for current parameters

4.1 Introduction of the practical part of the thesis

In the practical part of the thesis, a three-dimensional numerical calculation of the complete T10MW experimental steam turbine will be performed. This turbine is equipped with blades derived from the third turbine stage of a BFPT.

Before the calculation itself, it is necessary to first create a volume of flowing steam. To do this, the models and blades drawings, input confuser and output channel drawings will be used.

The first chapter of the practical part deals with the numerical calculation of the degree for the specified current parameters, which correspond to the maximum efficiency of the stage. The value of maximum efficiency and other important parameters have already been determined by experiments carried out in the Doosan Škoda Power laboratory in Pilsen. The task of the diploma thesis will be first to verify by calculation whether these parameters correspond and evaluate any differences.

In the second part, the geometry created in the first section will be used to simulate many different conditions and with those results, create a plot power versus relative velocities and finding a range that occurs ventilation phenomena. Again, the results of the experiments will need to be verified.

The practical part will be described as a creation process from creating geometry to analyzing results. It will include comments on images, tables, or graphs.

Bellow can be seen pictures of the T10MW experimental steam turbine with 3 stages. The rotor consists of 48 blades and the stator 64 blades:

Figure 4-1: Real rotor and diffuser of 10MW BFPT [Custom Processing]

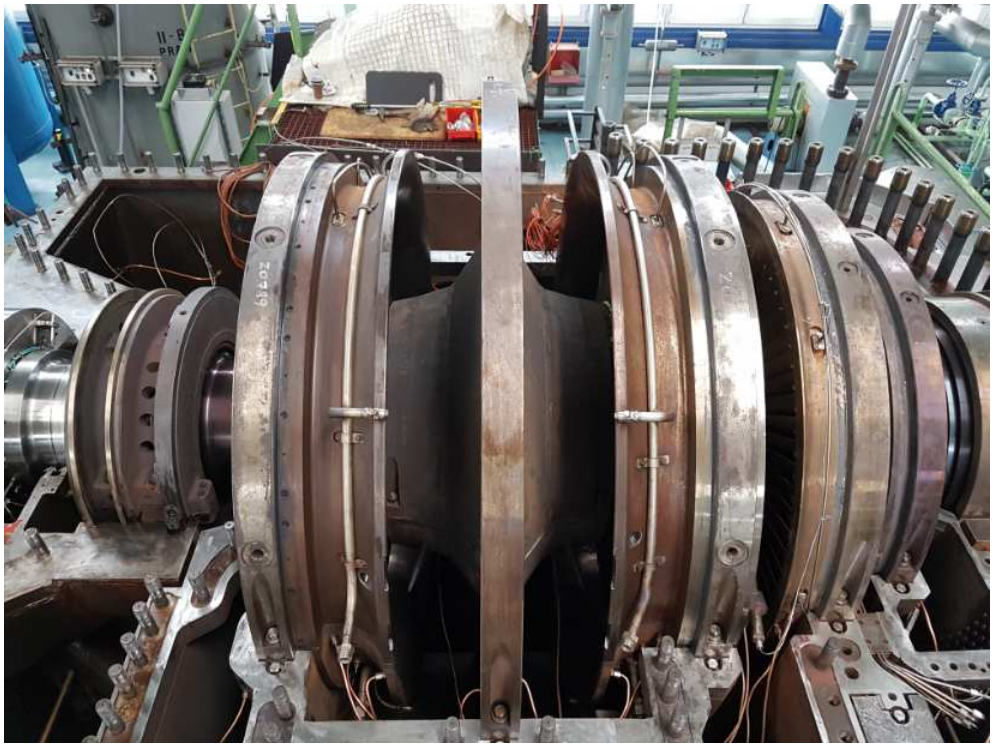

Figure 4-2: Real 10MW BFPT withot the upper casing [Custom Processing]

4.2 Resources of the thesis

Resources for the diploma thesis were provided by Doosan Škoda Power. These are models of blades, rotor and stator, of the examined steam turbine created in the Catia V5R21 modeling software. For the purpose of the thesis, they were first converted into formats suitable for Autodesk Inventor 2019.

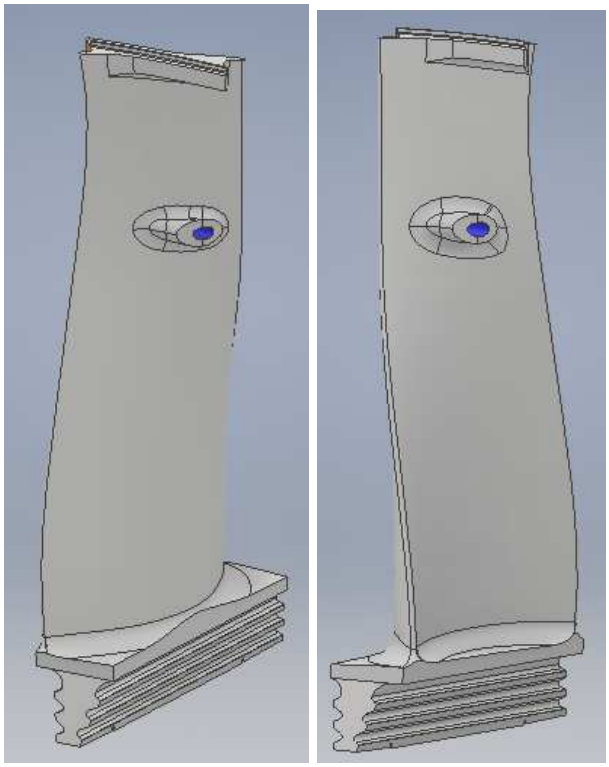

Figure 4-3: Isometric View of Switchgear and Rotor Blades Models [Custom Processing]

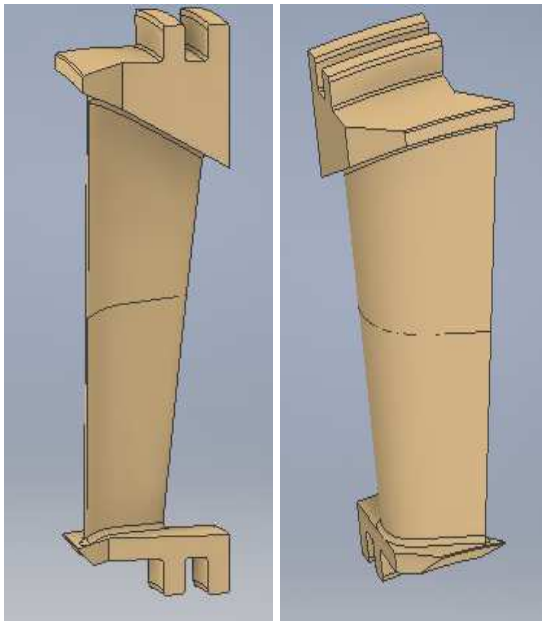

Figure 4-4: Isometric View of Switchgear and Stator Blades Models [Custom Processing]

However, the blades of Figure (4 - 3) are not suitable for computational operations in ANSYS CFX because their geometry includes the radius at the heel and at the vanes vane as well as at the head of the blade. Although the results of calculating such blades are more accurate, the complexity of the network and the more time consumed by such calculations make it possible to use rather modified (simplified) geometry of the blades in practice.

It was therefore necessary to remove the radiuses directly in Catia, where the blades were originally formed. The move itself was very simple. All you had to do was delete the object in the browser tree. The modified blades of Figure (4 - 5) are already suitable.

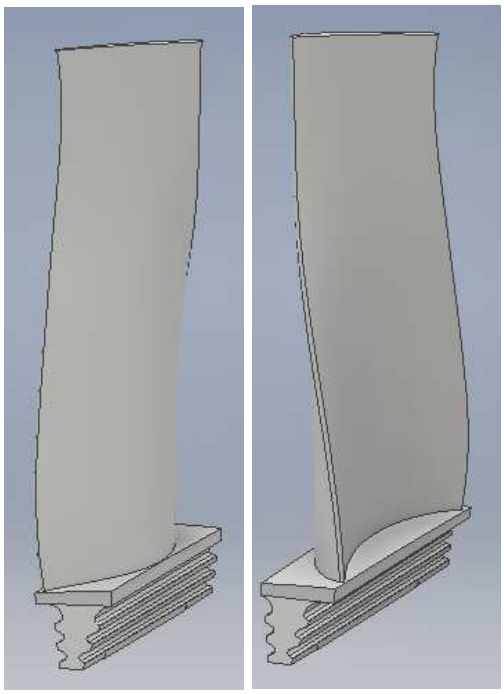

Figure 4-5: Isometric View of Distribution and Rotor Blade Models without Radius and vane [Custom Processing]

In the end the Doosan Škoda Power provided the simplified stator and rotor blades in .turbogrid format that could be imported on TurboGrid and create the mesh for stator and rotor chanels. However the diffuser it was created in Autodesk Inventor 2019 according the dimetions required. Nevertheless the diffuser outlet was extended for avoid backflow and give more stability for the calculations and the diffuser was simplificated. The recommendations of extended are ten time the width.

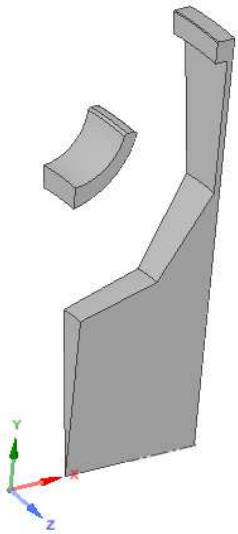

Figure 4-6: Isometric View of Distribution of original diffuser [Custom Processing]

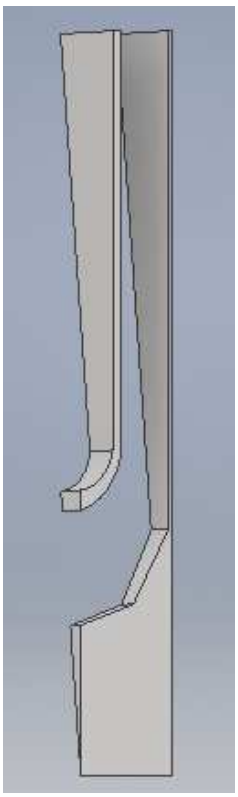

Figure 4-7: Isometric View of Distribution and extended and simplificaded diffuser [Custom Processing]

4.3 Creating the geometry of the steam volume in the inter-channel

The vapor volumes in the inter-channels were created for Turbo mode in CFX-Pre that is a specialist mode enabling you to set up turbomachinery simulations, such as compressors or turbines, in a simple manner. Each component of a rotating machine can be simply defined by selecting a mesh file and some basic parameters and then the boundary conditions and interfaces between the components are automatically generated. In addition to the quick setup, existing turbomachinery simulations can be easily modified to use alternative meshes or to add extra components with minimum effort. Turbo mode is designed to complement ANSYS TurboGrid but supports all the common mesh file formats that are supported in the general mode.

In a design process you may first want to construct the individual cases in order to check the flow around each individual component. Next you might want to analyze some of the "stator-rotor" portions of the machine. With it the flow vapor was created.

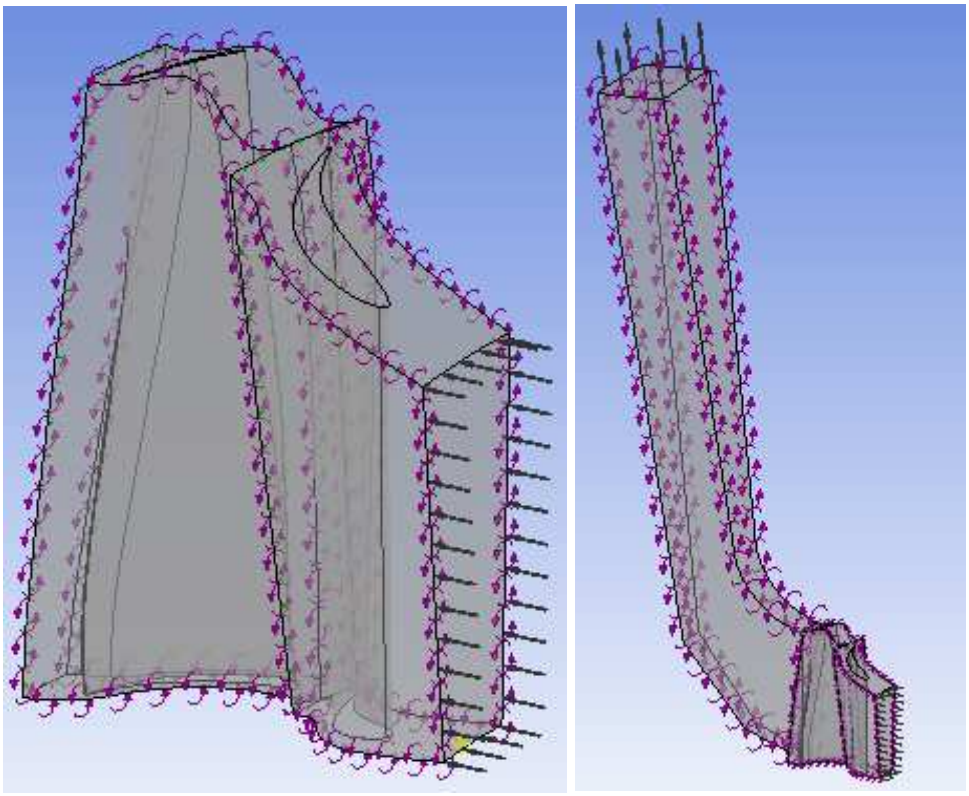

Figure 4-8: Vapor volumes in the inter-channels created for Turbo mode in CFX-Pre [Custom Processing]

4.3.1 Coupling geometry in the incoming confuser and guide vane

From the initial analysis of the problem and the dimensional geometry layout, it was found that it is advisable to minimize the number of surface areas, edges and points that could be trapped when creating a computational network, which would have a negative impact on the network itself and, above all, on the computation quality.

First, the model was trimmed to the required dimensions, the excess material was removed and only the blade blade was left. Furthermore, a set of straight lines converging on the axis of rotation "x" were created in 3D sketches. These lines were appropriately trimmed and the peaks of the resulting line segments connected by curves. This created a 3D surface representing the future channel boundary. This area had to be copied and a 5.29 ° pitch copy (68 Distributor Blades). This step yielded both boundaries between which the steam volume was generated, as shown in Figure (4 - 8).

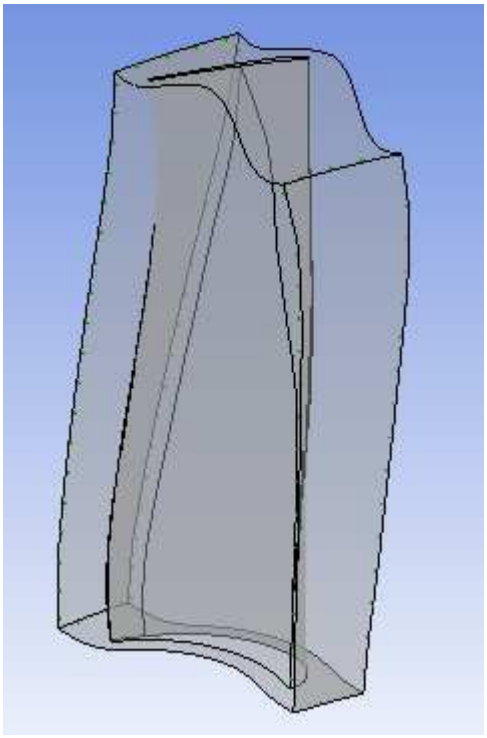

Figure 4-9: Adjustment Spreader Blades [Custom Processing]

4.4 Editing geometry in ANSYS

4.4.1 ANSYS Workbench 19.1

ANSYS is professional software for solving various problems such as acoustics, electromagnetism, mechanics and heat and mass transfer in both 2D and 3D. The Workbench is an administrator, but it can also edit geometry and create a compute network.

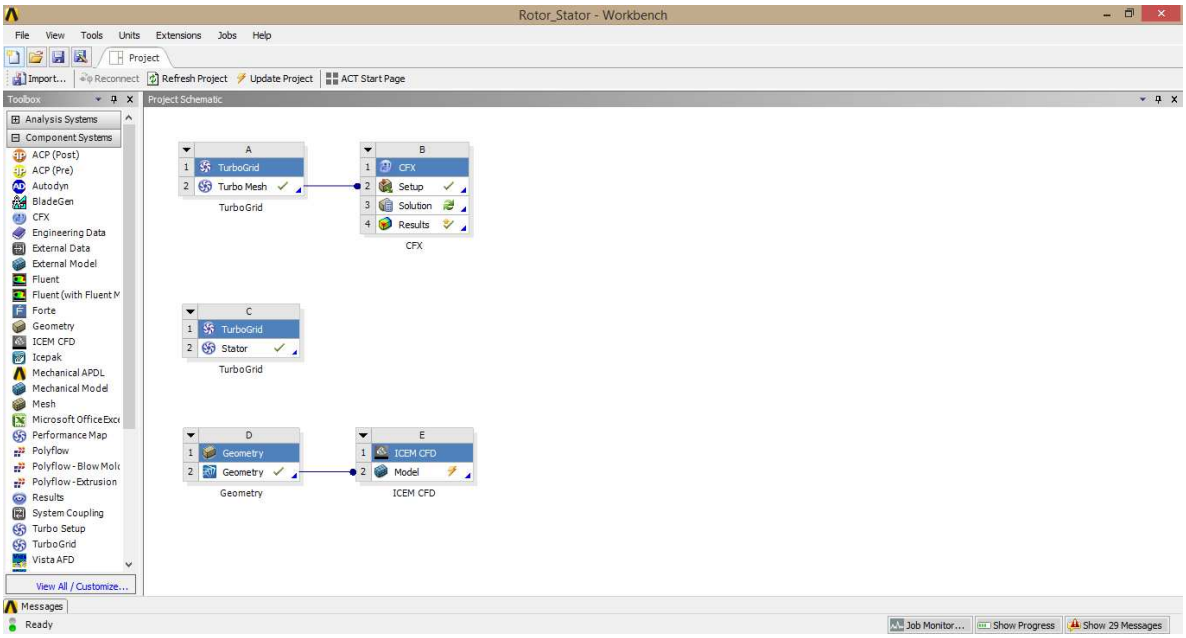

Figure 4-10: ANSYS Workbench 13.0 [Custom Processing]

4.4.2 ICEM CFD 19.1

ANSYS ICEM CFD provides advanced geometry acquisition, mesh generation, and mesh diagnostic and repair tools to provide integrated mesh generation for today's sophisticated analyses.

Maintaining a close relationship with the geometry during mesh generation, ANSYS ICEM CFD is designed for use in engineering applications such as computational fluid dynamics and structural analysis.

ANSYS ICEM CFD's mesh generation tools offer the capability to parametrically compute meshes from geometry in numerous formats:

- Multi-block structured
- Unstructured hexahedral
- Unstructured tetrahedral
- Cartesian with H-grid refinement
- Hybrid meshes comprising hexahedral, tetrahedral, pyramidal and/or prismatic elements
- Quadrilateral and triangular surface meshes.

ANSYS ICEM CFD provides a direct link between geometry and analysis. In ANSYS ICEM CFD, you can input geometry in almost any format, whether a commercial CAD design package, third-party universal database, scan data, or point data. Beginning with a robust geometry module that supports the creation and modification of surfaces, curves and points, ANSYS ICEM CFD's open geometry database offers the flexibility to combine geometric information in various formats for mesh generation. The resulting structured or unstructured meshes, topology, inter-domain connectivity, and boundary conditions are then stored in a database where they can easily be translated to input files formatted for a particular solver. [26]

For create the mesh of diffuser was used ICEM 19.1 was can be seen bellow figure (4 – 12). But first the geometry was imported from Autodesk Inventor 2019 figure (4 – 11).

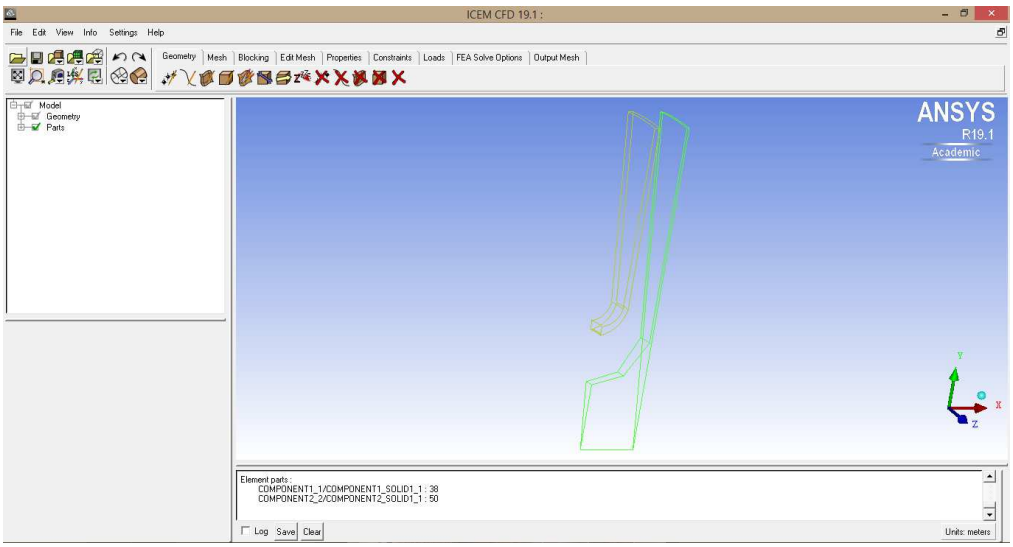

Figure 4-11: ICEM with Imported Geometry [Custom Processing]

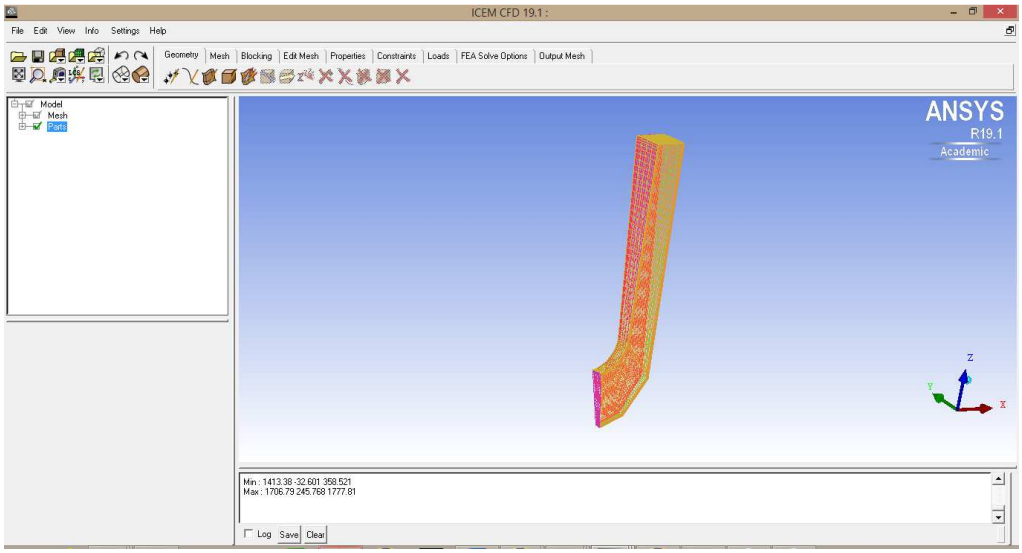

Figure 4-12: ICEM with Diffuser meshed [Custom Processing]

4.5 Creating a Computing Network

4.5.1 ANSYS Meshing

This software is used to create a computing network and is implemented in ANSYS Workbench. It was created separately, stator and rotor by TurboGrid and diffusor by ICEM.

ANSYS TurboGrid software includes novel technology that targets complete automation combined with an unprecedented level of mesh quality for even the most complex blade shapes. The desired final mesh size is defined (and, optionally, the blade boundary layer resolution), and all the other steps are performed automatically to produce a mesh of extremely high quality. Grid angles are exceptionally good, mesh sizes transition smoothly, and high aspect-ratio elements are generated in the near-wall regions to resolve these regions efficiently and capture boundary layer flows accurately. [31]

The flexible mesh-generation tools within ANSYS ICEM CFD offer the capability to parametrically create volume or surface meshes from geometry or mesh in multi-block structured, unstructured hexahedral, Cartesian, tetrahedral, tetra/prism hybrid, hexa hybrid and unstructured quad/tri shell formats. [32]

4.5.2 Stator in TurboGrid

ANSYS TurboGrid is a powerful tool that lets designers and analysts of rotating machinery create high-quality hexahedral meshes, while preserving the underlying geometry. These meshes are used in the ANSYS workflow to solve complex blade passage problems.

As mencioned before, the geometry was provided by Doosan Škoda Power in .turbogrid format that could be imported on TurboGrid and created the mesh as Figure (4 – 13).

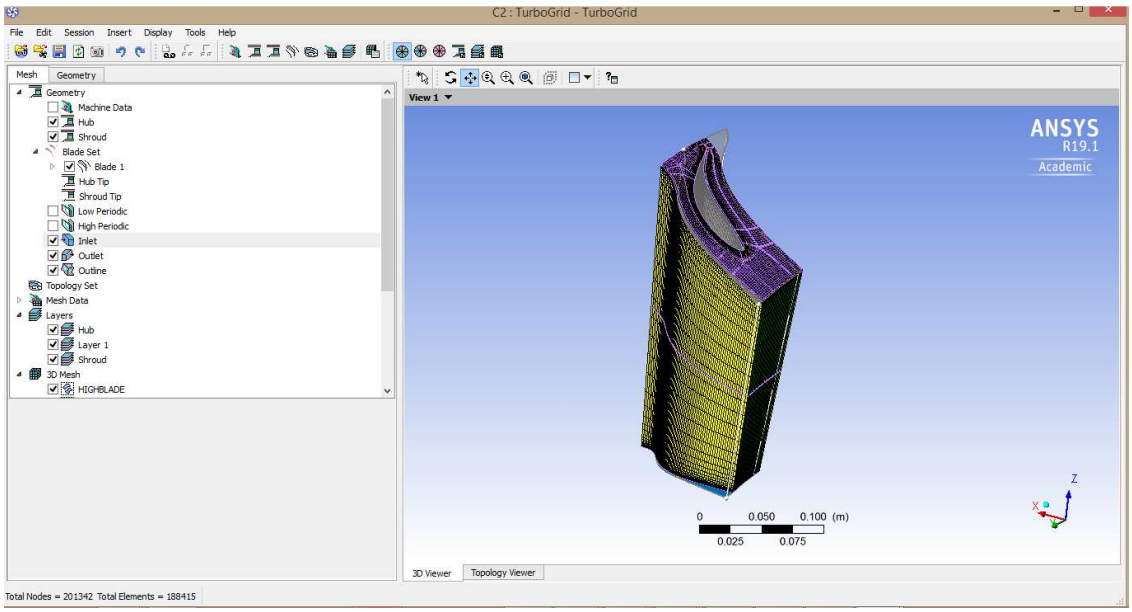

Figure 4-13: Stator meshing created in TurboGrid [Custom Processing]

4.5.3 Rotor in TurboGrid

The same process was made for the rotor as Figure (4 - 14).

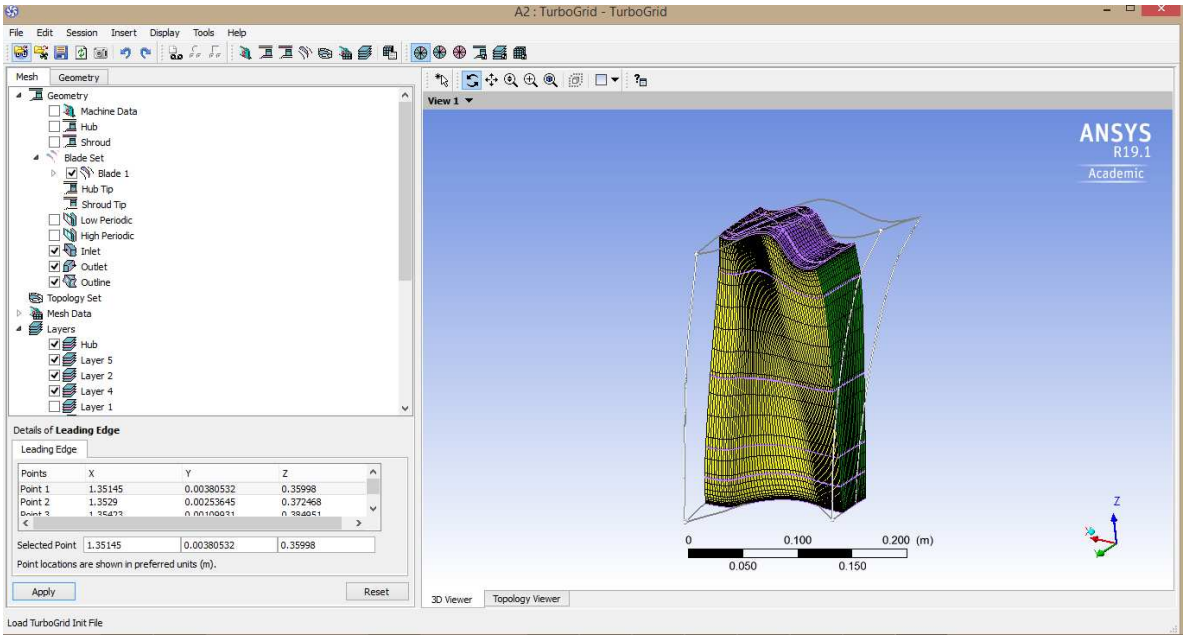

Figure 4-14: Stator meshing created in TurboGrid [Custom Processing]

4.5.4 Mesh Analysis

To analysis the mesh should be clicked at mesh analysis and check it out the mesh statitiscs, if the values are into the range means that the mesh are good as can seen on Figure (4 – 15).

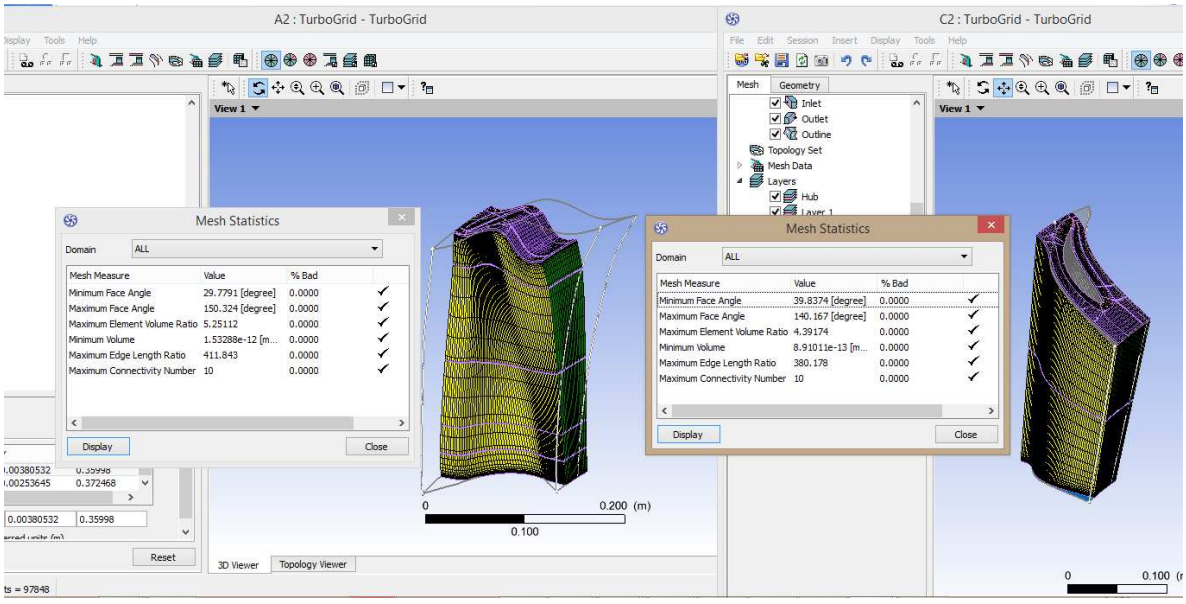

Figure 4-15: Mesh Analysis [Custom Processing]

4.6 ANSYS CFX-Pre 19.1

CFX can be run in two modes:

- CFX stand-alone, which refers to CFX running as a stand-alone application independent of the ANSYS Workbench software.
- CFX in Workbench, which refers to CFX running as a component inside of the ANSYS Workbench software. This is described in ANSYS CFX in ANSYS Workbench.

ANSYS CFX stand-alone has the launcher, which makes it easy to run all the modules of CFX without having to use a command line. The launcher enables you to:

- Set the working directory for your simulation.
- Start CFX and ANSYS products.
- Access various other tools, including a command window that enables you to run other utilities.
- Access the online help and other useful information.
- Customize the behavior of the launcher to start your own applications.

The launcher automatically searches for installations of CFX and ANSYS products including the license manager. Depending on the application, the search includes common installation directories, directories pointed to by environment variables associated with CFX and ANSYS products, and the Windows registry. In the unlikely event that a product is not found, you can configure the launcher using steps outlined in Customizing the ANSYS CFX Launcher in the CFX Reference Guide. [27]

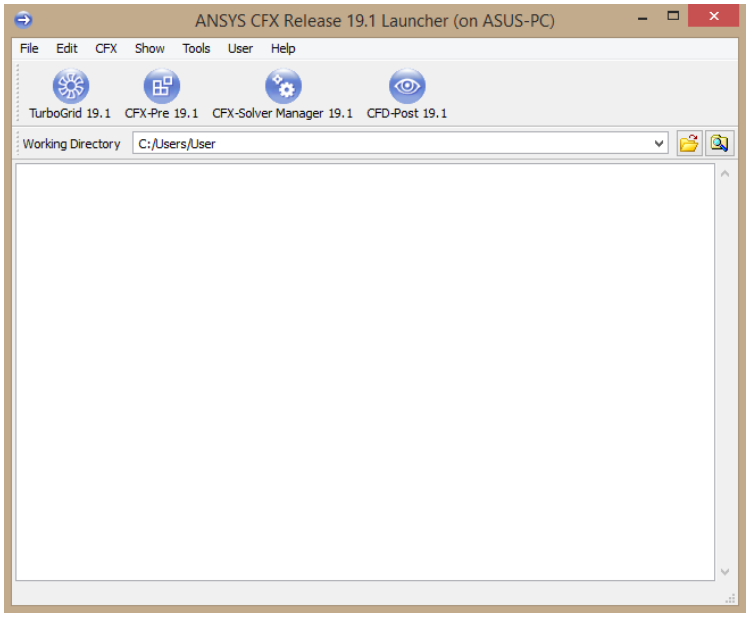

Figure 4-16: ANSYS CFX 19.1 Welcome Screen [Custom Processing]

The following subsections describe the ANSYS CFX settings. The most important steps that will be performed in each tab will be mentioned.

4.6.1 General

As the name suggests, the general parameters are set here. First, it was necessary to set the Scale dimension scale in which the computational network was created. In the Units section *Units* it was advisable to change the default angular speed by default $\left[rad \cdot s^{-1}\right]$ to the rotor speed $\left[\min^{-1}\right]$. Furthermore, this tab performs the quality control of the computational network and the geometrical setting, which should be performed several times during the setting of boundary conditions. Last but not least, it is possible to set the display of various parts of geometry and network.

4.6.2 Models

In this tab, computational models are set, the list of which is shown in Figure (3 - 10) and described in subchapter 3.7. As already mentioned, the two-equation turbulent model SST, K - ω will be used in this work.

4.6.3 Materials

As the name suggests, flowing fluid or solid wall material is chosen here. In this case, water vapor was selected from the material database for fluid flowing fluid and steel for solid walls. However, it was necessary to adjust the steam parameters according to the specification.

The water vapor density will be calculated automatically by the program from the ideal gas equation.

Specific heat capacity has been set as constant, but its exact value has to be calculated, see calculation below.

Thermal conductivity, dynamic viscosity and molar mass were left as default constants.

4.6.3.1 Specific gas constant

Specific gas constant for water $r_{H2O}\left[J \cdot kg^{-1} \cdot K^{-1}\right]$ is calculated from the universal molar gas constant from [28] of value: $R = 8314{,}3\left[J \cdot kmol^{-1} \cdot K^{-1}\right]$. Molar mass of water determined from ANSYS CFX $M_{H2O} = 18{,}01534\left[kg \cdot kmol^{-1}\right]$ from the relationship (4.1):

$$r_{H2O} = \frac{R}{M_{H2O}} = \frac{8314,3}{18,01534} \doteq 461,512$$
$$r_{H2O} = \underline{\underline{461,512\left[J \cdot kg^{-1} \cdot K^{-1}\right]}} \tag{4.1}$$

4.6.4 Cell Zone Conditions

This tab is dedicated to setting the boundary conditions in each zone of the flowing medium.

4.6.4.1 Part of Inlet Confuser and Distributor Blades

First, it is necessary to set the material of the flowing medium from subchapter 4.6.4, namely superheated steam. Furthermore, the sense of rotation must be correctly defined. ANSYS CFX-Pre works according to the clockwise rotation, as shown in Figure (4-17). This conclusion is to be compared with the coordinate system. It follows that the axis of rotation is a negative "x" axis.

Figure 4-17: Rotation sense ANSYS CFX-Pre [28]

The zone is absolute with zero speed because it is the stator part of the turbine stage.

4.6.4.2 Domains

CFX-Pre uses the concept of domains to define the type, properties, and region of the fluid, porous, or solid. Domains are regions of space in which the equations of fluid flow or heat transfer are solved. This section describes how to use the domain details view to define the physics of fluid, porous or solid domains in your simulation. This includes selecting the 3D bounding regions and choosing appropriate physical models. In your case the rotation is 4000 RPM in all simulations.

It was created 3 domains: Diffuser, stator and rotor. All of it was configured according the pre-settings from Doosan Škoda Power as can be seen on figure (4 - 18).

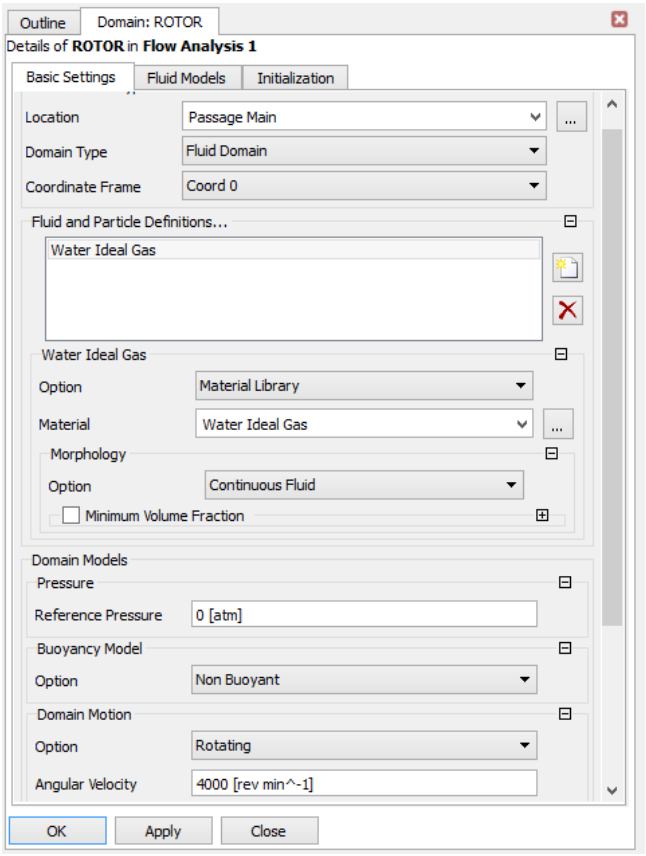

Figure 4-18: Rotor domain settings [Custom Processing]

4.6.5 Boundary Conditions

Boundary conditions must be applied to all the bounding regions of your domains. Boundary conditions can be inlets, outlets, openings, walls, and symmetry planes.

Unspecified external regions are automatically assigned a no-slip, adiabatic wall boundary condition. Such regions assume the name <Domain> Default, where <Domain> corresponds to the name of the domain. Unspecified internal boundaries are ignored.

You can apply boundary conditions to any bounding surface of a 3D primitive that is included in a domain (including internal surfaces). If you choose to specify a boundary condition on an internal surface (for example, to create a thin surface), then boundary conditions must be applied to both sides of the surface.

4.6.6 Specifying Well Posed Boundary Conditions

At first the idea was to create the boundary conditions as inlet static pressure and outlet static pressure. But the calculations were very unstable so we decided to follow the most robust parameters for the calculatations.

When there is 1 Inlet and 1 Outlet:

- Most Robust: Velocity/Mass Flow at an Inlet; Static Pressure at an Outlet. The Inlet total pressure is an implicit result of the prediction.

- Robust: Total Pressure at an Inlet; Velocity/Mass Flow at an Outlet. The static pressure at the Outlet and the velocity at the Inlet are part of the solution.
- Sensitive to Initial Guess: Total Pressure at an Inlet; Static Pressure at an Outlet. The system mass flow is part of the solution.
- Very Unreliable: Static Pressure at an Inlet; Static Pressure at an Outlet. This combination is not recommended as the inlet total pressure level and the mass flow are both an implicit result of the prediction (the boundary condition combination is a very weak constraint on the system). [29]

4.6.6.1 Inlet, Outlet

Channel input has been set as mass flow. This means that you had to enter the mass flow at the inlet to the stage $\dot{m}_0 = 4{,}385\,[Kg/s]$, and static inlet temperature $t_0 = 376{,}53\,[K]$.

The channel output was set as Pressure Outlet. It was necessary to define the static pressure at the outlet of the stage $p_2 = 28000\,[Pa]$. As can be seen in the figures (4 - 19 and 4 - 20).

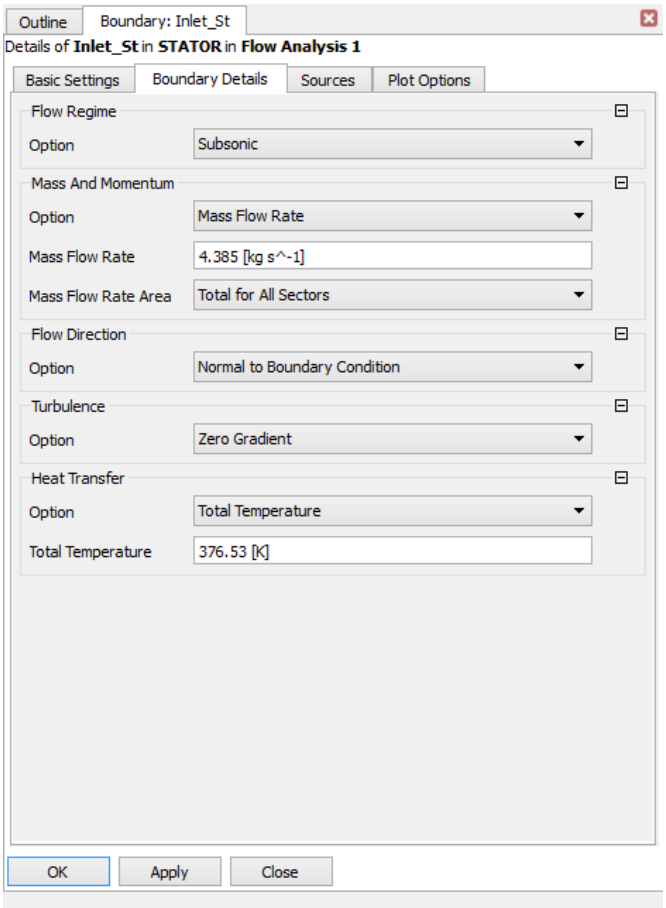

Figure 4-19: Stator inlet boundary conditions [Custom Processing]

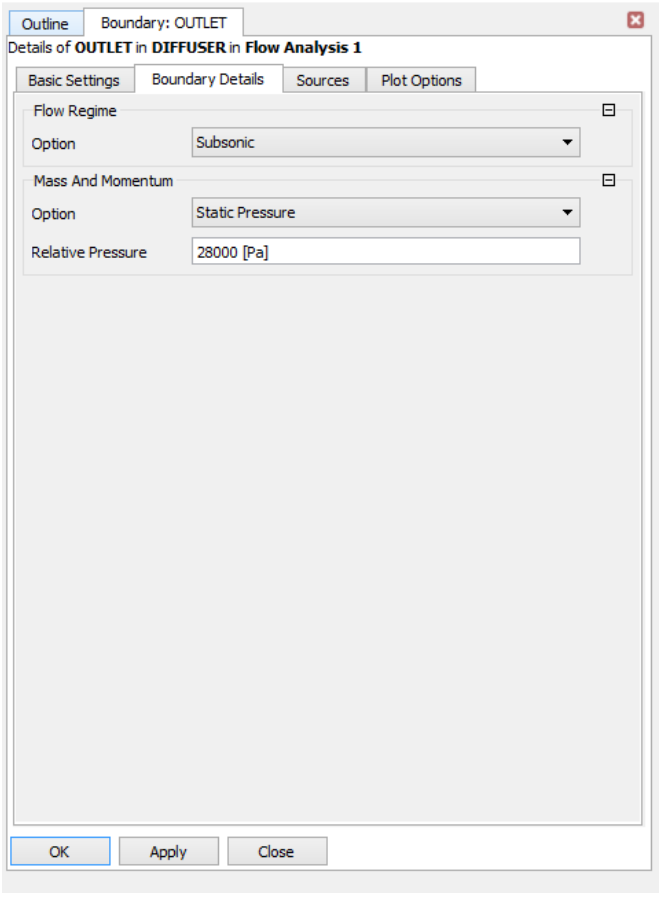

Figure 4-20: Diffuser outlet boundary conditions [Custom Processing]

The boundary conditions on diffuser outlet had a decrease step of pressure of 1000 [Pa] up to 13000 [Pa] in diffuser outlet pressure.

4.6.6.2 Mixing Plane a Mesh Interface

Mixing Plane, it is one of the methods of defining leap area between non-conforming networks. In this case, it is the area at the outlet of the Pressure Outlet and the surface at the entrance to the Mass flow Inlet. The advantage of this is that you no longer need to define any numeric values. All the data you define as Mixing Plane is taken automatically from the calculation. The disadvantage is that the contours of the resulting values will not follow each other, but will be interrupted at this point. This also affects the distortion of the current field and, for example, the inadequate mass flow value in subchapter 4.8.1 used when the transition areas do not have the same sector.

Mesh interface is another way of defining a landing area. This method has been defined on the output surface from the Interface and on the input surface into the Interface. Again, no other numeric parameters need to be set. The advantage of this method is that the contours between the parties pass smoothly and are not interrupted. The disadvantage is greater

computational complexity and longer computing time. It is used in the case of an identical segment of transition surfaces.

4.6.6.3 Periodicity

Frequency is one of the basic conditions for numerical calculation of parts of rotational geometries. In this case, the periodicity was preset in the mesher and was now loaded into the computator. In Figure (4 - 21), the areas of Periodicity and Shadow area are shown indicating the boundary of the calculated sector of the total channel.

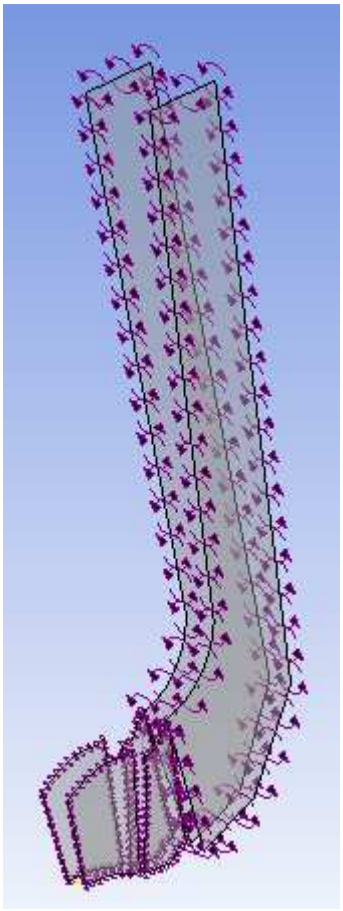

Figure 4-21: Periodicity limits [Custom Processing]

4.6.6.4 Interfaces

Domain interfaces are used to connect multiple assemblies together, to model frame change between domains, and to create periodic regions within and between domains. Domain interfaces are automatically generated based on the region information.

Nevertheless it was created 5 interfaces:

- Stator periodicity;
- Rotor to Staror;
- Rotor periodicity;
- Rotor to Diffuser;

- Diffuser Periodicity.

Bellow is the configurations of those interfaces.

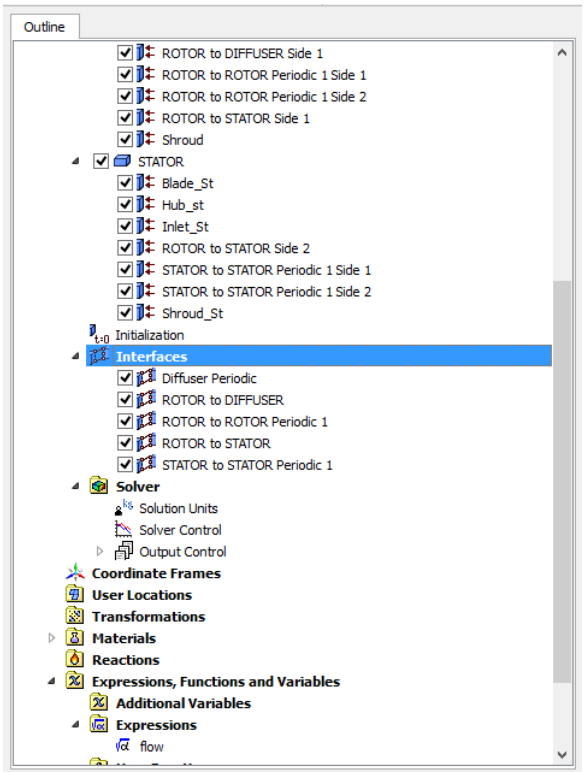

Figure 4-22: Interfaces [Custom Processing]

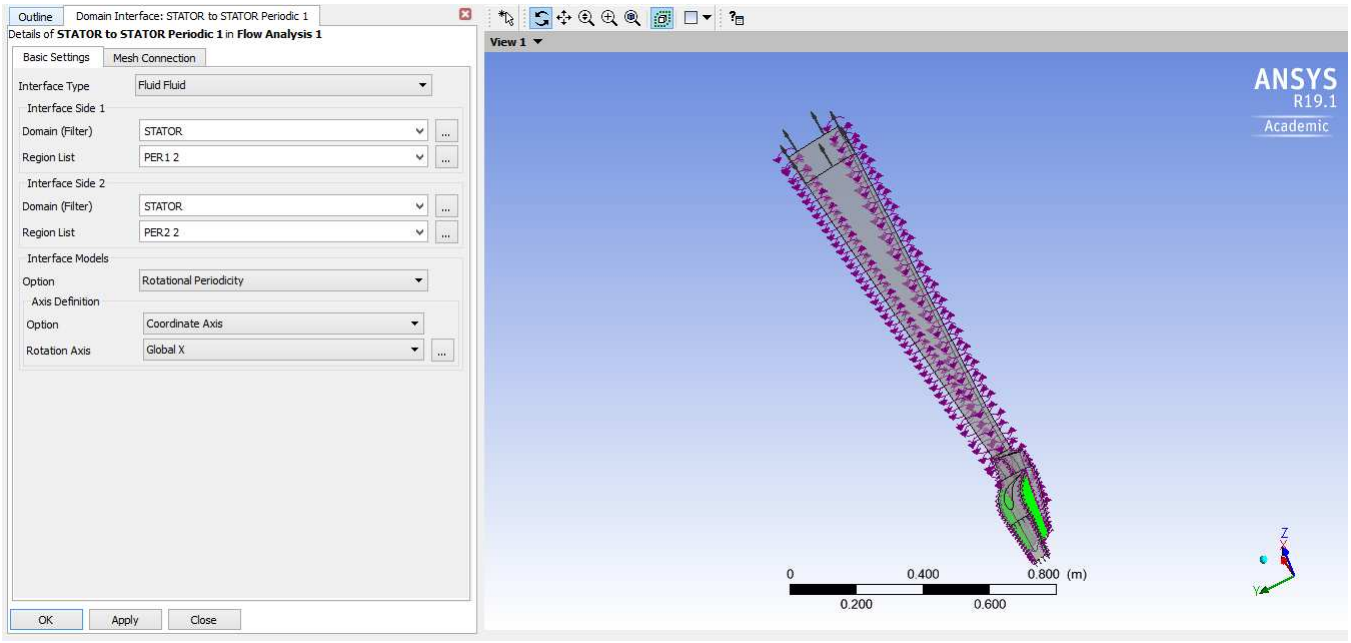

Figure 4-23: Interface Stator periodicity [Custom Processing]

4.6.6.5 Walls

Any remaining areas are marked as Walls. These are the upper and lower surfaces of the channel and the walls of the blades. In the unstable part of the calculation, all walls must be defined to be moving rotating walls in the direction of rotation of the negatively defined axis

"x". The walls must also be relative to the zone to which they belong. Only in this way will it be ensured that not only the flowing medium, ie the superheated water vapor, but also the walls it flows around will rotate in a zone that has a defined nonzero speed.

In the stable part of the calculation, the settings of the walls of the Input Confuser Zone and the Spreader Blade and Output Channel are changed. These walls will be stationary stationary. This is due to the correct calculation of the boundary layer velocity for these walls.

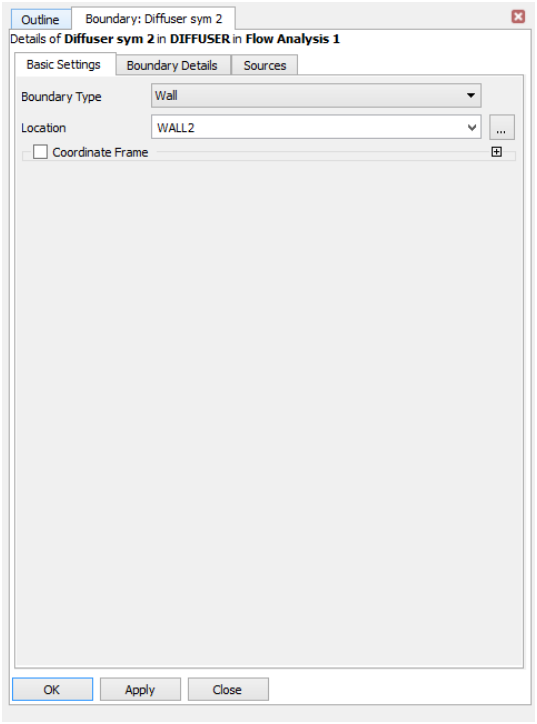

Figure 4-24: Relatively Set Intermediate Channel Walls [Custom Processing]

4.6.7 Solver Control

On the Solver Control form, it is recommend that you use the Central Difference advection scheme rather than the High Resolution scheme because it is less dissipative and it has provided good answers in CFX. Select the transient scheme as 2nd Order Backward Euler.

4.6.7.1 LES Timestep Considerations

First order fully implicit methods in time are usually too diffusive, and the turbulence is damped out. For highly unstable problems, such as cyclones, lower order methods may work, but the results will be very damped, unless very small timesteps are used.

For accuracy, the average Courant (or CFL) number should be in the range of 0.5-1. Larger values can give stable results, but the turbulence may be damped. For compressible flows where the acoustic behavior is being modeled (eg, for noise calculations), this

conclusion still holds, but for the CFL number based on the acoustic velocity as well as the convective velocity.

1,000 - 10,000 timesteps are typically required for getting converged statistics. More steps are required for second order quantities (for example, variances) than for means. Check the convergence of the statistics. For a vortex-shedding problem, several cycles of the vortex shedding are required.

The implicit coupled solver used in CFX requires the equations to be converged within each timestep to guarantee conservation. The number of coefficient loops required to achieve this is a function of the timestep size. With CFL numbers of order 0.5-1, convergence within each timestep should be achieved quickly. It is advisable to test the sensitivity of the solution to the number of coefficient loops, to avoid using more coefficient loops (and hence longer run times) than necessary. LES tests involving incompressible flow past circular cylinders indicates that one coefficient loop per timestep is sufficient if the average CFL number is about 0.75. If the physics or geometry is more complicated, additional coefficient loops (3-5) may be required. Timesteps sizes that require more coefficient loops than this will tend to degrade solution accuracy.

The solver control was configured according the pre-settings from Doosan Škoda Power.

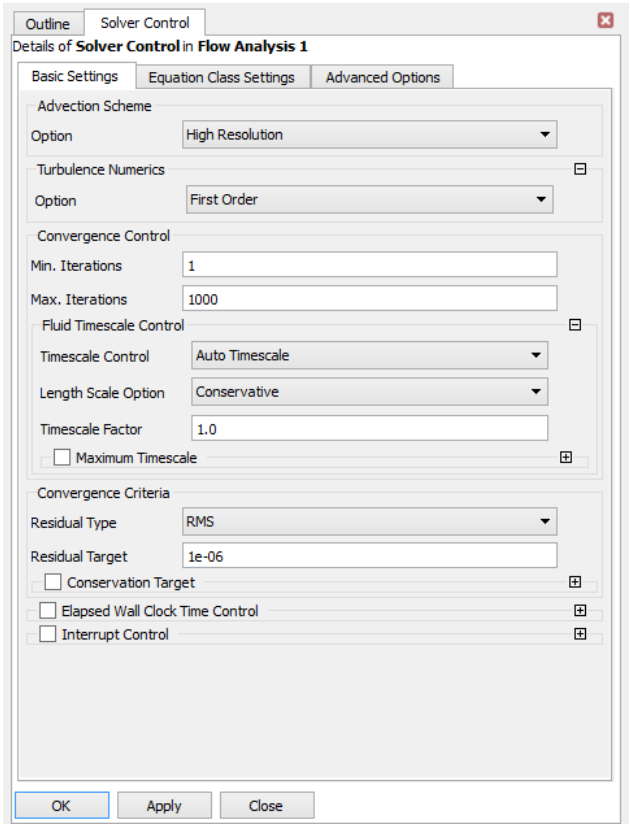

Figure 4-25: Solver control tab [Custom Processing]

4.6.8 Monitors

Monitors are used to observe the state of individual variables during the calculation. It is possible to estimate whether the measured variables will be changed or their final value is calculated in the required accuracy.

For this task, a monitor point was created for monitoring the static pressure at inlet hub of the Stator. Because it was provided the static pressure on this point so we could change the inlet pressure according to those measurements on this point. This is represented by a yellow dot in the figure below.

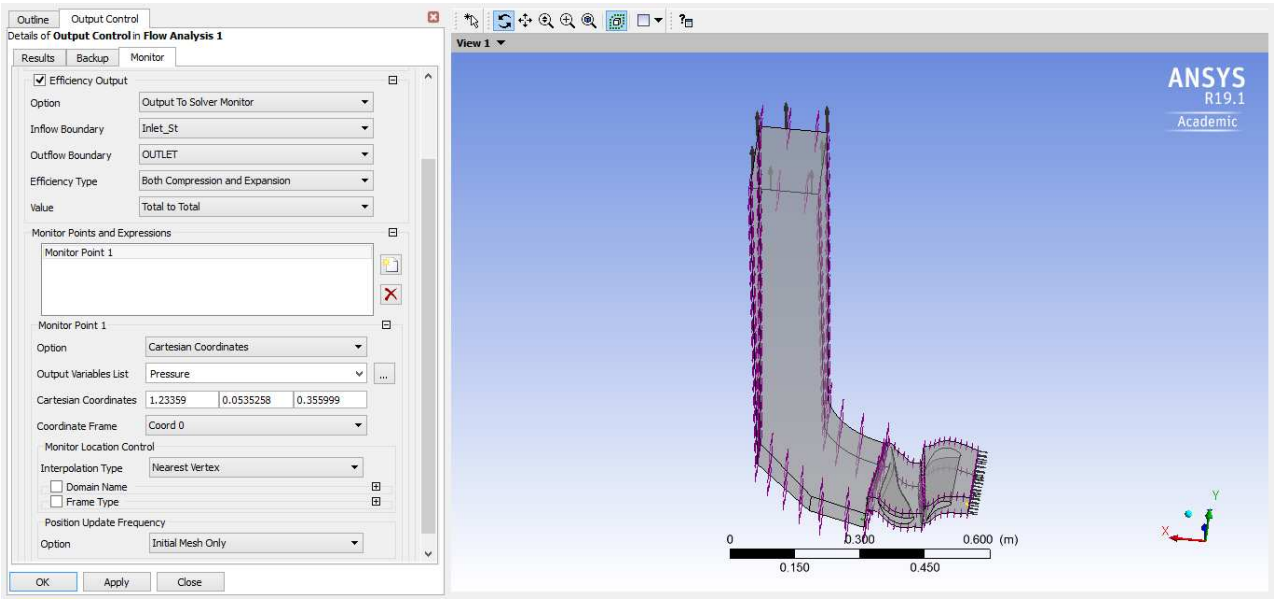

Figure 4-26: Output control tab [Custom Processing]

4.7 CFX-Solver manager 19.1

CFX-Solver Manager is a graphical user interface that enables you to set attributes for your CFD calculation, control the CFX-Solver interactively, and view information about the emerging solution. As an alternative to using the CFX-Solver Manager interface, you can also operate CFX-Solver from the command line, which is particularly useful for batch mode operations. [30]

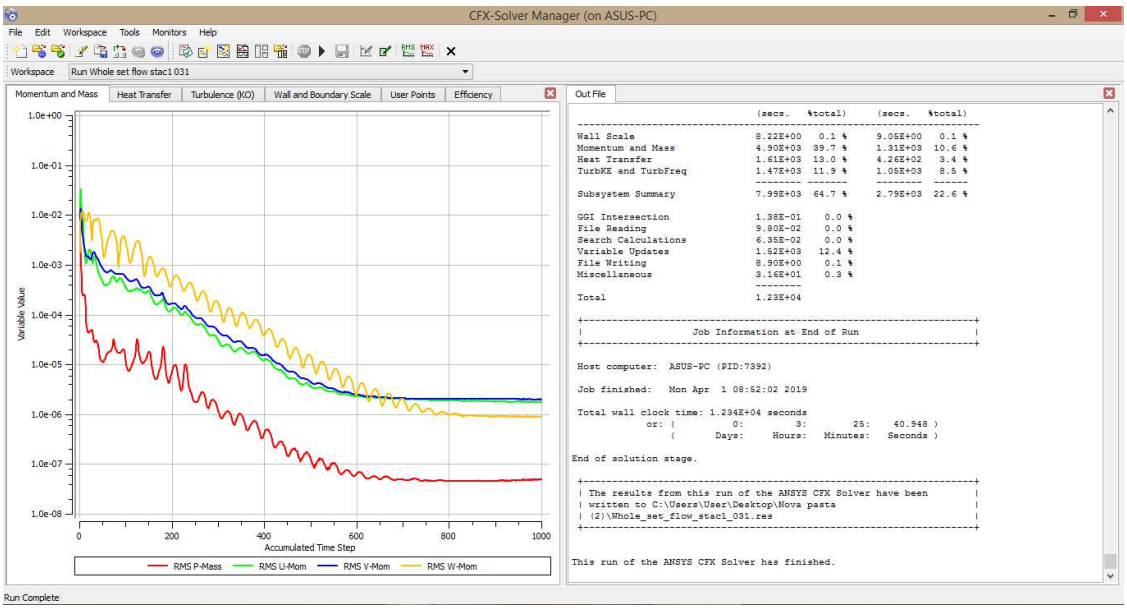

Figure 4-27: CFX-Solver manager 19.1 [Custom Processing]

4.8 CFX-Post 19.1

In CFX-Post are going to be presented all of the results after simulations. It can be made in many different ways. It will be represented the pressures, temperatures, velocities and Mach number for p_2 = 22000 [Pa] in 3 layers (planes) of the domain, 5%, 50% and 95% according to the hight of the domain. This p_2 = 22000 [Pa] pressure was used because it was the pressure that Doosan Skoda provided to be compared.

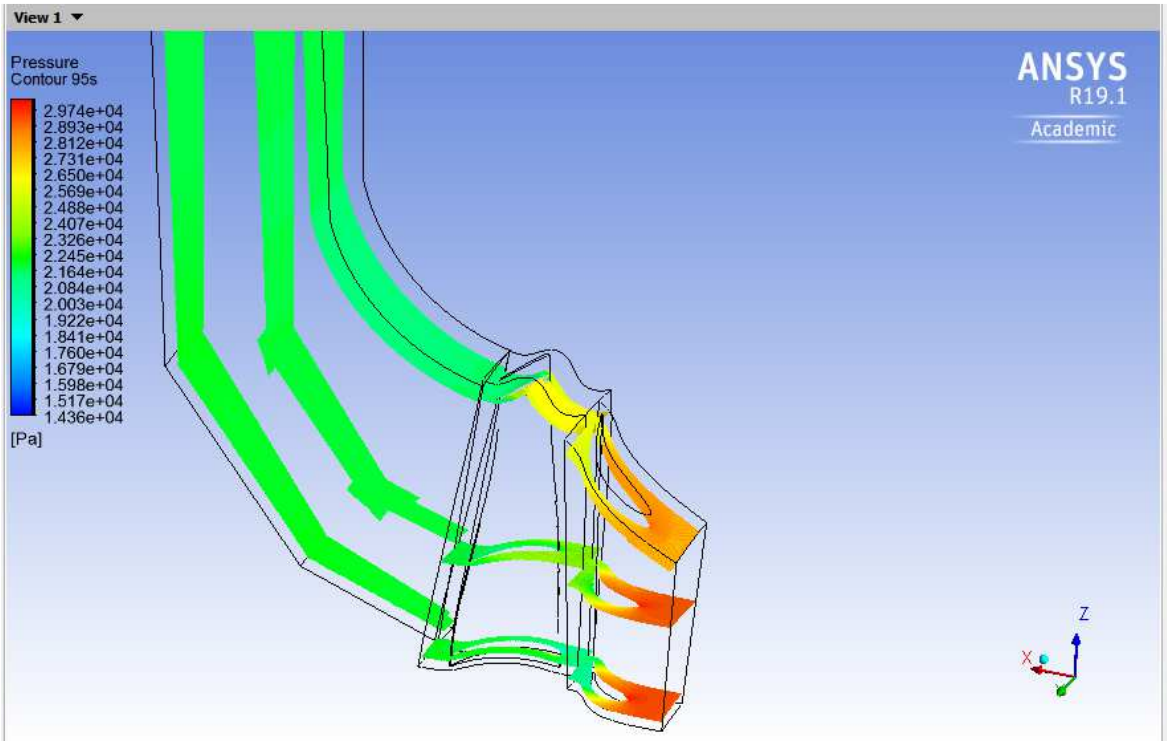

Figure 4-28: CFX-Pos represention pressures in 3 layers (planes) of the domain, 5%, 50% and 95% with p_2 = 22000 [Pa] [Custom Processing]

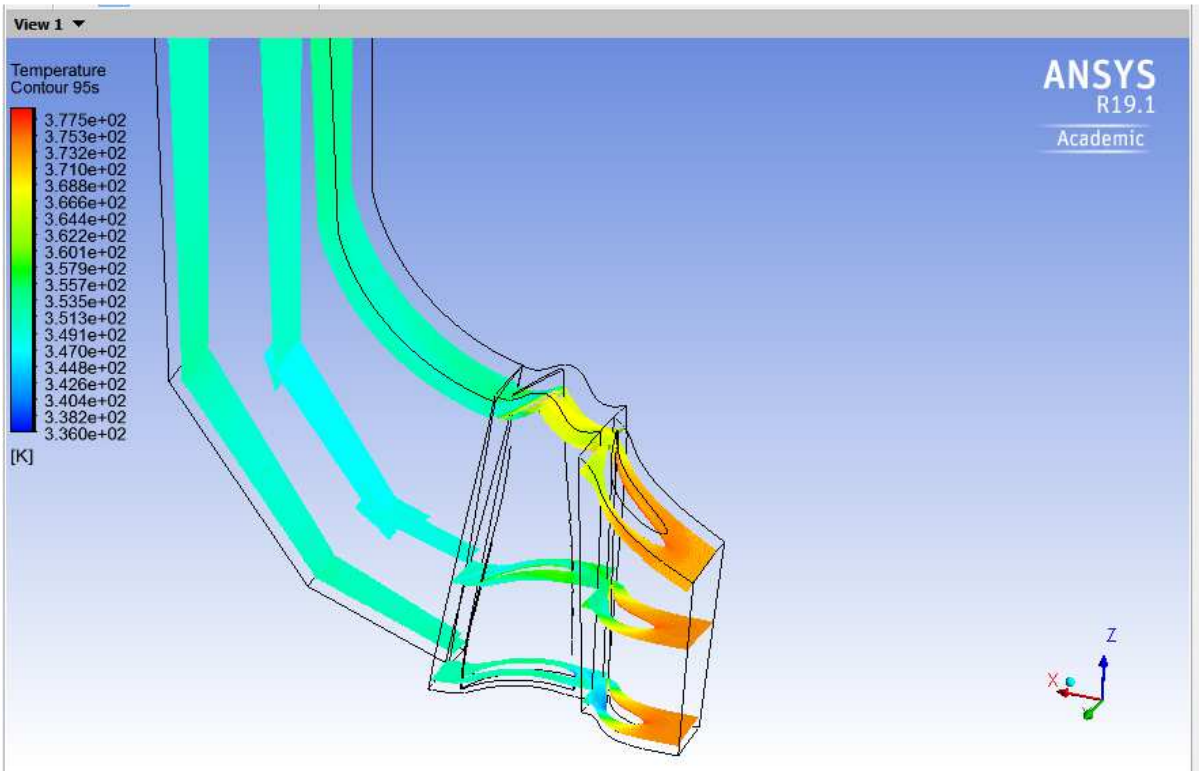

Figure 4-29: CFX-Pos represention temperatures in 3 layers (planes) of the domain, 5%, 50% and 95% with p_2 = 22000 [Pa] [Custom Processing]

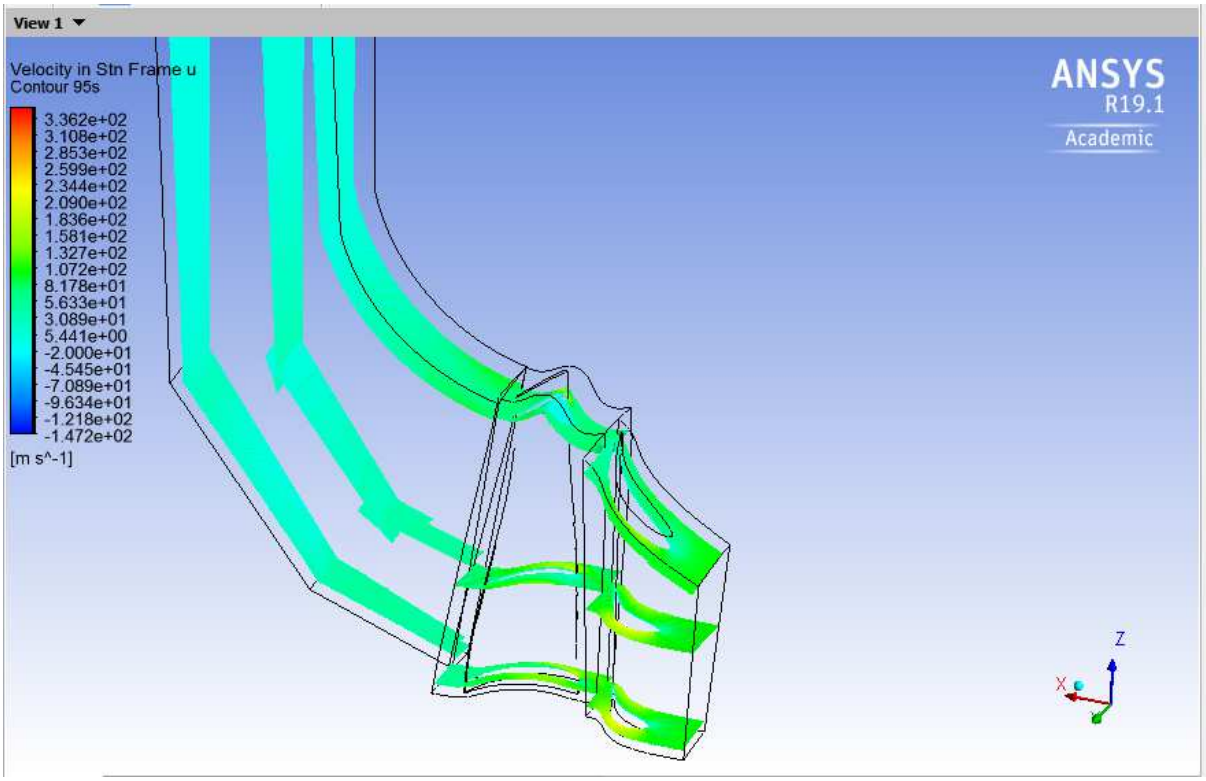

Figure 4-30: CFX-Pos represention axial velocities in 3 layers (planes) of the domain, 5%, 50% and 95% with p_2 = 22000 [Pa] [Custom Processing]

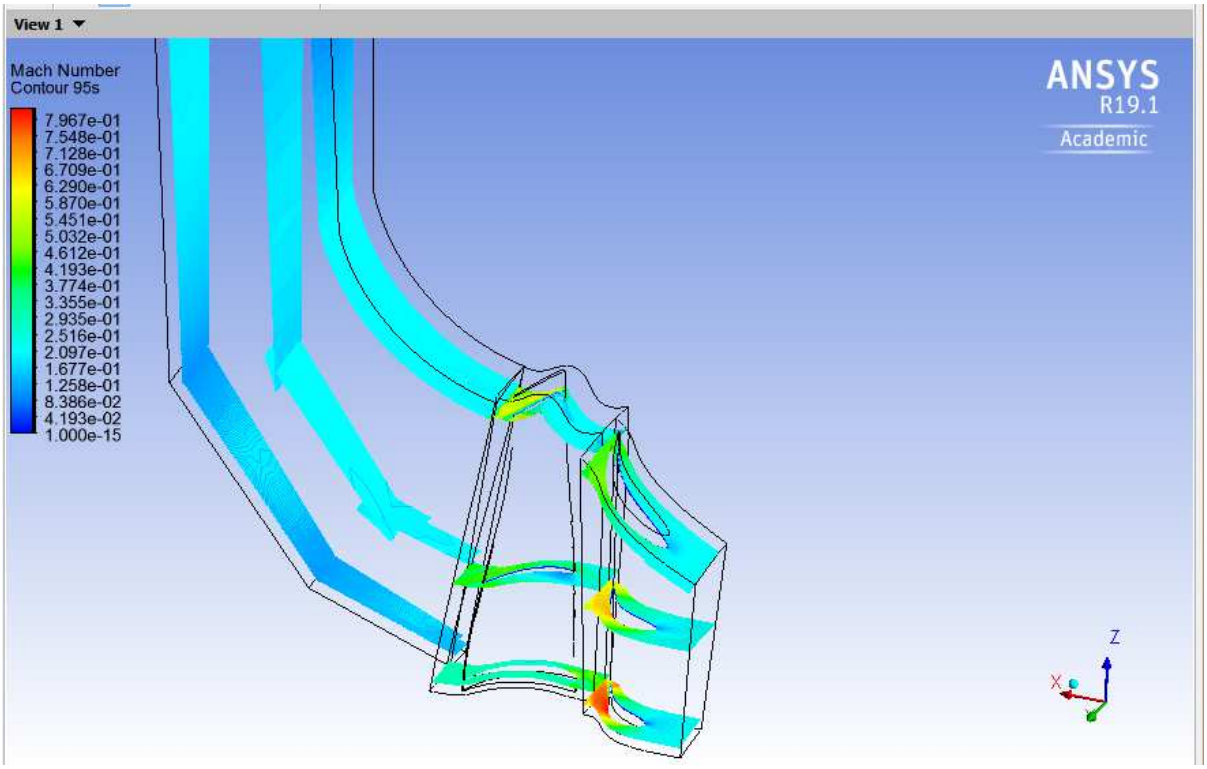

Figure 4-31: CFX-Pos represention Mach number in 3 layers (planes) of the domain, 5%, 50% and 95% with p_2 = 22000 [Pa] [Custom Processing]

3D numerical calculation of BFPT T10MW for current parameters

Bellow is the table representing all the simulations with the outlet pressure, inlet pressures, temperatures, velocities and Mach number. All the simulations had the boundary conditions with the mass flow at the inlet to the stage $\dot{m}_0 = 4{,}385\,[Kg/s]$, and static inlet temperature $t_0 = 376{,}53\,[K]$.

Simulations	p_2 [Pa]	p_0 [Pa]	T_2 [K]	c_{0x} [m/s]	Mach Number on Rotor blade
1	13000	24367,2	327,093	119,185	0,699
2	14000	24890,9	330,740	117,412	0,670
3	15000	25399,1	333,345	115,634	0,638
4	16000	25901,3	336,976	113,743	0,602
5	17000	26513,5	339,911	111,893	0,573
6	18000	26939,6	342,806	110,145	0,542
7	19000	27402,0	345,456	108,309	0,513
8	20000	27903,1	347,824	106,388	0,487
9	21000	28427,5	350,073	104,448	0,465
10	22000	28971,6	352,147	102,509	0,445
11	23000	29546,3	354,065	100,536	0,428
12	24000	30160,0	355,817	98,512	0,412
13	25000	30820,7	357,380	96,419	0,397
14	26000	31541,1	358,741	94,233	0,384
15	27000	32284,6	360,008	92,077	0.372
16	28000	32847,9	362,516	89,918	0,359
17	33000	33559,2	364,795	87,712	0,345
18	36000	34145,7	366,918	85,561	0,330
19	40000	34889,3	369,010	83,305	0,317

Table 4-1: Simulations with the outlet pressur, inlet pressures, temperatures, velocities and Mach number [Custom Processing]

Below is the table with the real measurements provided by Doosan Skoda with p_2 = 22000 [Pa]:

p_2 [Pa]	p_0 [Pa]	T_2 [K]	c_{0x} [m/s]	Mach Number on Rotor blade
22000	27914,1	355,99	103,768	0,613

Table 4-2: Real measuramets provided by Doosan Skoda [Custom Processing]

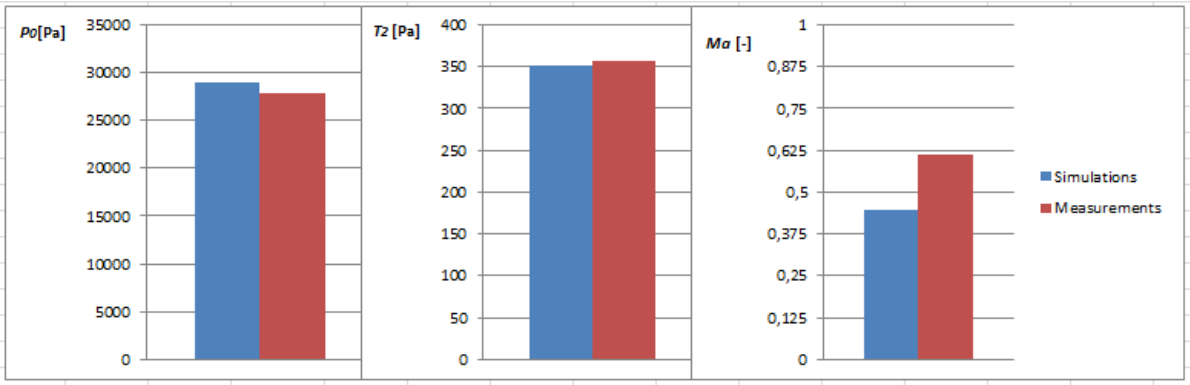

Figure 4-32: Comparison between measured and simulation data

Another requiremets from Doosan Skoda was to create a plot of efficiency versus ratio of velocities as can be seen on figure (4 – 33):

p_2 [Pa]	M [N.m]	c_{0x} [m/s]	h_0 [J/Kg]	h_2 [J/Kg]	h_{2is} [J/Kg]	c_{is} [m/s]
16000	159,477	113,743	2692870	2672710	2680420	200,798
17000	133,237	111,893	2692790	2675920	2682420	183,685
18000	108,872	110,145	2692690	2679020	2684290	165,348
19000	87,139	108,309	2692600	2681710	2685960	147,580
20000	67,454	106,388	2692490	2684100	2687500	129,538
21000	49,641	104,448	2692390	2686280	2688960	110,544
22000	33,264	102,509	2692290	2688270	2690230	89,666
23000	18,271	100,536	2692190	2690090	2691380	64,807
24000	4,362	98,512	2692100	2691770	2692410	25,690
25000	0,947	96,419	2692100	2691770	2691640	25,690

$$\omega = 2 \,.\, \pi \,.\, \frac{RPM}{60} \tag{4.2}$$

$$P = M \,.\, \omega \tag{4.3}$$

$$u = \frac{D_{mid}}{2} \,.\, \omega \tag{4.4}$$

$$h_{is} = h_0 - h_{2is} \tag{4.5}$$

$$\eta = \frac{P}{\dot{m}_0 \,.\, (\frac{c_{0x}^2}{2} + h_{is})} \tag{4.6}$$

$$C_{is} = \sqrt{2 . (h_0 - h_2)} \quad (4.7)$$

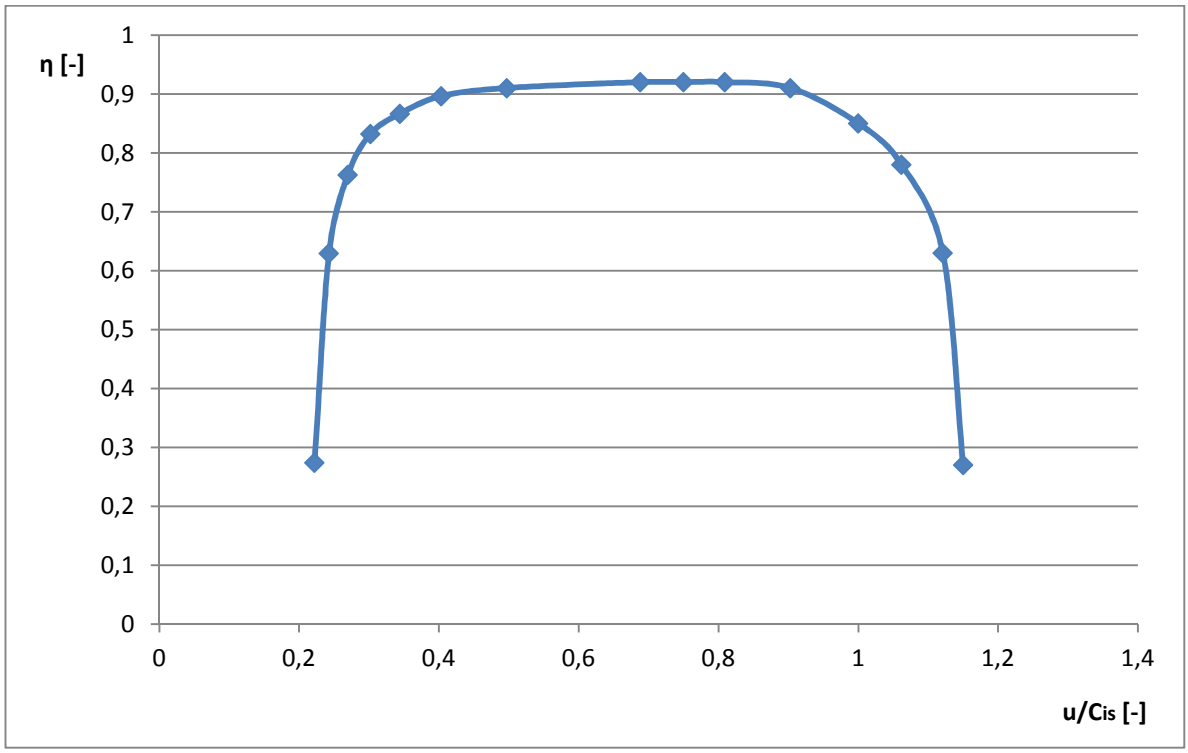

Figure 4-33 Efficiency of steam turbine

4.9 Ventilation phenomena

To cope up with the power generation needs and satisfying environmental requirements, combined cycle power plants have been widely developed. The system should be reliable and flexible but it would bring risk to steam turbine designs. The critical components of steam turbine in terms of flexible operation are those sustaining higher temperature and higher pressure such as the inlet valves or the rotor which can suffer from low cycle fatigue under high thermal transients. Other vulnerable parts are the Last Stage Moving Blades (LSMBs) of the low-pressure turbines. The operating regime of the LSMB is characterized by the volume flow leaving the stage. The volumeflow can vary due to a reduction in inlet mass flow to the stage under low load conditions of the power plant, or with large extraction mass flows for district heating, or steam used for chemical processes. Also a poor condenser pressure also leads to a reduced volume flow as the fluid density is rising while maintaining the mass flow.

With a reduction in volume flow the work output is reduced and consequently the power output. A further reduction in volume flow leads to a power consumption of the stage, where energy is returned from the shaft to the fluid. This region is sometimes called ventilation region because the rotor blade is swirling in the globally slow moving fluid with small pressure differences. Here the term Low Volume Flow (LVF) operation is used. [1]

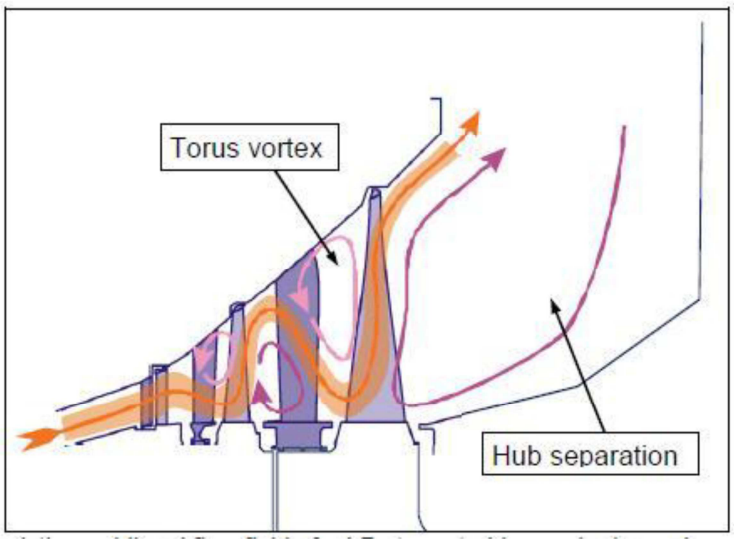

Figure 4-34: Flow Field of A Low Pressure Turbine Under Low Volume Flow Operation [Custom Processing]

Such off design conditions may cause aero elastic problems mainly to the LSMBs and also putting them at a risk of damage due to windage .i.e. strongly separated flow. It has been observed that since a steam turbine may undergo variable part load operation for a considerable part of time, high dynamic stresses that are associated with the blade excitation must be avoided or at least controlled to be at below at certain level. Therefore it is necessary to investigate the flow behavior of LSMBs and corresponding aero elastic phenomena's under low volume flow operations. This would directly help the designers in prediction of any mechanical failure and to reduce the risk. Thus this would play a major role in extending the working range and improving the flexibility of steam turbines.In past there were many different methods has been used to understand the unsteady aerodynamic flow phenomenon described. A computational study has been performed for measuring unsteady pressure measurements and will be created a general characteristic of power (load) turbine under velocities according the acquired datas that will have the same characteristic of the graph represented bellow figure (4-30).

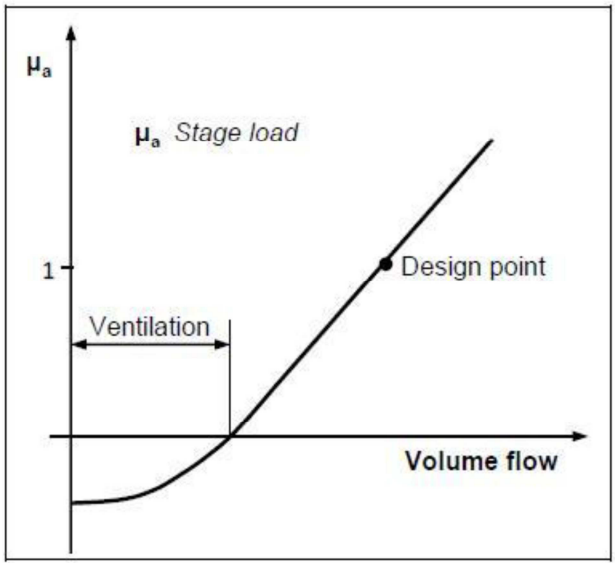

Figure 4-35: General characteristic of low pressure turbine under variable flow [Custom Processing]

Stresses get increased sharply with 2-3 times higher than the dynamic stresses at rated conditions while operated at LVF. This increase of stress is due to the change of turbine operational mode to compressor type mode where there is drastic increase of pressure and velocity of flow in tip region of LSMB. Engelke et al. showed the variation of stress in a model steam turbine close to the point where the last stage produces zero power refers figure (4-32). With that we will find the optimal range for our turbine avoiding these phenomena.

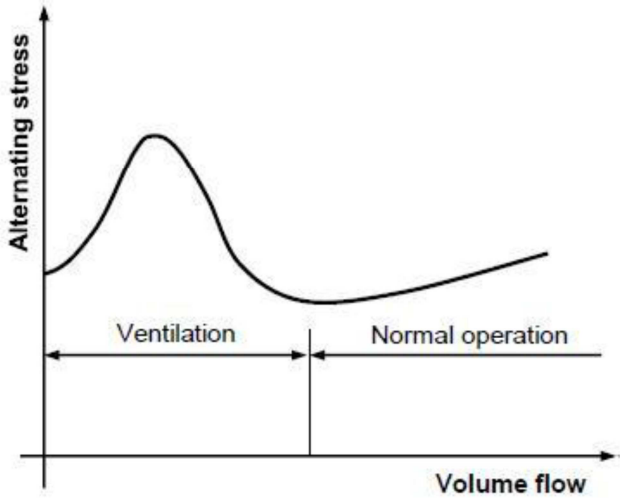

Figure 4-36: Variation of Stresses with the Volume Flow [Custom Processing]

4.9.1 Mesuared points and general characteristic of power (load) turbine under velocities

Bellow we have a table with the results of the simulations for create a general characteristic of load turbine under variable velocities on rotor and after a graph representation of those values.

Simulations	P [W]	c_{2x} [m/s]	c_{2x}/u
1	58345	62,6	0,281
2	49681	58,3	0,262
3	42198	54,7	0,245
4	35563	51,6	0,231
5	29712	49,1	0,220
6	24278	47,0	0,211
7	19432	45,4	0,203
8	15042	44,1	0,198
9	11070	42,1	0,189
10	7418	40,8	0,183
11	4075	39,7	0,178
12	973	38,5	0,173
13	-1923	37,6	0,169
14	-4638	36,9	0,165
15	-7190	36,3	0,163
16	-9650	35,4	0,159
17	-19718	30,4	0,136
18	-24706	27,6	0,124
19	-23905	24,3	0,109

Table 4-3: The load turbine acording variable velocities on rotor [Custom Processing]

$$\omega = 2 \,.\, \pi \,.\, \frac{RPM}{60} \tag{4.8}$$

$$P = M \,.\, \omega \tag{4.9}$$

$$u = \frac{D_{mid}}{2} \,.\, \omega \tag{4.10}$$

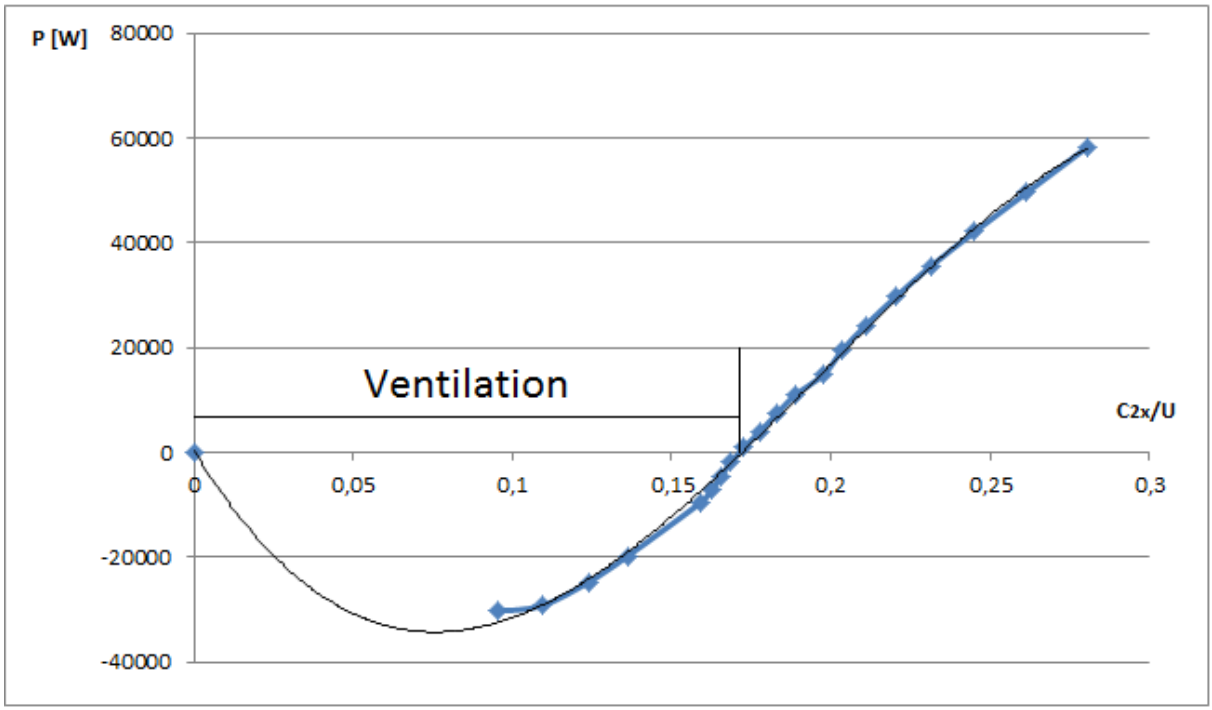

Figure 4-37: General characteristic of load turbine under velocities on rotor [Custom Processing]

4.9.1.1 Stremlines and vectors showing the ventilation phenomena

It would be a tedious task for doing numerical investigation of the flow field under ventilation.

Various experimental measurements are needed to estimate the onset of separation of flow. But the analysis is limited only to a minimum mass flow of 20%. It is known that the mostly used coordinate system for use in turbo machinery rotors is the relative or rotating coordinate system. The frame of reference is attached to the rotor so it rotates with an angular velocity ω about the main axis. The basic reason behind using moving reference of frame is if the flow field is transient when viewed in a stationary frame can become steady when viewed in this frame. Below we can see the ventilation on streamlines figure (4 - 33).

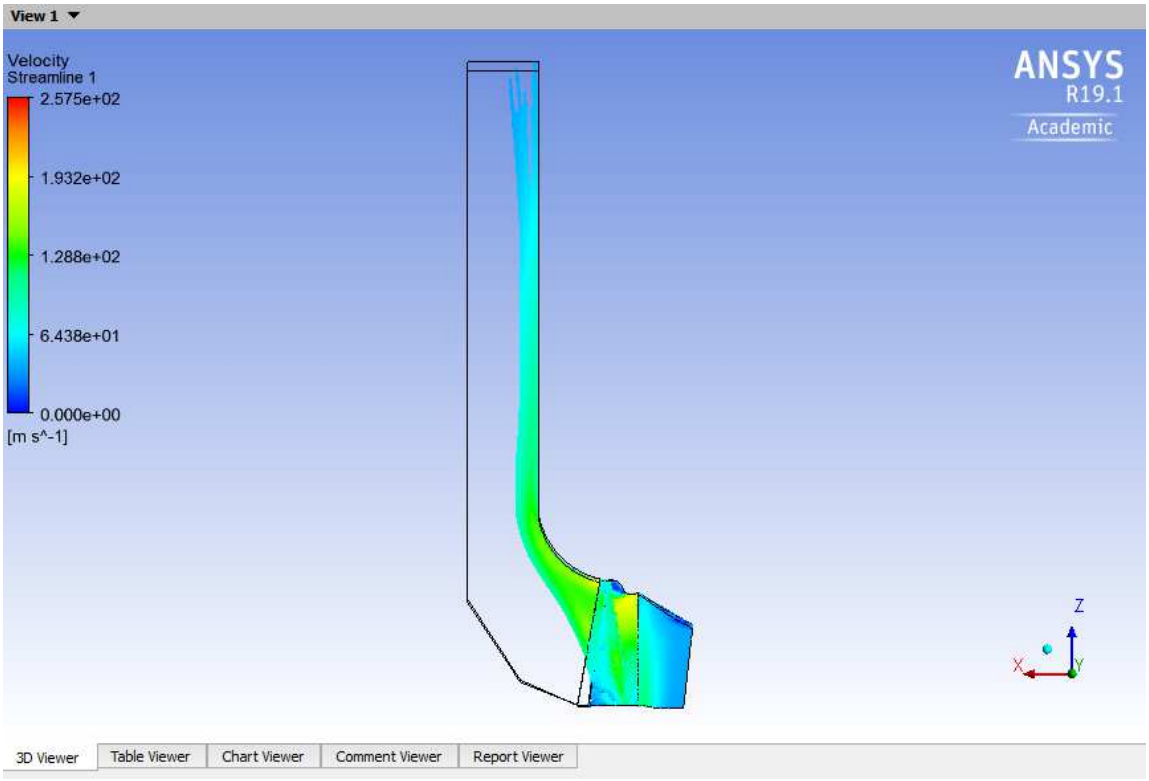

Figure 4-38: Streamlines showing the ventilation with p_2 = 27000 [Pa] (low load) [Custom Processing]

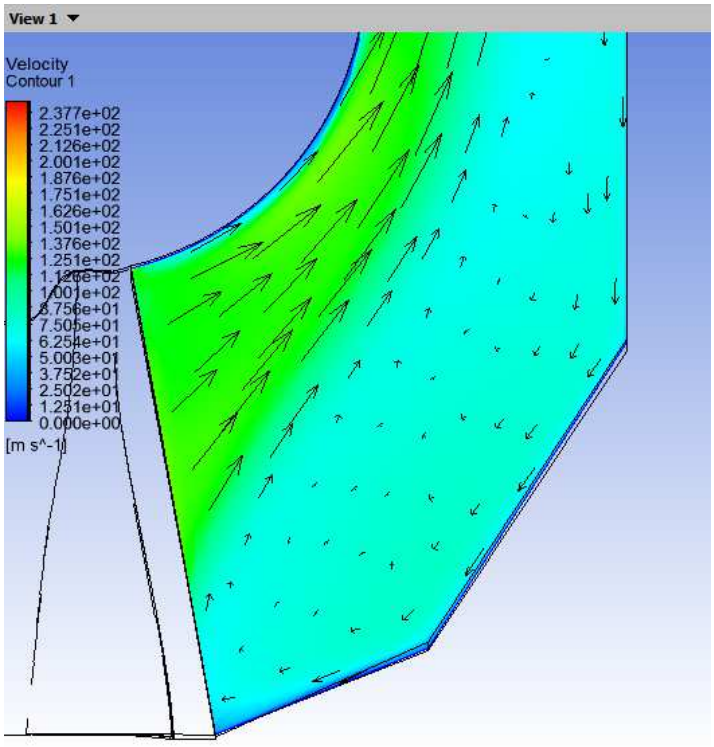

Figure 4-39: Vectors showing the starting point ventilation p_2 = 25000 [Pa] [Custom Processing]

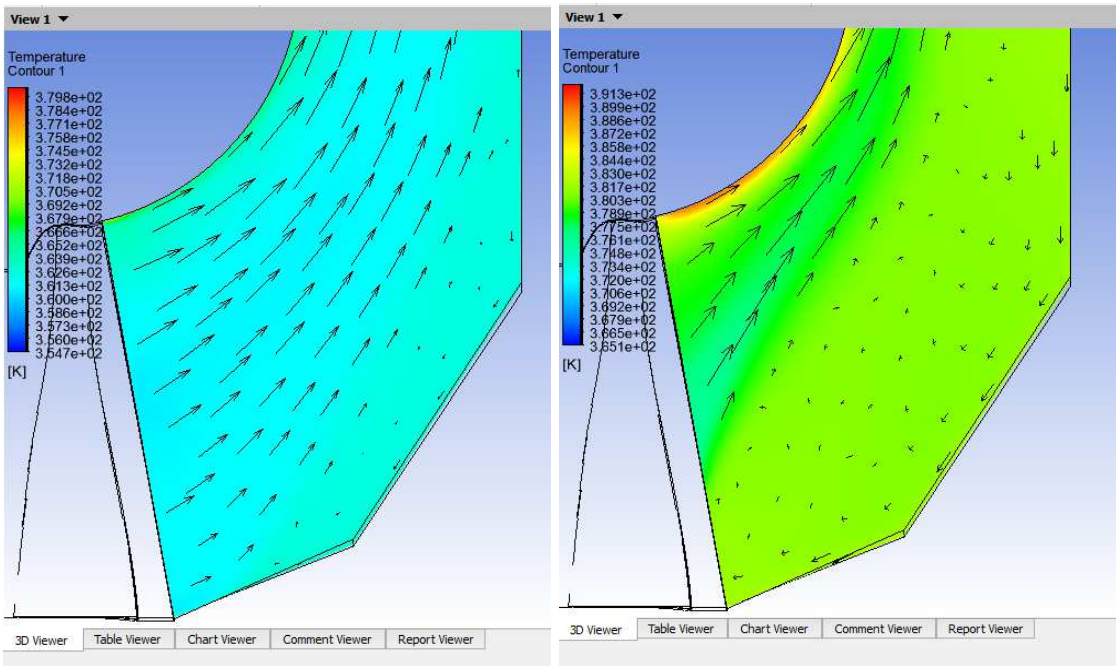

Figure 4-40: Temperature Comparation with intense ventilation (right side) and without ventilation (left side) [Custom Processing]

5. Conclusion

The diploma thesis deals with three-dimensional numerical simulation of steam flow through the complete turbine stage of the experimental Boiler Feed Pump Turbines T10MW located in the Doosan Škoda Power laboratory in Pilsen.

In the theoretical part of the thesis, information on the past and presence of Doosan Škoda Power was presented. Furthermore, the theory of steam turbines was written with an emphasis on the working process and energy transformation in the stator and rotor parts. This information has been provided for both turbine and positive pressure stages. In the last chapter of the theoretical part, an insight into a complex industry such as turbulent fluid flow was introduced. It has been found that this issue is not yet reliably elucidated, but that there are a number of computational models that try to define it. One of these models is the numerical simulation of turbine flow in the practical part of this work.

In the practical part of the thesis, a three-dimensional numerical calculation of the complete T10MW experimental steam turbine will be performed. This turbine is equipped with blades derived from the third turbine stage of a BFPT.

Before the calculation itself, it is necessary to first create the 3D models of the rotor and stator blades and diffuser by Inventor 2019. The blades and diffuser were simplified and slight modified (diffuser) for better results and stabilization. After that, the flow steam was created by for Turbo mode in TurboGrid, then creating the computational network that was generated in the universal mesher ANSYS Meshing. It was created separately, stator and rotor by TurboGrid and diffusor by ICEM. As it was explained on chapter 4.5.1.

With the 3D model and mesh, it could start to set the boundary conditions according to the requirements of Doosan Skoda Power. It was made with success as can be seen in chapter 4.6.

The next step was to start the calculation with CFX-solver with 1000 interactions and the monitor setting according to chapter 4.6 and 4.7.

It was made 19 simulations starting with boundary conditions of, static inlet temperature and pressure outlet. After was increased steps of 1000 [Pa] for each simulation until 28000 [Pa] after the steps were bigger due to lack of time.

With all the results we could start to analyze it on CFX-Post. The first requirement from Doosan Skoda represented the pressures, temperatures, velocities, and Mach number for = 22000 [Pa] in 3 layers (planes) of the domain, 5%, 50% and 95% according to the hight of the domain. The results were quite good as can be seen on the table (4 – 1 and 4 - 2) and figure (4

– 32). It's important to mention that my results were analyzed with plans on the region required and the measurement provided was punctual sensors that can explain the differences.

After the requirement from Doosan Skoda was create a plot representation the efficiency versus ratio of velocities was can be seen on figure (4 – 33). The results were very good once the expected result should be efficiency= 0,9 and u/cis = roughly 0,65. We had efficiency= 0,92 and u/cis = 0,69.

On the next chapter and more important Doosan Skoda required creating a plot that we could see in which conditions the ventilation phenomena occurs. So it was created a plot with the general characteristic of load turbine under velocities on rotor and the results were very good the ventilations phenomena starts on 0,17 on axis x. The expectation was that this value should be between 0,17 - 0,16. So loads lower than 0,17 occur the ventilation phenomena that we want to avoid for many reasons that it was explained in chapter 4.9. For concluding it was demonstrated on the figure (4 – 40) how the phenomena is damaged for the turbine considering how much the temperature increases in those regions. For matters of security normally are used water sprinklers to decrease the temperature.

6. List of used literature

[1] SOFT IN WAY INCORPORATED- *Design Challenges of Boiler Feed Pump Turbines in Thermal Power Stations* [online]. [cit. 2019-13-05]. Available from: < http://blog.softinway.com/en/design-challenges-of-boiler-feed-pump-turbines-in-thermal-power-stations/#comment-4126 >

[2] IDNES - *Škoda* [online]. This page was last modified on 11.09.2017 [cit. 2019-13-05]. Available from: < https://www.idnes.cz/finance/prace-a-podnikani/historie-financi-osobnosti-managementu-rytir-skoda.A170908_154121_podnikani_kho >

[3] DOOSAN ŠKODA POWER - *Nuclear Power Plants* [online]. Doosan Škoda Power Co., Ltd, © 2019. Available from: < http://www.doosanskodapower.com/en/steam/nuclearpowerplants/ >

[4] ŠMÍDA, Z. *3D numerický výpočet proudění v kompletním stupni experimentální parní turbíny T1MW vliv geometrie a proudových parametrů na účinnost:* Thesis. Ostrava: VŠB - Technical University of Ostrava, Faculty of Mechanical Engineering, Department of Power Engineering, 2014, 135 p.

[5] WIKIPEDIA. *Škoda (Enterprise)* [online]. This page was last modified on 15 September 2013, 16:54 [cit. 2013-24-10]. Available from: < http://cs.wikipedia.org/wiki/%C5%A0koda_(podnik) >

[6] ALCHETRON – *Doosan Škoda Power* [online]. This page was last modified on 12.07.2018 [cit. 2019-13-05]. Available from: < https://alchetron.com/Doosan-%C5%A0koda-Power >

[7] TECHINICAL UNIVERSITY OF OSTRAVA -TUO - ZZO Energy Basics [online]. © 2013 [cit. 2013-24-10]. Available from: < http://www1.vsb.cz/ke/vyuka/zaklady_energetiky/Zaklady_energetiky_ZZO.pdf >

[8] ŠMÍDA,Zdeněk. *Steam turbines, lecture 1, 2, 3, 4 and 5*. Ostrava: VSB - Technical University of Ostrava, 2018. 394 p.

[9] WIKIPEDIA. *Aeolipile* [online]. This page was last modified 09.04.2019, 14:11 [cit. 2019-13-05]. Available from: < https://en.wikipedia.org/wiki/Aeolipile >

[10] WIKIPEDIA. *Steam turbine* [online]. This page was last modified 07.05.2019, 07:14 [cit. 2019-13-05]. Available from: < https://en.wikipedia.org/wiki/Steam_turbine >

[11] WIKIPEDIA. *Dynamo* [online]. This page was last modified 28.05.2019, 12:50 [cit. 2019-13-05]. Available from: < https://en.wikipedia.org/wiki/Dynamo >

[12] MPOWERUK. *Laval Impulse Steam Turbine* [online]. This page was last modified 02.08.2012, 16:56 [cit. 2019-13-05]. Available from: < https://www.mpoweruk.com/figs/Laval.htm >

[13] RESEARCHGATE. *Tip leakage / main flow interaction in multi-stage HP turbines with short-height blading* [online]. This page was last modified 01.12.2003 [cit. 2019-13-05]. Available from: < https://www.researchgate.net/publication/216474270_Tip_leakage_main_flow_interaction_in_multi-stage_HP_turbines_with_short-height_blading >

[14] BEČVÁŘ, Josef. *Tepelné turbíny*. Praha: SNTL, 1968. 544 p.

[15] WIKIPEDIA. *Newton's laws of motion* [online]. This page was last modified 25.04.2019 [cit. 2019-14-05]. Available from: < https://en.wikipedia.org/wiki/Newton%27s_laws_of_motion >

[16] WIKIPEDIA. *Degree of reaction* [online]. This page was last modified 11.05.2019, 02:56 [cit. 2019-14-05]. Available from: < https://en.wikipedia.org/wiki/Degree_of_reaction >

[17] KRBEK, Jaroslav. *Tepelné turbíny a turbokompresory*. 3. vyd. Brno: VUT, 1990, 241 s. ISBN 80-214-0236-9

[18] TRANSFORMATION TECHNOLOGY. Design of turbomachine with regard to spatial character of flow [online]. Jiří Škorpík, © 2004 - 2012 [cit. 2019-14-05]. Available from: < http://www.transformacni-technologie.cz/navrh-stupne.html >

[19] KRBEK, Jaroslav. *Tepelné turbíny a turbokompresory*. 3. vyd. Brno: VUT, 1990, 241 s. ISBN 80-214-0236-9

[20] ASME DIGITAL COLLECTION. *Modeling of a Steam Turbine Including Partial Arc Admission for Use in a Process Simulation Software Environment* [online]. This page was last modified 03.06.2014 [cit. 2019-14-05]. Available from: < http://gasturbinespower.asmedigitalcollection.asme.org/article.aspx?articleid=1852173 >

[21] NUCLEAR POWER. *Boundary Layer* [online]. [cit. 2019-14-05]. Available from: < https://www.nuclear-power.net/nuclear-engineering/fluid-dynamics/boundary-layer/>

[22] KOZUBKOVÁ, Milada. *Modeling of heat, mass and momentum transfer*. Ostrava: VSB - Technical University of Ostrava, 2018. 184 s.

[23] MCCABISM. *Hairpin vortices and other turbulent phenomena* [online]. Gordon McCabe, [cit. 2014-28-3]. Available from: < http://mccabism.blogspot.cz/2011/06/hairpin-vortices-and-other-turbulent_18.html >

[24] THE TAME AERODYNAMICIST. *The Evolution of CFD* [online]. This page was last modified 04.11.2014 [cit. 2019-14-05]. Available from: < https://tameaero.wordpress.com/2014/11/04/the-evolution-of-cfd/>

[25] SPRINGER LINK. *Models of Turbulent Flows and Particle Dynamics* [online]. This page was last modified 27.07.2016 [cit. 2019-14-05]. Available from: <https://link.springer.com/chapter/10.1007/978-3-319-41567-3_3>

[26] ANSYS, Inc., *ANSYS ICEM CFD User's Manual* [online]. [cit. 2019-14-05]. Available from: < https://haman.academy/wp-content/uploads/2017/11/ANSYS-ICEM-CFD-Users-Manual.pdf >

[27] SHARCNET, *Chapter 4: Using the ANSYS CFX Launcher* [online]. [cit. 2019-14-05]. Available from: < https://www.sharcnet.ca/Software/Ansys/16.2.3/en-us/help/cfx_intr/i1303196.html>

[28] APLUSPHYSICS. *Rotationals kinematics* [online]. Silly Beagle Productions, © 2014 [cit. 2014-3-4]. Available from: < http://www.aplusphysics.com/courses/honors/rotation/honors_rot_kinematics.html >

[29] G. ANZALDO ,MUÑOZ. *DOMAINS, BC´s AND SOURCES ANSYS CFD, CFX 16.0 [online]. ©2012* [cit. 2019-14-05]. Available from: <https://www.academia.edu/16970139/DOMAINS_BC_s_AND_SOURCES_ANSYS_CFD_CFX_16.0 >

[30] SHARCNET, *Chapter 1: CFX-Solver Manager Basics* [online]. [cit. 2019-14-05]. Available from: < https://www.sharcnet.ca/Software/Ansys/16.2.3/en-us/help/cfx_solv/i1311656.html>

[31] ANSYS, *ANSYS TurboGrid* [online]. [cit. 2019-16-05]. Available from: < https://www.ansys.com/products/fluids/ansys-turbogrid>

[32] ANSYS, *Extend your ANSYS Meshing Capabilities with ANSYS® ICEM CFD ™*

Meshing Software [online]. [cit. 2019-16-05]. Available from: < https://www.ansys.com/-/media/Ansys/corporate/resourcelibrary/brochure/ansys-icem-cfd-brochure.pdf>

7. List of Annexes

Annexe A – Tables of basic values [Doosan Škoda Power]

Annexe B – Parameters of computer technology [Custom processing]

Annexe C – Photographic documentation from Doosan Škoda Power [Custom processing]